View metadata, citation and similar papers at core.ac.uk
brought to you by CORE
provided by VBN

CHANNEL ESTIMATION AND PREDICTION IN UMTS LTE

Aalborg University
Institute of Electronic Systems
Signal and Information Processing for Communications

Lathaharan Somasegaran

The Faculty of Engineering and Science

Aalborg University

10th. Semester

TITLE:

Channel Estimation and Prediction in UMTS LTE

PROJECT PERIOD:

22nd. February - 25th. June, 2007

PROJECT GROUP:

1094

GROUP MEMBERS:

Lathaharan Somasegaran

SUPERVISORS:

Bernard Fleury

Maxime Guillaud

Thomas Zemen

NUMBER OF COPIES: 5

REPORT PAGE COUNT: 75

APPENDIX PAGE COUNT: 15

TOTAL PAGE COUNT: 89

ABSTRACT:

The 3rd Generation Partnership Project (3GPP) currently works on developing the third generation (3G) mobile telecommunication system towards a future 4th generation system. The evolution of the current 3G UMTS system was given the name Long Term Evolution (LTE). This project focuses on the downlink of the UMTS LTE, where orthogonal frequency division multiplexing (OFDM) is utilized as multiple access scheme. Based on working assumptions of 3GPP the project probes into different low-complexity methods in order to estimate and predict a time-varying channel for the UMTS LTE. The estimation is performed in two dimensions, i.e. the channel frequency response (frequency-domain) needs to be estimated at different time indices (time-domain). Common for all methods is the utilization of discrete prolate spheroidal (DPS) sequences for interpolation in the time-domain. The investigated methods are evaluated by simulations in Matlab. The channel model is chosen as a typical urban scenario modeled by Spatial Channel Model Extended (SCME), which is implemented with the LTE downlink structure in this project. The performance is measured using the mean square error (MSE) between the actual and the estimated frequency response. The performance is compared to the performance of a 2x1 dimensional Wiener interpolator, which consistently yields the lowest MSE but also the highest complexity. In general the investigated estimators have the same performance for channel prediction and which is close to the one of the 2x1D Wiener interpolation at a speed of 120 km/h. One of the investigated estimators, the linear minimum mean square error channel impulse response (LMMSE CIR) is a good compromise between complexity and performance. It is shown that the performance of this estimator for channel estimation purpose is close to the 2x1D Wiener filter at 120 km/h for different signal-to-noise ratios.

Preface

This report documents the master thesis written by the 10th semester group 1094, Section of Signal & Information Processing for Communications at the Department of Electronic Systems, Aalborg University, in the period from February 22nd to June 28th 2007. The thesis has been carried out at the Telecommunications Research Center (ftw) in Vienna. It is addressed to anyone interested in UMTS LTE and channel estimation.

Reading Guidelines

Appendix A provides an introduction to OFDM and can be skipped by readers already familiar with this technique.

Nomenclature

References are denoted by brackets as [] and may also contain a reference to a specific page. The number in the brackets refers to the bibliography which can be found at the back of the main report on the page 75. Reference to figures (and tables) are denoted by ”Figure/Table x.y” and equations by ”(x.y)” where x is a chapter number and y is a counting variable for the corresponding element in the chapter. A vector is denoted by boldface lowercase letter (”$\boldsymbol{a}$”) and matrix by boldface uppercase letter (”$\boldsymbol{A}$”), while the identity matrix of size $L \times L$ is denoted by $\boldsymbol{I}_L$.

Enclosed Material

A CD-ROM containing Matlab source code used within the project is enclosed in the back of the report. Furthermore, a postscript, DVI and PDF version of this report is also included in the CD-ROM. The DVI and PDF version includes hyperlinks.

Acknowledgements

I am very grateful to my supervisors Professor Bernard Fleury, Dr. Maxime Guillaud and Dr. Thomas Zemen for their great support and inputs and for giving me permission to perform my master thesis at ftw.

Aalborg University, June 25th,

Lathaharan Somasegaran

Contents

1 Introduction

1.1 Background

Long Term Evolution (LTE) is a project within the Third Generation Partnership Project (3GPP) in order to improve the UMTS (Universal Mobile Telecommunications System) mobile phone standard such that future requirements can be met. 3GPP is a collaboration agreement established in December 1998 and it is a co-operation between ETSI (Europe), ARIB/TTC (Japan), CCSA (China), ATIS (North America) and TTA (South Korea). The good aspect of 3GPP is the centralization of the standards, since a single organization for these technologies ensures global interoperability[1].

3GPP standards are structured as releases, which incorporate several individual standards. Table 1.1 shows the latest releases and emphasizes some of the specifications.

Developments currently done by 3GPP (Release 7 and above) are under the title *UMTS Long Term Evolution*.

Version	Date	Description
Release 99	End of 1999	Specification of the first UMTS 3G (3rd generation) networks with Wideband Code Division Multiple Access (WCDMA) air interface.
Release 5	2002	Specification of High Speed Downlink Packet Access (HSDPA).
Release 6	End of 2004	Specification of High Speed Uplink Packet Access (HSUPA).
Release 7	In progress. Final release expected at mid of 2007	Includes LTE. Focuses on decreasing latency and improvements to real-time applications like voice over IP (VoIP). This specification also focus on OFDM techniques in downlink.
Release 8	In progress	Long Term Evolution

Table 1.1: *Releases from 3GPP[19, 23].*

1.1.1 Scope of UMTS Long Term Evolution

Release 5 and 6 incorporate enhancements such as HSDPA and HSUPA offering up to 10 Mbps in downlink and 5.7 Mbps in uplink [23]. Using these enhancements, the 3GPP radio access technology will be competitive for the next years. However, to ensure competitiveness for the next

[1] http://www.3gpp.org/About/about.htm

several years and beyond, a long-term evolution of the 3GPP radio-access technology is currently considered [23].
In particular, to enhance the capability of the 3GPP system to cope with the rapid growth in IP data traffic [16], the packet-switched technology utilized within 3G mobile networks requires further enhancement. A continued evolution and optimization of the system concept is also necessary in order to maintain a competitive advantage in terms of both performance and cost [23].
Hence important parts of the long-term evolution include reduced latency, higher user data rates, improved system capacity and coverage, and reduced cost for the operator. In order to achieve this, an evolution of the radio interface as well as the radio network architecture is considered.
The present 3G network utilizes 5 MHz bandwidth for transmission between terminal also denoted as user equipment (UE) and base station (NodeB), but if higher data rates are desired, future spectrum allocations for LTE will evolve towards supporting wider transmission bandwidth. At the same time, support for transmission bandwidths of 5 MHz and less than 5 MHz allows more flexibility in whichever frequency bands the system may be deployed. The main objectives of LTE are the following [23]:

- User plane latency below 5 ms with 5 MHz or higher spectrum allocation. With narrower spectrum allocation, latency below 10 ms should be facilitated.
- Scalable bandwidth up to 20 MHz, with smaller bandwidths covering 1.25 MHz, 2.5 MHz, 5 MHz, 10 MHz and 15 MHz for narrow allocations.
- Downlink peak data rates up to 100 Mbps.
- Uplink peak data rates up to 50 Mbps.
- Support for packet switched (PS) domain only.
- Up to 4 Tx-antennas at the NodeB and 4 Rx-antennas at the UE.
- Optimized performance for mobile speed of less than 15km/h, and high performance for speeds up to 120km/h, and the connection should be maintained with mobile speeds up to 350 km/h.

In order to achieve the future requirements orthogonal frequency division multiplexing (OFDM) is used in the physical layer for downlink purpose, which is specified in the current Release 7 [4]. Unlike HSDPA or HSUPA, high speed orthogonal packet access (HSOPA) is an entirely new air interface system, unrelated to and incompatible with WCDMA.

1.2 Scope of the Project

One of the most important aspects in an OFDM system is a reliable and accurate channel estimation. It is important to estimate the channel as close to the true channel as possible since the estimation has an impact on the equalization of the received symbols. Furthermore prediction is necessary at the NodeB in order to improve bandwidth allocation when serving multiple users. Several methods for channel estimation for OFDM have been already presented [8, 18, 13]. This project investigates methods for channel estimation and prediction in the LTE downlink.
The report is structured as follows:

- Firstly the structure of the LTE downlink is studied in Chapter 2.
- Chapter 3 describes the channel model used within the project in order to validate the estimation methods.
- Chapter 4 discusses different channel estimation methods for estimation of frequency response without taking the time-variant channel into account.
- In Chapter 5 channel estimation methods for time-varying channel are presented and Chapter 6 presents methods for channel prediction.
- In Chapter 7 the different estimation methods are investigated by simulations in Matlab.
- The last chapter contains the conclusion of the thesis and proposals for possible future work.

Physical Layer in the LTE Downlink 2

One of the main changes in the LTE system compared to 3G-UMTS is the physical layer. In third generation systems, Wideband Code Division Multiple Access (WCDMA) is the most widely adopted technology. A highlight of the characteristics of the UMTS before Release 7 is listed below [12]:

- User information bits are spread over a wide bandwidth by multiplying the user data with a spreading code. The use of variable spreading factor allows a variation of the bit rate.
- The bandwidth is 5 MHz. The chip rate used is 3.84 Mcps. A network operator can deploy multiple 5 MHz bands to increase capacity.
- The frame length is 10 ms. During this phase, the user data rate is kept constant. However, the data rate among the users can change from frame to frame.

In the LTE system, this will be very different. The new system will present an OFDM based structure. The main aspects important for channel estimation in the physical layer are presented in the following section.

2.1 Overview of OFDM Based Structure

The technique of OFDM is based on the technique of frequency division multiplexing (FDM). Appendix A gives a detailed description of OFDM. The OFDM technique differs from traditional FDM by having subcarriers, which are are orthogonal to each other. The modulation technique used in an OFDM system helps to overcome the effects of a frequency selective channel. A frequency selective channel occurs when the transmitted signal experiences a multipath environment. Under such conditions, a given received symbol can be potentially corrupted by a number of previous symbols. This effect is commonly known as inter-symbol interference (ISI). To avoid such interference, the symbol duration has to be much larger than the delays caused by multipath channel.
Hence each symbol is prolonged with a copy of its tail denoted as cyclic prefix (CP) such that the ISI is minimized. Also, the spectral efficiency of the OFDM modulation technique is superior to

FDM since the subcarriers are overlapping, but orthogonal. The frequency spacing between the subcarriers $f_{\text{space}} = \frac{f_s}{N_{\text{IFFT}}}$ is either 15 kHz or 7.5 kHz according to working assumption in Release 8 [5]. In contrast to an OFDM transmission scheme, OFDMA allows multiple users to share the available bandwidth. Each user is assigned a specific time-frequency resource referred as resource block (RB). The fundamental principle of the Evolved UMTS Terrestrial Radio Access (E-UTRA) is that the data channels are shared channels, i.e. for each transmission time interval (TTI) of 1 ms, a new scheduling decision is made at NodeB regarding which users are assigned to which time/frequency resources during this transmission time interval.
In the LTE only packet-switched transmission is utilized [1]. OFDMA fits perfectly into packet-switched transmission, since different number of subcarriers (RBs) can be assigned to different users, in order to support differentiated Quality of Service (QoS).
The scheduling is dynamic and performed for each subframe, hence the number of RBs can be adjusted dynamically depending on the channel quality.

2.2 Frame Structure

The structure of the radio frame, illustrated in Figure 2.1, is described in the current study from 3GPP. It should be noticed that for time division duplex (TDD), subframes for uplink and downlink purpose should be assigned. Other frame structures are proposed in order to make the structure compatible with the present structure used in 3G. For simplicity it is chosen to work with the illustrated generic frame structure.
The duration of one frame is 10 ms and is composed of 20 slots of 0.5 ms, where one subframe consists of two slots. The number of OFDM symbols in one slot N_{sym} depends on the chosen length of the cyclic prefix (CP) and can be either 6 (long CP) or 7 (short CP).

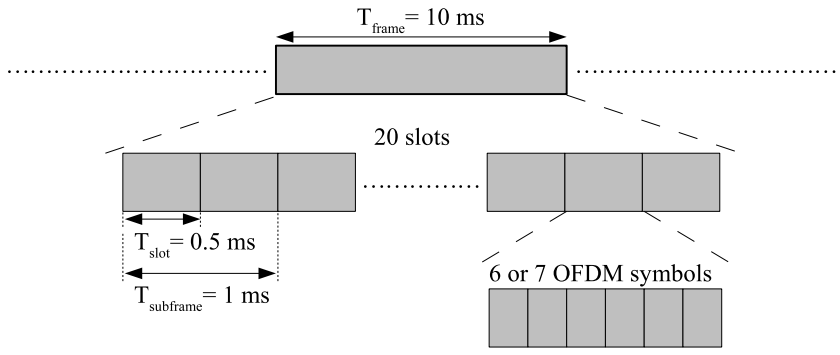

Figure 2.1: *Frame structure in LTE [4]. A radio frame is divided into 20 slots of 0.5 ms each having 6 or 7 OFDM symbols. Two slots make one subframe, which corresponds to the minimum downlink TTI.*

Transmission BW		1.25 MHz	2.5 MHz	5 MHz	10 MHz	15 MHz	20MHz
Subframe duration T_{sub}		0.5 ms					
Sub-carrier spacing f_{space}		15 kHz					
Sampling frequency f_{s}		1.92 MHz	3.84MHz	7.68 MHz	15.36 MHz	23.04 MHz	30.72 MHz
FFT size N_{IFFT}		128	256	512	1024	1536	2048
Number of occupied sub-carriers N_{BW}		75	150	300	600	900	1200
Number of OFDM symbols per subframe (short/long CP)		7/6					
CP length (μs / sample)	Short	(4.69/9)×6 (5.21/10)×1	(4.69/18)×6 (5.21/20)×1	(4.69/36)×6 (5.21/40)×1	(4.69/72)×6 (5.21/80)×1	(4.69/108)×6 (5.21/120)×1	(4.69/144)×6 (5.21/160)×1
	Long	(16.67/32)	(16.67/64)	(16.67/128)	(16.67/256)	(16.67/384)	(16.67/512)

Table 2.1: *Downlink parameters for OFDM transmission. The occupied subcarriers $\{1, \ldots, N_{BW}\}$ are centered around the frequency $f = 0$ [4].*

2.3 Downlink OFDM Parameters

The parameters used for downlink are listed in Table 2.1. The subcarrier frequency spacing $f_{\text{space}} = \frac{f_{\text{s}}}{N_{\text{IFFT}}} = 15$ kHz is used, and it is always constant, hence f_{s} and N_{IFFT} are proportional. The downlink parameters for $f_{\text{space}} = 7.5$ kHz are not yet defined [5].
The number of OFDM symbols N_{sym} per slot depends on the length of the CP as described in section 2.2. If 128-point IFFT and short CP is used, the first 6 OFDM symbols have a CP of 9 samples and the last symbol a CP of 10 samples, such that the duration of the subframe of 0.5 ms is preserved. Not all subcarriers are occupied, in Release 7 [4] approximately $2/3$ of the total frequency band is used. According to technical specifications in Release 8 [5] the number of used subcarriers (here denoted as N_{BW}) can be varied. The values of N_{BW} however are not specified. In this project the values N_{BW} are the same as in Release 7. Other downlink parameters than number of FFT-points and sampling frequency are not yet determined, but the above assumption is used for evaluation purpose in 3GPP, hence these parameters are also used in the project.

2.3.1 Mapping of Subcarriers

The subcarriers are mapped into the frequency spectrum as illustrated in Figure 2.2. According to Table 2.1, N_{BW} is $75/150/300/600/900/1200$ when the transmission bandwidth is $1.25/2.5/5/10/15/20$ MHz. Since the occupied subcarriers are centered around the frequency 0, half of the occupied subcarriers are placed in the negative spectrum and the other half in the positive spectrum. Let us denote the occupied subcarriers in the negative spectrum as $\{1, \ldots, N_{\text{n}}\}$ and in the positive spectrum as $\{N_{\text{n}} + 1, \ldots, N_{\text{BW}}\}$, where N_{n} (also shown on Figure 2.2) is $37/75/150/300/450/600$ [4]. The unused carriers are placed at the edges of the spectrum such that the utilized bandwidth is less than the specified bandwidth. This can be based on reducing the requirements for the analog filters at the transmitter and receiver side.

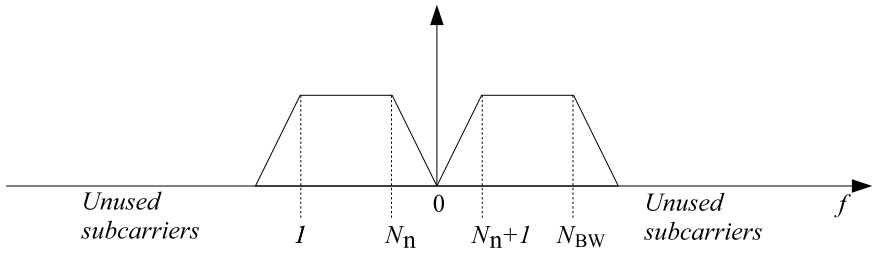

Figure 2.2: *Placement of occupied subcarriers [4]. N_{BW} and N_n are the total number of occupied subcarriers and the number of carriers in the negative spectrum respectively.*

2.4 Downlink Data Transmission

The transmitted signal in each slot is described by a resource grid of N_{BW} subcarriers and N_{sym} OFDM symbols. In order to achieve multiple access, bandwidth is allocated to the UEs in terms of resource blocks. A physical resource block, N_{RB} consists of 12 consecutive subcarriers in the frequency domain. In the time domain, a physical resource block consists of N_{sym} consecutive OFDM symbols, see Figure 2.3. N_{sym} is equal to the number of OFDM symbols in a slot. The

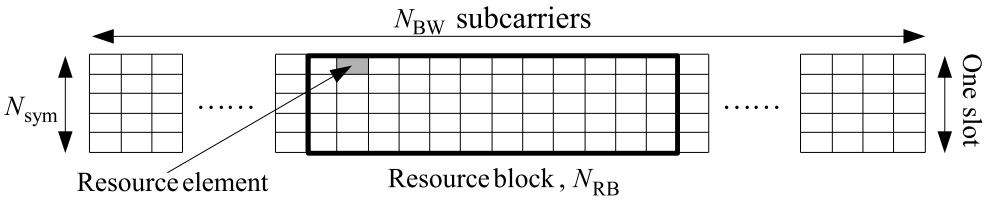

Figure 2.3: *Downlink resource grid [5].*

resource block size is the same for all bandwidths, hence the number of available physical resource blocks depends on the bandwidth. Depending on the required data rate, each UE can be assigned one or more resource blocks in each transmission time interval of 1 ms. The scheduling decision is done at the NodeB. The user data is carried on the Physical Downlink Shared Channel (PDSCH). Downlink control signaling on the Physical Downlink Control Channel (PDCCH) is used to transport the scheduling decisions to individual UEs. The PDCCH is placed in the first OFDM symbols of a slot [5].

2.4.1 Modulation

According to the working assumptions for PDSCH in Release 8, the transmitted bits are modulated using quadrature amplitude modulation (QAM). The available modulation schemes are 4-QAM, 16-QAM, and 64-QAM [4].

2.4.2 Downlink Reference Signal Structure

The downlink reference signal structure is important for cell search and channel estimation. Resource elements in the time-frequency domain are carrying the reference signal sequence, which is predefined for each cell.

Appendix **??** gives a detailed description of how the reference symbols are generated and on their positions. In this section we focus on the main properties of the structure.

The reference symbols are placed in the first OFDM symbol of one slot and on the third last OFDM symbol [4]. The spacing between the reference symbols is always 6 subcarriers [4] and the norm is always 1 no matter which modulation scheme is utilized for the data symbols as described in Section 2.4.2.

In the LTE the NodeBs and UEs can have 2 or 4 antennas and when two or more transmitter antennas are applied, the reference symbols are transmitted such that they are orthogonal in space. The orthogonality in space is obtained by letting all other antennas be silent in the resource element in which one antenna transmits a reference symbol [5].

Figure 2.4 shows the positions of the reference symbols for transmission with two antennas as an example. When antenna 1 transmits a reference symbol, antenna 2 is silent and vice versa. This

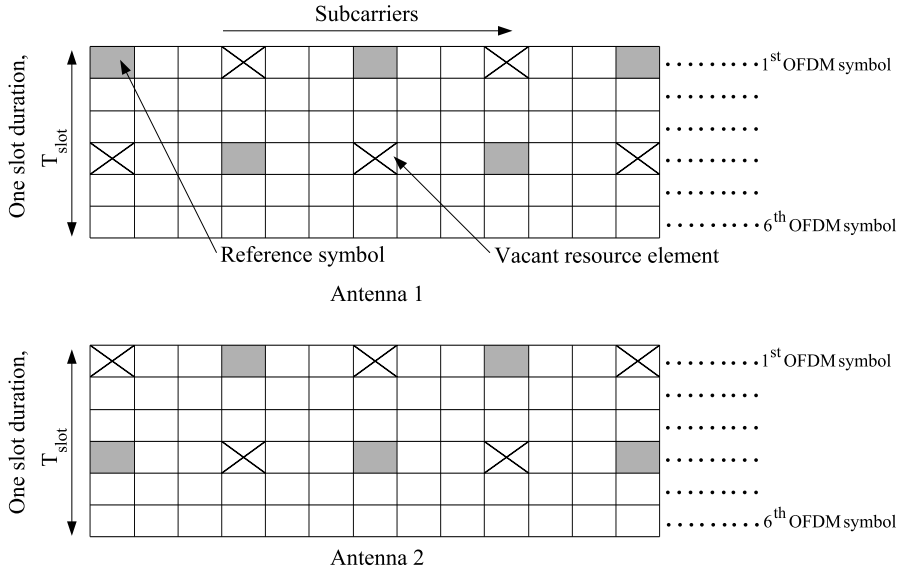

Figure 2.4: *The reference symbol structure for one slot with 6 OFDM symbols using two antennas. Note that only the used subcarriers are depicted. In this thesis we consider one antenna and makes use of the reference symbol structure depicted for antenna 1.*

thesis considers one antenna and makes use of the reference symbol structure depicted for antenna 1 on Figure 2.4.

The reference signal sequence also carries the cell identity. The reference signal sequence is generated as a symbol-by-symbol product of an orthogonal sequence (OS) $\boldsymbol{R}^{\text{OS}} \in \mathbb{C}^{340\times 2}$ (3 different sequences are predefined) and a pseudo-random sequence (PRS) $\boldsymbol{R}^{\text{PRS}} \in \mathbb{R}^{340\times 2}$ (170 different sequences are predefined). Each cell identity corresponds to a unique combination of one orthog-

onal sequence $\boldsymbol{R}^{\mathrm{OS}}$ and one pseudorandom sequence $\boldsymbol{R}^{\mathrm{PRS}}$, allowing 510 different cell identities [5].
Frequency hopping can also be applied to the downlink reference signals. The frequency hopping pattern has a period of one frame duration.

2.4.3 Cell Search

During cell search, different types of information need to be identified by the UE such as radio frame timing, frequency, cell identification, overall transmission bandwidth, antenna configuration, cyclic prefix length. Besides the reference symbols, synchronization signals are therefore needed during cell search. In E-UTRA (Evolved UMTS Terrestrial Radio Access) the synchronization acquisition and the cell group identifier are obtained from different synchronization channels (SCH).
A primary synchronization channel (PSCH) for synchronization acquisition and a secondary synchronization channel (SSCH) for cell group identification have a pre-defined structure. They are transmitted on the 72 subcarriers centered around subcarrier at frequency $f = 0$ within the same predefined slots (1st and 11th slot in one frame). PSCH and SSCH are however placed on the second last and third last OFDM symbol respectively [5].
Hence cell search is always performed using the 72 central subcarriers independent of the overall transmission bandwidth.

2.5 Latency Requirement

As mentioned in Section 1.1.1 the user plane latency should be below 5 ms [1]. For the downlink case the user plane is defined in terms of a one-way transit time between a packet being available at the IP layer at the NodeB and the availability of this packet at IP layer at the UE. The NodeB provides the interface towards the core network (see also Appendix **??**).
From a channel estimation point of view a latency below 5 ms results in a block length less than 5 ms for channel estimation purpose.

2.6 Implementation of the OFDM Transceiver

Based on the mentioned information on the physical layer, a structure of the transmitter in LTE is designed as illustrated on Figure 2.5. The transmitter is based on conventional OFDM system structure. The structure of the implemented receiver is depicted in Figure 2.6.

2.6.1 Binary Source Generator

The binary source generator generates the signal randomly. The number of the generated binary symbols depends on the modulation scheme, i.e. the number of bits per QAM-symbol (sec. 2.4.1) and the number of subcarriers (sec. 2.3).

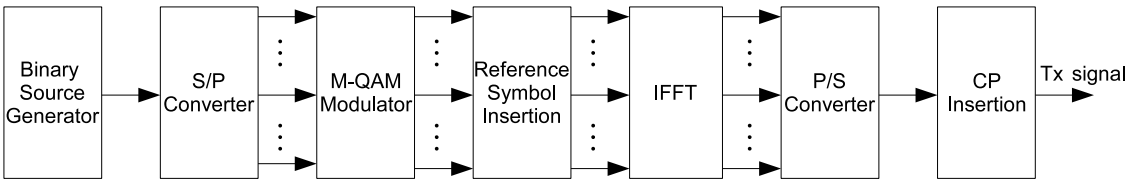

Figure 2.5: *Block diagram of the OFDM transmitter in LTE.*

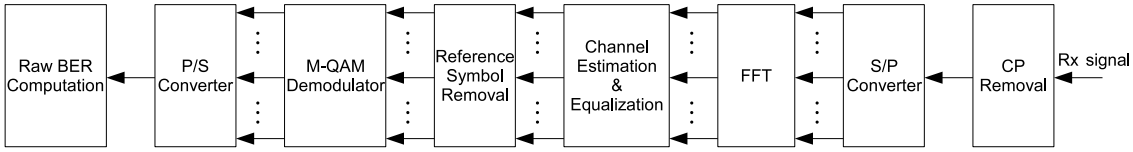

Figure 2.6: *Block diagram of the OFDM receiver in LTE.*

2.6.2 Modulation

During modulation it is necessary to normalize the transmitted symbols in order to adjust the signal-to-noise ratio. The normalization is achieved by scaling the symbols as listed in Table 2.2. The bits are modulated using Gray labeling, which is depicted in Figure 2.7 for 16-QAM as an

Modulation	K_{norm}
4-QAM	$\frac{1}{\sqrt{2}}$
16-QAM	$\frac{1}{\sqrt{10}}$
64-QAM	$\frac{1}{\sqrt{64}}$

Table 2.2: *Normalization factor for M-QAM modulation schemes in E-UTRA downlink [5].*

example.

2.6.3 Inverse Fast Fourier Transform

Figure 2.8 shows an illustration of the mapping of symbols under IFFT-operation, which corresponds to the mapping described in section 2.3.1.

2.7 Summary

Important properties of the physical layer in the LTE downlink have been described. For the purpose of channel estimation, one antenna at transmitter side and receiver side is considered. The channel estimation can be achieved separately for each antenna since the reference symbols are orthogonal in space. OFDMA is utilized as multiple access scheme in the downlink, where each user is allocated one or several resource blocks and scheduling is performed for each subframe. Based on specifications in Release 7 [4] and on working assumptions in Release 8 [5] an OFDM

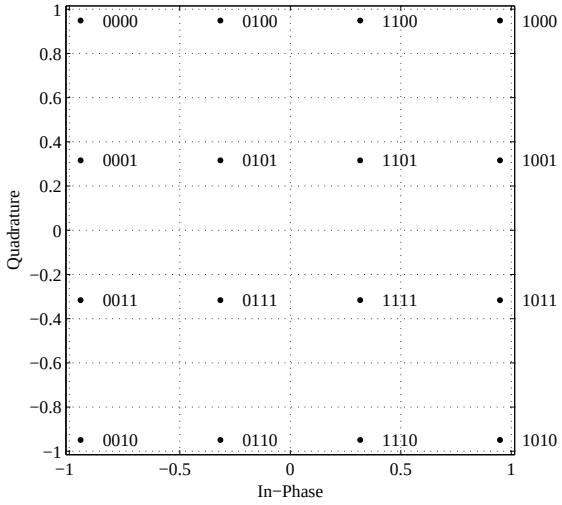

Figure 2.7: *16-QAM constellation with the corresponding binary values after normalization.*

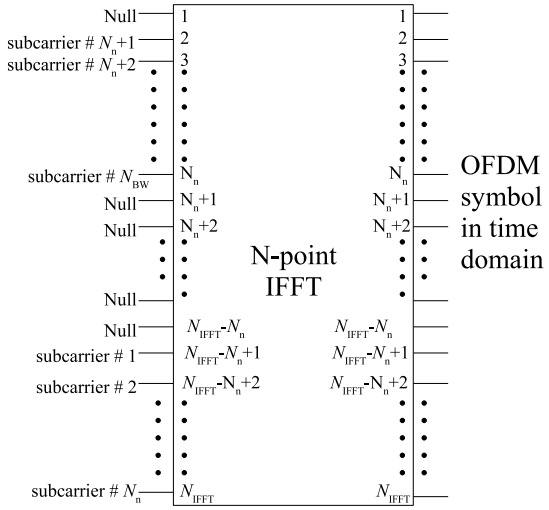

Figure 2.8: *OFDM symbol generation using an N-point IFFT operation.*

transceiver is implemented in MatLab. In order to analyze different channel estimation methods, an appropriate channel model needs to be used, as described in the next

Channel Model

3

3.1 Multipath transmission

Radio wave propagation can be described by multiple paths occurring due to reflection (buildings, trees, etc.) in the environment. When modeling a radio channel, only a finite number of paths is considered to approximate the real environment, which is illustrated by Figure 3.1. The received

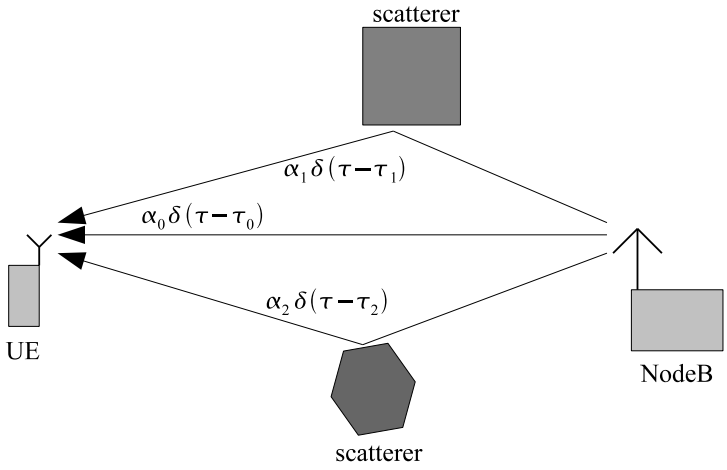

Figure 3.1: *Multipath radio environment [28, p. 7].*

signal at the UE is a superposition of all paths. There are infinite number of paths closely spaced in time, but only a finite number is modeled. Equation (3.1) describes a model for the channel impulse response,

$$h'(\tau) = \sum_{k=0}^{K-1} \alpha_k \delta(\tau - \tau_k), \text{ where} \tag{3.1}$$

K is the number of paths, α_k is the complex fading coefficient for a given path at delay τ_k. In this thesis a baseband representation of the channel is used, hence the effect of up-converting/transmit filter and down-converting/receive filter is modeled by $h_T(\tau)$ and $h_R(\tau)$ respectively [28].

$$h(\tau) = h_T(\tau) * h'(\tau) * h_R(\tau), \tag{3.2}$$

where $*$ denotes convolution.
Applying the sampling operation at rate $1/T_C$ equation (3.2) is transformed into

$$h\left[k\right] = h\left[kT_c\right], \text{ where} \tag{3.3}$$

where the discrete time index $k \in \{0, ..., L-1\}$ and L denotes the length of the sampled impulse response. One channel model is the wide-sense stationary uncorrelated scattering (WSSUS). In WSSUS model, the time-varying fading process is assumed to be wide-sense stationary random process and the signal reflections from the scatterings by different objects are assumed to be independent. The following parameters are often used to characterize a WSSUS channel:

- In order to describe the average delay of the channel the term delay spread, τ_{RMS} is used.
- Coherence bandwidth $\Delta f_{(c)}$ gives an indication of how far apart, in frequency, the signal has to be spaced to in order to achieve correlation of value c.
- Coherence time $\Delta t_{(c)}$ gives a measure of the time duration over which the correlation between two channel impulse response has a value c. The coherence time is related to the Doppler spectrum which depends on the velocity of the UE.
- Doppler spread f_{Dmax} which indicates a maximum range of Doppler shifts.

The mentioned parameters are now described in detail and calculated for the signal structure of the physical layer in the LTE downlink. Furthermore standard channel models will be described in order to find a suitable model for simulation purposes.

3.2 Delay Spread

The impact of the environment on the transmitted signal (fading) can also be classified as follows:

- Long-term fading: the fading varies slowly compared to the symbol time, it is not of interest when estimating a channel. Typically it is caused by reflections from the geographical surroundings, e.g. landscape.
- Short-term fading: Short-term fading can vary as fast as the symbol time. Short-term fading is caused by the interference of multiple reflections, scattering and diffractions on small elements in near surroundings., e.g. trees and other obstacles in the near.

The channel delay spread τ is closely related to the short-term fading. In order to describe the average delay of the channel, the root-mean-square (RMS) average of the delay spread, which is defined as the second central moment of the channel power delay profile, is used [11, p. 540].

$$\tau_{RMS} = \sqrt{\frac{\sum_{k=0}^{K-1} P_k(\tau_k - \tau_m)^2}{\sum_{k=0}^{K-1} P_k}} \text{ , where} \tag{3.4}$$

$$\tau_m = \frac{\sum_{k=0}^{K-1} P_k \tau_k}{\sum_{k=0}^{K-1} P_k} \quad \text{is the mean excess delay} \tag{3.5}$$

and P_k is the power of $h[k]$ at time index k. When the channel is viewed in frequency domain the coherence bandwidth is of concern. Using the uncertainty relationship found in [9] the coherence bandwidth is calculated as

$$\Delta f_{(c)} \geq \frac{1}{2\pi\tau_{RMS}} \arccos(c), \tag{3.6}$$

where $\Delta f_{(c)}$ is the minimal coherence bandwidth in which the autocorrelation of the channel power delay profile, R_{hh} has the value c.
A multipath channel is characterized as frequency flat or frequency selective in the following way: Frequency flat fading: Coherence bandwidth $\Delta f_c >> B_\text{s}$ Symbol bandwidth . The frequency components of the signal would roughly undergo the same fading.
Frequency selective fading: $\Delta f_c \leq B_\text{s}$, with $c = 0.5$ is in both cases. The different frequency components of the signal, which differ by more than Δf_c will undergo different degrees of fading. In order to avoid ISI the delay spread τ_{RMS} should always be less than symbol duration T_s, such that frequency flat fading is achieved. The data rate however will be decreased if the symbol duration is extended.

3.2.1 Position of Reference Symbols in the Frequency Domain

The position of the reference symbols in frequency domain is investigated. Section 2.4.2 describes the positions in detail. The goal is to compare the spacing between the reference symbols with the coherence bandwidth of the channel.

3.2.2 Coherence Bandwidth

The spacing in frequency between the subcarriers is known from Section 2.3,

$$f_\text{space} = 15 \text{ kHz}. \tag{3.7}$$

According to Section 2.4.2 the reference symbols are placed at every 6th subcarrier:

$$f_\text{R} = f_\text{space} \cdot 6 = 90\text{kHz}. \tag{3.8}$$

Using the uncertainty relationship described in Section 3.2 the bandwidth $B_{(c)}$ in which the channel is constant is defined for $c = 0.9$ and the value $c = 0.5$ for when the channel has changed.
Based on these assumptions the coherence bandwidths are now calculated:

$$B_{(0.5)} \geq \frac{1}{2\pi\tau_{RMS}} \arccos(c) = \frac{1}{2\pi 0.65\mu s} \arccos(0.5) = 256.4\text{kHz} \tag{3.9}$$

$$B_{(0.9)} \geq \frac{1}{2\pi 0.65\mu s} \arccos(0.9) = 110.4\text{kHz} \tag{3.10}$$

Equations (3.9) and (3.10) show that the spacing of the reference symbols in frequency approximately corresponds to the bandwidth in which the channel is constant, furthermore the channel is estimated at least twice before the autocorrelation has the value 0.5.

3.3 Time-Varying channel

The mobile movement introduces Doppler frequency shifts. There are multiple Doppler shifts, which add up and form a Doppler spectrum. In the following we consider one path.

3.3.1 Doppler shift

The main factor that affects the rate of fading is the mobility of the receiver relative to the transmitter. As a UE moves with velocity v_{UE} relative to NodeB, it causes a Doppler shift f_d which is given by (3.11) for a singe path:

$$f_{\text{d}} = f_{\text{Dmax}} \cos(\theta), \tag{3.11}$$

where θ is the angle of arrival of the received signal relative to the direction of the UE and

$$f_{\text{Dmax}} = \frac{v_{\text{UE}}}{c_0} f_c, \tag{3.12}$$

where f_{Dmax} is the maximum Doppler frequency , v_{UE} is the velocity of the receiver, f_c is the carrier frequency and c_0 speed of light.
The time varying impulse response of the channel can be expressed as an extension of Equation (3.1).

$$h(t,\tau) = \sum_{k=0}^{L-1} \alpha_k e^{j2\pi f_d t} \delta(\tau - \tau_k), \tag{3.13}$$

where t is the time at which the channel impulse response is measured. The signal $h(t,\tau)$ has a band-limited spectrum, also denoted as Doppler spectrum. The spectrum is limited to the range

$$\mathcal{W} = [-\nu_{\text{Dmax}}, \ldots, \nu_{\text{Dmax}}], \quad \text{where} \tag{3.14}$$

$$\nu_{\text{Dmax}} = f_{\text{Dmax}} T_{\text{s}}, \tag{3.15}$$

with T_{s} as the symbol duration and ν_{Dmax} as the normalized maximum Doppler-shift. In mobile radio channels, the maximum Doppler spread is used to characterize how fast in time the channel changes. For this purpose the coherence time is calculated as [9]

$$\Delta t_{(c)} \geq \frac{1}{2\pi f_{\text{Dmax}}} \arccos(c), \tag{3.16}$$

where $\Delta t_{(c)}$ is the difference in time for which the autocorrelation in the time-domain has the value c.
A channel is said to be time-invariant, in the sense that the channel appears as time invariant to the transmitted signal.
Hence the terms are relative to the symbol duration: time selective fading occurs when the channel changes within one symbol period T_{s} while time-invariant fading occurs when the channel is constant within at least one symbol period.

Time-invariant fading: $\Delta t_{(0.5)} >> T_\text{s}$, where $c = 0.5$. If the symbol duration is small compared with $\Delta t_{0.5}$ then the channel is classified as time-invariant.
Time selective fading: $\Delta t_{(0.5)} \leq T_\text{s}$. On the other hand if $\Delta t_{(c)}$ is close to or smaller than the symbol duration , the channel is considered to have time selective fading. In general, it is difficult to estimate the channel parameters for a time selective channel.
In order to estimate a channel for a period of T_s it is of importance to be in the time-invariant case.

3.3.2 Position of Reference Symbols in Time-Domain

The duration of one slot T_slot is known from Section 2.3. There are $N_\text{sym} = 6$ OFDM symbols in one slot, which results in a symbol duration

$$T_\text{s} = \frac{T_\text{slot}}{N_\text{sym}} = \frac{0.5 \text{ ms}}{6} = 83.3 \ \mu\text{s}. \tag{3.17}$$

Reference symbols are placed at each fourth OFDM symbol, but are not always found at same subcarriers. Nevertheless the channel can be estimated after each third OFDM symbol and hence the spacing of reference symbols in the time-domain is set to,

$$T_\text{R} = 3T_\text{s} = 0.250 \text{ ms} \tag{3.18}$$

Using the uncertainty relationship described in Section 3.2 the coherence bandwidth $\Delta f_{(c)}$ in which the channel is constant is defined for $c = 0.9$ and the value $c = 0.5$ for when the channel has changed.
A UE with a maximum speed of 120 km/h, has a maximum Doppler shift of 185.4 Hz. Based on these assumptions the coherence times are now calculated

$$\Delta t_{(0.5)} \geq \frac{1}{2\pi f_{d,\,max}} \arccos(c) = \frac{1}{2\pi 185.4\text{Hz}} \arccos(0.5) = 0.750 \text{ ms} \tag{3.19}$$

$$\Delta t_{(0.9)} \geq \frac{1}{2\pi 222.15\text{Hz}} \arccos(0.9) = 0.323 \text{ ms} \tag{3.20}$$

Equations (3.19) and (3.20) show that the spacing of the reference symbols in time is less than the coherence time . Furthermore the channel is estimated at least three times before the autocorrelation of the channel estimates has the value 0.5.

3.4 Time-Frequency Correlation

For channel estimation purposes the channel correlation properties are of importance. Following properties of the channel can be shown from [13, p. 93]:

$$R(\Delta t, \Delta f) = R(\Delta t)\, R(\Delta f) \tag{3.21}$$

Equation (3.21) is the autocorrelation of the time-varying channel frequency response, which is the Fourier transform of (3.13) in the delay domain. The difference in time is denoted as Δt, while Δf

is the difference in frequency. Equation (3.21) is based on the fact that in mobile radio channels the time-correlation function is independent from the frequency correlation function [13]. Moreover different assumptions can be made for these correlation functions. The frequency correlation function is the Fourier transform of the power delay profile of the channel, hence it is based on the power delay profile. The time-correlation depends on the Doppler power spectral density. The Doppler power spectral density can be assumed uniform or having Jake's spectrum [7]. In this thesis the uniform spectral density is used. The constant spectrum can be expressed as,

$$S_h(\nu, \mathcal{W}) = \begin{cases} \frac{1}{2\nu_{\text{Dmax}}} & , \nu \in \mathcal{W} \\ 0 & \text{otherwise,} \end{cases} \tag{3.22}$$

where ν_{Dmax} is defined in equation (3.15) with ν as $\nu_{\text{Dmax}} = f_d T_\text{s}$ and $\mathcal{W}$ in (3.14). The discrete correlation function with $R_\text{d}(k) = R(kT_\text{s})$, based on [27], is then expressed as,

$$\begin{aligned} R_\text{d}\,(k, \mathcal{W}) &= \frac{1}{j2\pi k|\mathcal{W}|}\left(e^{j2\pi k\nu_{\text{Dmax}}} - e^{-j2\pi k\nu_{\text{Dmax}}}\right) \\ &= \frac{\sin(2\pi k\nu_{\text{Dmax}})}{\pi k|\mathcal{W}|} \end{aligned} \tag{3.23}$$

3.5 Standard Channel Models

Several models exist and are used in the industry to simulate radio wave propagation. Each model is suitable for a certain type of environment. The channel model used in this project is based on recommendations from 3GPP. The recommended channel models are chosen as simplifications, or typical realizations of the COST 259 model [3]. Testing with a common channel model is imperative to facilitate comparisons. The 3GPP typical urban (TU) channel model has been designed to simulate high delay spread in urban environments using bandwidths up to 5 Mhz.
A simplified model for the power delay profile is given in (3.24) [26]. The tap powers are normalized so that the sum of all tap powers is equal to 1.

$$P_k = \eta^2[k] = \frac{e^{-\frac{k}{L_D}}}{\sum_{k'=0}^{L-1} e^{-\frac{k'}{L_D}}}\text{, where} \tag{3.24}$$

$$L_D = \frac{\tau_{\text{RMS}}}{T_C} \tag{3.25}$$

denotes the RMS delay spread τ_{RMS} normalized to the sampling rate $1/T_C$ and η is the amplitude of the fading coefficient.
Assuming perfect power control and neglecting pathloss results in

$$\sum_{k=0}^{L-1} \eta^2[k] = 1 \tag{3.26}$$

The supported length L of the sampled impulse response should be chosen with respect to the signal-to-noise ratio (SNR) ($\frac{E_\text{s}}{\sigma^2_\text{z}}$), at which the system is operating [28, p.8],

$$L \geq 1 + \frac{\tau_{\text{RMS}}}{T_C}\ln\left(\text{SNR}\right) \tag{3.27}$$

Hence the components of the impulse response smaller than the SNR are not taken into account. Generation of a channel impulse response when the power delay profile is known is achieved assuming Rayleigh fading, which is described in next section.

3.6 Rayleigh Fading Channels

When a signal is transmitted in an environment with obstacles resulting in non line-of-sight (NLOS) propagation, more than one transmission path will appear as a result of the reflections. The receiver will then have to process a signal which is a superposition of several main transmission paths.

Each of the main paths is in reality the result of multiple scattered waves, or subpaths. If there exists a large number of subpaths they may be modeled as statistically independent; the central limit theorem will give the channel the statistical characteristics of a Rayleigh distribution [11, pp. 542-543].

The real and imaginary parts of the fading coefficient of one main path α are independent and identically Gaussian distributed with zero mean and variance $\frac{\sigma^2}{2}$, which leads to the probability density function

$$p(\eta) = \frac{\eta}{\sigma^2} e^{-\frac{\eta^2}{2\sigma^2}},\ \eta \geq 0 \tag{3.28}$$

$$p(\phi) = \frac{1}{2\pi},\ -\pi \leq \phi \leq \pi \tag{3.29}$$

where $p(\eta)$ is the Rayleigh distribution, η is the amplitude of the fading coefficient and the phase ϕ uniformly distributed.

Each tap is hence modeled as Gaussian real and imaginary part with zero mean with a variance according to the power delay profile. The goal is to model the time variation of the channel properties too. One method to simulate this phenomenon is to use Jake's model [7]. However a model developed by 3GPP, the Spatial Channel Model (SCM), described in the following Section 3.6.1, is used in this thesis in order to get as close to a true time varying channel as possible.

3.6.1 Spatial Channel Model

3GPP has developed a Spatial Channel Model (SCM) [2] for multiple input multiple output (MIMO) systems in order to specify parameters intended for the three most common cellular environments: suburban macrocells, urban macrocells, and urban microcells.

Since the goal of this project is channel estimation, pathloss is neglected.

The overall difference between the models are the amount and size of the scatterers. The macrocell environments assume height of NodeB well above the height of scatterers, while the scatterers and BS are at same height for the microcell scenario. From a UE's point of view the delay spread is one of the main parameters affected by the change in channel model as shown in Table 3.1. SCM has been implemented in Matlab [21] and can be used to generate channel fading coefficients, depending on several parameters such as the speed of UE, number of antennas and their properties

Channel Model	Delay spread / τ_{RMS}
Urban micro cell	0.251 μs
Urban macro cell	0.65 μs
Suburban macro cell	0.17 μs

Table 3.1: *Root mean square delay spread for different channel models according to [2].*

on transmitter and receiver side.
The SCM is designed for bandwidths up to 5 MHz, however support for bandwidths up to 20 MHz is needed for modeling the LTE downlink, hence an extended version of SCM (SCME) has also been developed [21].
This project makes use of the "Urban macro cell" channel model which specifies parameters for an urban environment with up to 3 km distance to a base station and NLOS, since it is assumed that the scatterers surrounding the UE are about the same height or are higher. This implies that the received signal at the mobile antenna arrives from all directions after bouncing from the surrounding scatterers, but there is no line-of-sight (LOS) to the NodeB.

3.7 Implementation of the Channel Model

The channel model is implemented with the OFDM transceiver as depicted in Figure 3.2. The

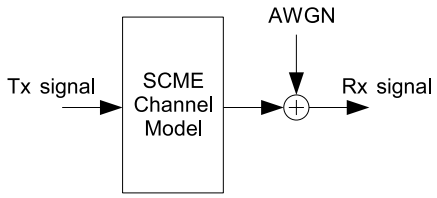

Figure 3.2: *Block diagram of implementation of the SCME channel model with the transmitter and receiver.*

transmitted signal is affected by the multipath channel generated by SCME and additive white Gaussian noise (AWGN) is added afterwards. In Section 3.3.2 it was concluded that the channel was time-invariant within one OFDM symbol duration. Hence in this thesis the SCME channel model is configured such that channel impulse responses are generated for each OFDM symbol and convolved with the symbol.

3.7.1 AWGN

Since the subcarriers of the transmitted signal are normalized, the signal-to-noise ratio is controlled by adjusting the noise variance σ_z^2. The average energy of one OFDM symbol is calculated as following,

$$E_S = \frac{N_{BW}}{N_{\text{IFFT}}}. \tag{3.30}$$

The resulting SNR is calculated as

$$SNR = \frac{E_S}{E_N} = \frac{N_{BW}}{N_{\text{IFFT}}} \frac{1}{\sigma_z^2}. \tag{3.31}$$

3.7.2 Impulse Response Length

The impulse response generated by the SCME model is based on 6 paths at different delays, which depend on the chosen channel scenario. The resolution of the delays is of $\frac{1}{16 \cdot 3.84 \text{ MHz}} = 0.0163\ \mu$s. For a given sampling rate T_c the impulse response is assumed lowpass filtered with cutoff at $f_{\text{cut}} = \frac{1}{2 \cdot T_c}$ according to the Nyquist criterion.
The lowpass filtering yields a convolution with a sinc in time domain, hence the generated impulse response is filtered with a sinc, with width T_c.
In Table 2.1 different sampling frequencies are listed for the LTE downlink. For $T_c = \frac{1}{3.84 \text{ MHz}}$, the essential support of taps is chosen as $L = 12$ resulting in a power delay profile depicted in Figure 3.3. The power delay profile is calculated over 2000 different channels generated by the SCME model. The simulations will be carried out in the SNR range 0 to 20 dB and the minimum noise level is also depicted on the figure. Hence components of the channel impulse response that are smaller than the minimum noise variance are not taken into account.

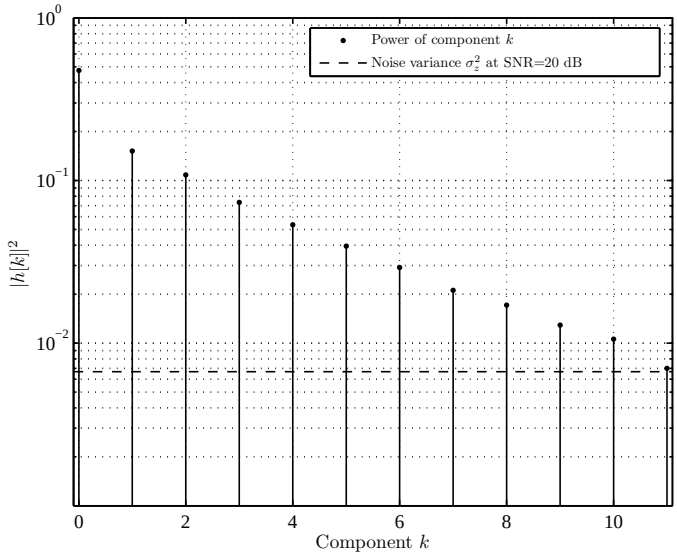

Figure 3.3: *Power Delay Profile of the channel.*

3.8 Summary

In order to do simulations as close to the reality as possible, it is important to have a good channel model. Mobile channel models with time invariant and time variant behavior have been investigated. The chosen channel model is the SCME (Spatial Channel Model Extended), which generates channel coefficients based on the 3GPP channel model specifications. The channel model supports a typical urban area scenario as well as mobility of the UE. Moreover the selection of the impulse response length and adapting the impulse response to a sampling frequency T_c has been described in order perform simulation of channel estimation methods with the LTE downlink structure.

4 Time-Invariant Channel Estimation

This chapter describes different channel estimation techniques to be used for the time-invariant downlink case.
By focusing on time-invariant channels, only the frequency-domain needs to be considered. Hence three different channel estimators are applied in the frequency-domain and compared. Since the estimation is aimed for the UE, the complexity should be minimized.

4.1 OFDM Signal Model

In Appendix A.7 the OFDM signal model is presented. As stated in (A.29), the signal model for OFDM transmission can be expressed as

$$\boldsymbol{y}[m] = \text{diag}(\boldsymbol{g})\boldsymbol{d}[m] + \boldsymbol{z}[m]. \tag{4.1}$$

In order to ease the calculation of the channel estimation, the signal model is simplified in the following section.

4.1.1 Signal Model Simplification

The channel is estimated for each OFDM symbol and the general focus of the channel estimation will be on only one OFDM symbol. For the sake of simplicity the index m is dropped and equation (4.1) is rewritten as

$$\boldsymbol{y} = \boldsymbol{X}\boldsymbol{F}\boldsymbol{h} + \boldsymbol{z}, \tag{4.2}$$

where $\boldsymbol{y} \in \mathbb{C}^{N_{\text{IFFT}}}$ is the received OFDM symbol, $\boldsymbol{X} \in \mathbb{C}^{N_{\text{IFFT}},N_{\text{IFFT}}}$ is a diagonal matrix with data, reference symbols or zeros while $\boldsymbol{h} \in \mathbb{C}^{N_{\text{IFFT}}}$ is the channel impulse response and $\boldsymbol{z} \in \mathbb{C}^{N_{\text{IFFT}}}$ is the noise which is assumed to be white Gaussian. $\boldsymbol{F} \in \mathbb{C}^{N_{\text{IFFT}} \times N_{\text{IFFT}}}$ is the same DFT-matrix as described in (A.13),

$$\boldsymbol{F} = \begin{bmatrix} f_{1,1} & \cdots & f_{1,N_{\text{IFFT}}} \\ \vdots & \ddots & \vdots \\ f_{N_{\text{IFFT}},1} & \cdots & f_{N_{\text{IFFT}},N_{\text{IFFT}}} \end{bmatrix}. \tag{4.3}$$

The channel estimation will be based on transmitted reference symbols, which are scattered as described in Section 2.4.2, i.e. an interpolation has to be performed in order to obtain the channel estimates for the subcarriers with data symbols. Before the first estimation method is introduced, prior knowledge about the channel is used to reduce the complexity of the estimator.
Based on the knowledge of the channel model and of the reference symbols two following assumptions can be made [24]:

- If the channel $\boldsymbol{h}$ has the maximum delay at tap $L-1$, only the first L columns of F can be considered, since the rest is multiplied by zero. $\boldsymbol{h}' \in \mathbb{C}^L$ denotes the first L coefficients of $\boldsymbol{h}$.

- The transmitted reference symbols are scattered (see Figure 2.4), hence only rows corresponding to the position of these symbols need to be considered for the diagonal matrix $\boldsymbol{X}$.

Equation (4.2) is rewritten as

$$\boldsymbol{y}_r = \boldsymbol{X}_\mathrm{r}\boldsymbol{T}_\mathrm{r}\boldsymbol{h}' + \boldsymbol{z}_\mathrm{r}, \tag{4.4}$$

where $\boldsymbol{X}_\mathrm{r} = \mathrm{diag}\,(x_\mathrm{r}(1) \dots x_\mathrm{r}(N_\mathrm{r}))$ and

$$\boldsymbol{T}_\mathrm{r} = \begin{bmatrix} f_{t_\mathrm{r}(1),1} & \cdots & f_{t_\mathrm{r}(1),L} \\ \vdots & \ddots & \vdots \\ f_{t_\mathrm{r}(N_\mathrm{r}),1} & \cdots & f_{t_\mathrm{r}(N_\mathrm{r}),L} \end{bmatrix}. \tag{4.5}$$

N_r denotes the number of reference symbols for one OFDM symbol, while $x_\mathrm{r}(i)$ and $t_\mathrm{r}(i)$ denote the i'th reference symbol in the frequency-domain and the index of the subcarrier carring the symbol respectively. $\boldsymbol{z}_\mathrm{r} \in \mathbb{C}^{N_\mathrm{r}}$ is the truncated noise and is still white Gaussian.
The channel $\boldsymbol{h}'$ is estimated based on the knowledge of transmitted reference symbols $\boldsymbol{x}_\mathrm{r}$.

4.2 Least Squares Estimator

Knowing the the transmitted reference symbols, the first estimate to be calculated is the least squares estimator in the frequency-domain for the channel impulse response:

$$\boldsymbol{g}_\mathrm{LS} = \left[\frac{y_\mathrm{r}(1)}{x_\mathrm{r}(1)}, \frac{y_\mathrm{r}(2)}{x_\mathrm{r}(2)}, \cdots, \frac{y_\mathrm{r}(N_\mathrm{r})}{x_\mathrm{r}(N_\mathrm{r})}\right], \tag{4.6}$$

where $\boldsymbol{g}_\mathrm{LS} \in \mathbb{C}^{N_\mathrm{r}}$ can only be estimated over the subcarriers carrying reference symbols. Hence this result has to be interpolated over the full frequency range in order to give an estimate for subcarriers with data symbols.
The interpolation can be performed in frequency domain or in time domain. For the latter case the interpolation is carried out by only taking the first L channel taps into account and setting all other taps to zero. After estimating the L-tap channel, the channel is transformed back into frequency domain. This approach is investigated by applying linear minimum mean square error (LMMSE) estimator in Section 4.3 and least-squares (LS) estimator in Section 4.4.

4.3 Linear Minimum Mean Squared Error Estimator

The LMMSE estimator, calculates the channel impulse response (CIR) $\tilde{h}$, that minimizes the mean squared error $\mathbb{E}\left\{\tilde{\boldsymbol{h}} - \boldsymbol{h}'\right\}$, given $\boldsymbol{y}_\mathrm{r}$ and $\boldsymbol{X}_\mathrm{r}$ [24].

$$\tilde{h} = \boldsymbol{R}_{hy_\mathrm{r}} \boldsymbol{R}_{y_\mathrm{r}y_\mathrm{r}}^{-1} \boldsymbol{y}_\mathrm{r} \tag{4.7}$$

The autocorrelation matrices are calculated as follows:

$$\begin{aligned}
\boldsymbol{R}_{y_\mathrm{r}y_\mathrm{r}} &= E\left[\boldsymbol{y}_\mathrm{r}{\boldsymbol{y}_\mathrm{r}}^H\right] \\
&= \boldsymbol{X}_\mathrm{r}\boldsymbol{T}_\mathrm{r} E\left[\boldsymbol{h}\boldsymbol{h}^\mathrm{H}\right] \boldsymbol{X}_\mathrm{r}^\mathrm{H}\boldsymbol{T}_\mathrm{r}^\mathrm{H} + E\left[\boldsymbol{z}_\mathrm{r}\boldsymbol{z}_\mathrm{r}^\mathrm{H}\right] + \boldsymbol{X}_\mathrm{r}\boldsymbol{T}_\mathrm{r}\left[\boldsymbol{h}\boldsymbol{z}_\mathrm{r}^\mathrm{H}\right] + \left[\boldsymbol{n}_\mathrm{r}\boldsymbol{h}^\mathrm{H}\right]\boldsymbol{T}_\mathrm{r}^\mathrm{H}\boldsymbol{X}_\mathrm{r}^\mathrm{H} \\
&= \boldsymbol{X}_\mathrm{r}\boldsymbol{T}_\mathrm{r}\boldsymbol{R}_{h'h'}\boldsymbol{T}_\mathrm{r}^\mathrm{H}\boldsymbol{X}_\mathrm{r}^\mathrm{H} + {\sigma_z}^2\boldsymbol{I}_{N_\mathrm{r}} \qquad (4.8) \\
&= \frac{1}{L}\boldsymbol{X}_\mathrm{r}\boldsymbol{T}_\mathrm{r}\boldsymbol{T}_\mathrm{r}^\mathrm{H}\boldsymbol{X}_\mathrm{r}^\mathrm{H} + {\sigma_z}^2\boldsymbol{I}_{N_\mathrm{r}} \qquad (4.9)
\end{aligned}$$

In order to simplify calculations it is assumed that the channel coefficients are independent and the energy for each tap is $1/L$, i.e. the power delay profile is uniform $\boldsymbol{R}_{h'h'} = E\left[\boldsymbol{h}'\boldsymbol{h}'^\mathrm{H}\right] = \frac{1}{L}\boldsymbol{I}$.

$$\begin{aligned}
\boldsymbol{R}_{h'y_\mathrm{r}} &= E\left[\boldsymbol{h}'{\boldsymbol{y}_\mathrm{r}}^H\right] = E\left[\boldsymbol{h}'\boldsymbol{h}'^\mathrm{H}\boldsymbol{T}_\mathrm{r}^\mathrm{H}\boldsymbol{X}_\mathrm{r}^\mathrm{H} + \boldsymbol{z}_\mathrm{r}\boldsymbol{h}^\mathrm{H}\boldsymbol{T}_\mathrm{r}^\mathrm{H}\boldsymbol{X}_\mathrm{r}^\mathrm{H}\right] \\
&= \boldsymbol{R}_{h'h'}\boldsymbol{T}_\mathrm{r}^\mathrm{H}\boldsymbol{X}_\mathrm{r}^\mathrm{H} \qquad (4.10) \\
&= \frac{1}{L}\boldsymbol{T}_\mathrm{r}^\mathrm{H}\boldsymbol{X}_\mathrm{r}^\mathrm{H}. \qquad (4.11)
\end{aligned}$$

Similar to (4.4), the transmission of data symbols can be described as

$$\boldsymbol{y}_d = \boldsymbol{X}_d\boldsymbol{T}_d\boldsymbol{h}' + \boldsymbol{z}_\mathrm{d}, \tag{4.12}$$

where $\boldsymbol{X}_\mathrm{d} = \mathrm{diag}\left(x_\mathrm{d}(1)\ldots x_\mathrm{d}(N_\mathrm{d})\right)$ and

$$\boldsymbol{T}_d = \begin{bmatrix} f_{t_\mathrm{d}(1),1} & \cdots & f_{t_\mathrm{d}(1),L} \\ \vdots & \ddots & \vdots \\ f_{t_\mathrm{d}(N_\mathrm{d}),1} & \cdots & f_{t_\mathrm{d}(N_\mathrm{d}),L} \end{bmatrix}. \tag{4.13}$$

N_d denotes the number of data symbols for one OFDM symbol, while $x_\mathrm{d}(i)$ and $t_\mathrm{d}(i)$ denote the i'th data symbol and the index of the subband carring the symbol respectively. $\boldsymbol{z}_\mathrm{d} \in \mathbb{C}^{N_\mathrm{d}}$ is the truncated Gaussian noise.

The calculated value for $\boldsymbol{h}'$ is transformed into frequency domain for the subcarriers containing data symbols,

$$\tilde{g} = \boldsymbol{T}_\mathrm{d}\tilde{h} \approx \boldsymbol{T}_\mathrm{d}\boldsymbol{h}'. \tag{4.14}$$

The frequency response of the channel is now interpolated using LMMSE estimation with low complexity and the estimate is passed to the equalizer. It should be noted that for the case with the true autocorrelation $\boldsymbol{R}_{h'h'}$ and not uniform as assumed this method is equal to the Wiener interpolation [14].

4.4 Downsampling

Section 4.2 gives an estimate for the LS frequency response of the channel. Now a LS estimate in the time domain is calculated. By modifying (4.2) it is transformed into the time domain. To understand the idea behind this method, let us consider the received signal $\boldsymbol{r}$ in time for one OFDM symbol.

$$\boldsymbol{r} = \boldsymbol{F}^{\mathrm{H}} \boldsymbol{X} \boldsymbol{F}_L \boldsymbol{h}' + \boldsymbol{z}_t, \tag{4.15}$$

where $\boldsymbol{h}' \in \mathbb{C}^L$ is the L-tap channel impulse response and $\boldsymbol{F}_L \in \mathbb{C}^{N_{\text{IFFT}} \times L}$ is the Fourier matrix that gives the frequency domain representation over N_{IFFT} subcarriers of the channel, while $\boldsymbol{X}$ is the transmitted symbols.
$\boldsymbol{F}^{\mathrm{H}} \in \mathbb{C}^{N_{\text{IFFT}} \times N_{\text{IFFT}}}$ transforms the attenuated signal in frequency domain into time domain, where $\boldsymbol{r}$ is the time domain representation of $\boldsymbol{y}$ from (4.2) and $\boldsymbol{z}_t$ is the complex Gaussian noise.

4.4.1 Least-Squares Estimation in Time

From (4.15) the received signal $\boldsymbol{r}$ is equivalent to

$$\boldsymbol{r} = \boldsymbol{S}\boldsymbol{h}' + \boldsymbol{z}_t, \tag{4.16}$$

where

$$\boldsymbol{S} = \boldsymbol{F}^{\mathrm{H}} \boldsymbol{X} \boldsymbol{F}_L, \tag{4.17}$$

and the diagonal matrix $\boldsymbol{X}$ containing the complex symbols modulated over the subcarriers can be expressed as:

$$\boldsymbol{X} = \boldsymbol{A}_{\mathrm{d}} + \boldsymbol{A}_{\mathrm{r}}, \tag{4.18}$$

where $\boldsymbol{A}_{\mathrm{d}} \in \mathbb{C}^{N_{\text{IFFT}} \times N_{\text{IFFT}}}$ and $\boldsymbol{A}_{\mathrm{r}} \in \mathbb{C}^{N_{\text{IFFT}} \times N_{\text{IFFT}}}$ are diagonal matrices containing non-zero elements in the positions of the transmitted data and of the transmitted reference symbols respectively. Since the transmitted symbols are unknown, an approximation of the matrix $\boldsymbol{S}$ is made such that only transmitted reference symbols are taken into account:

$$\widehat{\boldsymbol{S}} = \boldsymbol{F}^{\mathrm{H}} \boldsymbol{A}_{\mathrm{r}} \boldsymbol{F}_L. \tag{4.19}$$

The channel impulse response in least-squares sense is found as [6]

$$\boldsymbol{h}_{\mathrm{LS}} = \left(\widehat{\boldsymbol{S}}^{\mathrm{H}} \widehat{\boldsymbol{S}}\right)^{-1} \widehat{\boldsymbol{S}}^{\mathrm{H}} \boldsymbol{r}. \tag{4.20}$$

Inserting (4.19) into (4.20) yields,

$$\boldsymbol{h}_{\mathrm{LS}} = \left(\boldsymbol{F}_L^{\mathrm{H}} \boldsymbol{A}_{\mathrm{r}}^{\mathrm{H}} \boldsymbol{A}_{\mathrm{r}} \boldsymbol{F}_L\right)^{-1} \boldsymbol{F}_L^{\mathrm{H}} \boldsymbol{A}_{\mathrm{r}}^{\mathrm{H}} \boldsymbol{F} \boldsymbol{r} = \left(\boldsymbol{F}_L^{\mathrm{H}} \boldsymbol{A}_{\mathrm{r}}^{\mathrm{H}} \boldsymbol{A}_{\mathrm{r}} \boldsymbol{F}_L\right)^{-1} \boldsymbol{F}_L^{\mathrm{H}} \boldsymbol{A}_{\mathrm{r}}^{\mathrm{H}} \boldsymbol{y} \tag{4.21}$$

From a computational point of view the LS estimator is simple since the matrix

$$\left(\boldsymbol{F}_L^{\mathrm{H}} \boldsymbol{A}_{\mathrm{r}}^{\mathrm{H}} \boldsymbol{A}_{\mathrm{r}} \boldsymbol{F}_L\right)^{-1} \boldsymbol{F}_L^{\mathrm{H}} \boldsymbol{A}_{\mathrm{r}}^{\mathrm{H}}$$

is constant. In the LTE application, the matrix inversion can be computed once and used regardless of the varying channel statistics. This of course is based on the assumption that the positions of the reference symbols do not change. However, an ill-conditioned problem caused by the matrix inversion occurs in the implementation of the LS estimator. The problem can be solved by regularizing the eigenvalues of the matrix to be inverted by adding a small constant term to the diagonal [6] or by downsampling.

4.4.2 Downsampled impulse response LS channel estimation

The ill-conditioning problem stems from the structure of the subcarriers in the LTE downlink. Only the center of the frequency spectrum is utilized, while the rest is set to zero.
As an example the case of $N_{\text{IFFT}} = 2048$ from Table 2.1 is considered. The number of occupied subcarriers is only 1200. Hence, while the sampling frequency is 30.72 MHz ($N_{\text{IFFT}} \cdot f_{\text{space}}$), the occupied bandwidth is only 18 MHz ($N_{\text{BW}} \cdot f_{\text{space}}$). In LTE the occupied bandwidth is approximately $2/3$ of the whole bandwidth. The goal is to get the occupied bandwidth close to the sampling frequency which can be accomplished by downsampling to $2/3$ of the sampling frequency. In practice, the channel $\boldsymbol{h}'$ is not estimated in all the L taps but only in 2 out of 3 taps hereby obtaining the average downsampling factor $2/3$, as described in (4.23).

$$\boldsymbol{g}_{\text{DS}} = \boldsymbol{F}_L \boldsymbol{h}' = \begin{bmatrix} f_{1,1} & f_{1,2} & f_{1,3} & \cdots & f_{1,L} \\ f_{2,1} & f_{1,2} & f_{2,3} & \cdots & f_{2,L} \\ f_{3,1} & f_{3,2} & f_{3,3} & \cdots & f_{3,L} \\ f_{4,1} & f_{4,2} & f_{4,3} & \cdots & f_{4,L} \\ \vdots & \vdots & \vdots & \vdots & \vdots \\ f_{N,1} & f_{N,2} & f_{N,3} & \cdots & f_{N,L} \end{bmatrix} \begin{bmatrix} h'_0 \\ h'_1 \\ 0 \\ h'_3 \\ h'_4 \\ 0 \\ \vdots \\ h'_L \end{bmatrix} \tag{4.22}$$

$$= \boldsymbol{F}^{\text{DS}} \boldsymbol{h}^{\text{DS}} = \begin{bmatrix} f_{1,1} & f_{1,2} & f_{1,4} & \cdots & f_{1,L} \\ f_{2,1} & f_{1,2} & f_{2,4} & \cdots & f_{2,L} \\ f_{3,1} & f_{3,2} & f_{3,4} & \cdots & f_{3,L} \\ f_{4,1} & f_{4,2} & f_{4,4} & \cdots & f_{4,L} \\ \vdots & \vdots & \vdots & \vdots & \vdots \\ f_{N,1} & f_{N,2} & f_{N,4} & \cdots & f_{N,L} \end{bmatrix} \begin{bmatrix} h'_0 \\ h'_1 \\ h'_3 \\ h'_4 \\ \vdots \\ h'_{L-1} \end{bmatrix} \tag{4.23}$$

By removing each third column in $\boldsymbol{F}_L$ resulting in $\boldsymbol{F}^{\text{DS}} \in \mathbb{C}^{N_{\text{IFFT}} \times L_{\text{DS}}}$ the calculations are simplified and the complexity is reduced.
Equation (4.15) is now written as

$$\boldsymbol{r} = \boldsymbol{F}^{\text{H}} \boldsymbol{A}_{\text{r}} \boldsymbol{F}^{\text{DS}} \boldsymbol{h}^{\text{DS}} + \boldsymbol{z}_t, \tag{4.24}$$

and the least square channel impulse response can be calculated as

$$\boldsymbol{h}^{\mathrm{DS}} = \left(\boldsymbol{F}^{\mathrm{DS,H}}\boldsymbol{A}_{\mathrm{r}}{}^{\mathrm{H}}\boldsymbol{A}_{\mathrm{r}}\boldsymbol{F}^{\mathrm{DS}}\right)^{-1}\boldsymbol{F}^{\mathrm{DS,H}}\boldsymbol{A}_{\mathrm{r}}{}^{\mathrm{H}}\boldsymbol{y}. \tag{4.25}$$

The channel impulse response $\boldsymbol{h}^{\mathrm{DS}}$ is transformed into frequency domain by multiplying with F^{DS}, such that

$$\boldsymbol{g}^{DS} = F_{\mathrm{d}}^{\mathrm{DS}}\boldsymbol{h}^{\mathrm{DS}} = F_{d}^{\mathrm{DS}}\left(\boldsymbol{F}^{\mathrm{DS,H}}\boldsymbol{A}_{\mathrm{r}}{}^{\mathrm{H}}\boldsymbol{A}_{\mathrm{r}}\boldsymbol{F}^{\mathrm{DS}}\right)^{-1}\boldsymbol{F}^{\mathrm{DS,H}}\boldsymbol{A}_{\mathrm{r}}{}^{\mathrm{H}}\boldsymbol{y}, \tag{4.26}$$

where $\boldsymbol{F}_{\mathrm{d}}^{\mathrm{DS}}$ is the truncated version of $\boldsymbol{F}^{\mathrm{DS}}$, only containing rows coresponding to positions of the data symbols. Utilizing knowledge of the transmitted reference symbols the complexity of equations (4.25) and (4.26) can be reduced even further.

4.4.3 Further explanation on downsampling

In [6] the downsampling to $2/3$ of the sampling frequency is performed by estimating $\boldsymbol{h}'$ only in 2 out of 3 taps.

In order to explain the purpose of this step, the downsampling procedure is investigated. Figure 4.1 shows an equivalent representation the downsampling of the non-integer factor $2/3$ is performed [17]. $\boldsymbol{h}'$ is upsampled by a factor of two as follows,

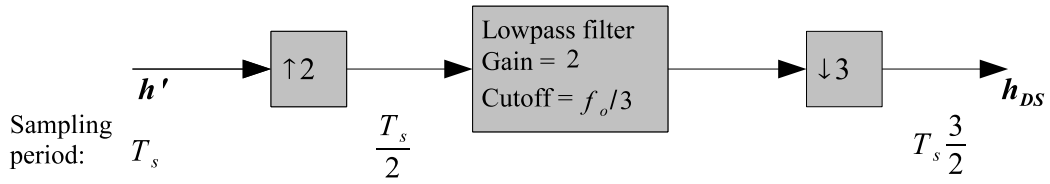

Figure 4.1: *System for changing the sampling rate by a non-integer factor [17].*

$$\boldsymbol{h}_{\mathrm{o}} = [h[0], 0, h[1], 0, h[2], 0, h[3], 0, \ldots, h[L-1], 0]\,. \tag{4.27}$$

The frequency response of the upsampled impulse response is illustrated on Figure 4.2(b). The frequency response of the channel is only illustrated as rectangular as an example. The one-sided bandwidth of the channel is assumed to be at most $2/3$ of half the sampling frequency,

$$f_{\mathrm{BW}} = \frac{2}{3}f'_{\mathrm{s}}, \tag{4.28}$$

where $f'_{\mathrm{s}} = \frac{f_{\mathrm{s}}}{2}$.

After 2x upsampling to sampling frequency $f_{\mathrm{o}} = 2f_{\mathrm{s}}$ the maximum one sided bandwidth of the channel is now at most $1/3$ of half the new sampling frequency,

$$f'_{\mathrm{BW}} = \frac{1}{3}f'_{\mathrm{o}}. \tag{4.29}$$

where $f'_{\mathrm{o}} = \frac{f_{\mathrm{o}}}{2}$.
In order to avoid aliasing when downsampling with factor three, a lowpass filter is introduced as in Figure 4.2(c). The method proposed in [6] is equivalent to the following lowpass filter:

$$\boldsymbol{h}_{\mathrm{lp}} = [1, 1]\,, \tag{4.30}$$

resulting in a filtered impulse response,

$$\boldsymbol{h}_{\mathrm{o}} = [h[0], h[0], h[1], h[1], h[2], h[2], h[3], h[3], \ldots, h[L-1], h[L-1]]\,. \tag{4.31}$$

Ideally the lowpass filter should have cutoff at $1/3f'_{\mathrm{o}}$ [17] but using $\boldsymbol{h}_{\mathrm{lp}}$ results in a sinc-function in frequency domain with an one-sided bandwidth of f'_{o} which is depicted in Figure 4.2(c). The

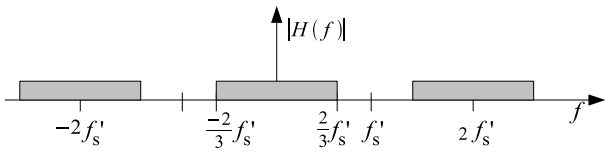

(a) Frequency response of the sampled $\boldsymbol{h}$.

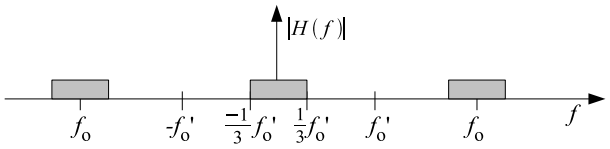

(b) Frequency response of the over sampled $\boldsymbol{h}_{\mathrm{o}}$.

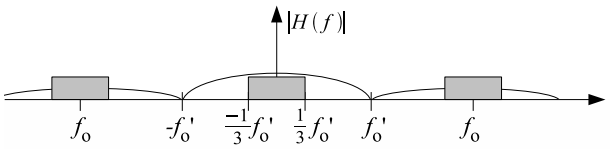

(c) Frequency response of the lowpass filter $\boldsymbol{h}_{\mathrm{lp}}$ and $\boldsymbol{h}_{\mathrm{o}}$.

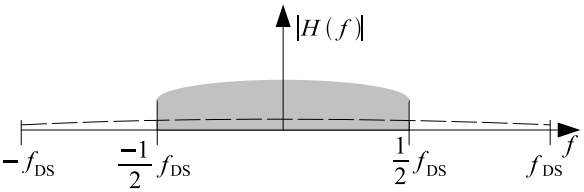

(d) Frequency response of the downsampled impulse response $\boldsymbol{h}_{\mathrm{DS}}$ with aliasing which is the dottet line.

downsampling of factor three is achieved by taking each third sample of $\boldsymbol{h}_{\mathrm{o}}$,

$$\begin{aligned}\boldsymbol{h}_{\mathrm{DS}} &= \Big[\underset{\uparrow}{h[0]}, h[0], h[1], \underset{\uparrow}{h[1]}, h[2], h[2], \underset{\uparrow}{h[3]}, h[3], \ldots, \underset{\uparrow}{h[L-1]}, h[L-1]\Big] \\ &= [h[0], h[1], h[3], h[4], \ldots, h[L-1]]\end{aligned} \tag{4.32}$$

where it is assumed that $h[L-1]$ is also an element to be selected in the downsampling. Equation (4.32) is exactly the result described in Section 4.4.2 equation (4.23). The downsampled sampled

frequency can be written as $f_{\text{DS}} = 1/3f_{\text{o}} = 2/3f_{\text{o}}$. The frequency response of the downsampled impulse response is depicted on Figure 4.2(d), where the presence of aliasing is illustrated with the dotted line.

4.4.4 Complexity Reduction

From the structure of the reference signals described in Section 2.4.2 it is known that the norm is 1. Hence the term $\boldsymbol{A}_{\text{r}}{}^{\text{H}}\boldsymbol{A}_{\text{r}}$ in (4.25) consists of ones at reference positions and zeros otherwise. The matrix inversion is rewritten according to this observation,

$$\left(\boldsymbol{F}^{\text{DS,H}}\boldsymbol{A}_{\text{r}}{}^{\text{H}}\boldsymbol{A}_{\text{r}}\boldsymbol{F}^{\text{DS}}\right)^{-1}\boldsymbol{F}^{\text{DS,H}} = \left(\boldsymbol{F}_r{}^{\text{DS,H}}\boldsymbol{F}_r^{\text{DS}}\right)^{-1}\boldsymbol{F}_r{}^{\text{DS,H}}, \tag{4.33}$$

where $\boldsymbol{F}_r^{\text{DS}}$ is the truncated version of $\boldsymbol{F}_L^{\text{DS}}$ only containing rows corresponding to reference symbol positions. Equation (4.26) with reduced complexity is now expressed as

$$\boldsymbol{g}_d^{DS} \;=\; F_d^{\text{DS}}\boldsymbol{h}^{\text{DS}} = F_d^{\text{DS}}\left(\boldsymbol{F}_r{}^{\text{DS,H}}\boldsymbol{F}_r^{\text{DS}}\right)^{-1}\boldsymbol{F}_r{}^{\text{DS,H}}\boldsymbol{X}_{\text{r}}{}^{\text{H}}\boldsymbol{y}_{\text{r}}, \tag{4.34}$$

with $\boldsymbol{X}_{\text{r}}^{\text{H}}$ and $\boldsymbol{y}_{\text{r}}$ only containing values corresponding to reference positions as described in Section 4.1.1.

4.5 Reduced Rank LMMSE

Least Squares and LMMSE channel estimation in time-domain have been presented so far. Now LMMSE estimation in frequency-domain using rank reduction is investigated.
Rank reduction is achieved by using the singular value decomposition (SVD) in the calculation of the LMMSE of the channel frequency response. The LMMSE estimator in frequency domain is found by [8]:

$$\boldsymbol{g}_{\text{LMMSE}} = \boldsymbol{R}_{g g_{\text{LS}}}\boldsymbol{R}_{g_{\text{LS}}g_{\text{LS}}}^{-1}\boldsymbol{g}_{\text{LS}}, \tag{4.35}$$

where $\boldsymbol{g}_{\text{LS}} \in \mathbb{C}^{N_{\text{r}}}$ is the least square channel frequency response, estimated using transmitted reference symbols as in (4.6). To be able to calculate the autocorrelation $\boldsymbol{R}_{g g_{LS}}$ between the full range, $\boldsymbol{g} \in \mathbb{C}^{N_{\text{IFFT}}}$, and least squares frequency response, the vector $\boldsymbol{g}_{LS}$ is set as a function of $\boldsymbol{g}$ by the following steps:

$$\boldsymbol{y}_{\text{r}} = \boldsymbol{X}_{\text{r}}\boldsymbol{T}_{\text{r}}\frac{1}{\sqrt{N_{\text{IFFT}}}}\boldsymbol{F}_L{}^{\text{H}}\boldsymbol{g} + \boldsymbol{z}_{\text{r}} \tag{4.36}$$

$\boldsymbol{g}$ is transformed into time domain by a DFT-matrix $\boldsymbol{F}_L \in \mathbb{C}^{\text{IFFT},L}$, where L is the number of channel taps and N is the DFT-size. The frequencies corresponding to the subcarriers of the reference symbols are then extracted by $\boldsymbol{T}_{\text{r}}$ and multiplied with the transmitted reference symbols. $\boldsymbol{g}_{\text{LS}}$ can now be expressed as

$$\boldsymbol{g}_{\text{LS}} \;=\; \boldsymbol{T}_{\text{r}}\frac{1}{\sqrt{N_{\text{IFFT}}}}\boldsymbol{F}_L{}^{\text{H}}\boldsymbol{g} + \boldsymbol{X}_{\text{r}}{}^{-1}\boldsymbol{z}_{\text{r}}. \tag{4.37}$$

Finally $\boldsymbol{R}_{gg_{\text{LS}}}$ is estimated using

$$\begin{aligned}\boldsymbol{R}_{gg_{\text{LS}}} &= E\left[\boldsymbol{g}{\boldsymbol{g}_{\text{LS}}}^{\text{H}}\right] &(4.38)\\ &= E\left[\boldsymbol{g}\left(\boldsymbol{g}^{\text{H}}\frac{1}{\sqrt{N_{\text{IFFT}}}}\boldsymbol{F}_L{\boldsymbol{T}_{\text{r}}}^{\text{H}}+{\boldsymbol{z}_{\text{r}}}^{\text{H}}\boldsymbol{X}^{-1,H}\right)\right]\\ &= \frac{1}{\sqrt{N_{\text{IFFT}}}}\boldsymbol{F}_L{\boldsymbol{T}_{\text{r}}}^{\text{H}} &(4.39)\end{aligned}$$

As in (4.9) each tap in the channel impulse response is assumed to have energy $\frac{1}{L}$, hence

$$E\left[\boldsymbol{g}\boldsymbol{g}^{\text{H}}\right]=\boldsymbol{F}_L\boldsymbol{R}_{h'h'}\boldsymbol{F}_L^{\text{H}}=\frac{1}{L}\boldsymbol{F}_L\boldsymbol{F}_L^{\text{H}}. \tag{4.40}$$

The same approach is used to calculate $\boldsymbol{R}_{g_{\text{LS}}g_{\text{LS}}}$.

$$\begin{aligned}\boldsymbol{R}_{g_{\text{LS}}g_{\text{LS}}} &= E\left[\boldsymbol{g}_{\text{LS}}{\boldsymbol{g}_{\text{LS}}}^{\text{H}}\right] &(4.41)\\ &= E\left[\boldsymbol{T}_{\text{r}}\frac{1}{\sqrt{N_{\text{IFFT}}}}{\boldsymbol{F}_L}^{\text{H}}\boldsymbol{g}\boldsymbol{g}^{\text{H}}\frac{1}{\sqrt{N_{\text{IFFT}}}}\boldsymbol{F}_L{\boldsymbol{T}_{\text{r}}}^{\text{H}}+{\boldsymbol{X}_{\text{r}}}^{-1}\boldsymbol{z}_{\text{r}}{\boldsymbol{z}_{\text{r}}}^{\text{H}}{\boldsymbol{X}_{\text{r}}}^{-1,H}\right]\\ &= \frac{1}{N_{\text{IFFT}}}\boldsymbol{T}_{\text{r}}{\boldsymbol{F}_L}^{\text{H}}\boldsymbol{F}_L{\boldsymbol{T}_{\text{r}}}^{\text{H}}+E\left[{\sigma_z}^2\left(\boldsymbol{X}_{\text{r}}{\boldsymbol{X}_{\text{r}}}^{\text{H}}\right)^{-1}\right]\\ &= \frac{L}{N_{\text{IFFT}}}\boldsymbol{T}_{\text{r}}{\boldsymbol{T}_{\text{r}}}^{\text{H}}+{\sigma_z}^2\boldsymbol{I}, &(4.42)\end{aligned}$$

where $\boldsymbol{F}_L^{\text{H}}\boldsymbol{F}_L=L\boldsymbol{I}_L$.
The average energy of the transmitted symbols are normalized to one, hence $E\left[\boldsymbol{X}_{\text{r}}{\boldsymbol{X}_{\text{r}}}^{\text{H}}\right]=\boldsymbol{I}_L$. In order to reduce the rank of the LMMSE estimate, (4.35) is factorized into [8],

$$\boldsymbol{g}_{\text{LMMSE}}=\boldsymbol{R}_{gg_{\text{LS}}}\boldsymbol{R}_{g_{\text{LS}}g_{LS}}^{-0.5}\boldsymbol{R}_{g_{\text{LS}}g_{LS}}^{-0.5}\boldsymbol{g}_{\text{LS}}. \tag{4.43}$$

The SVD is performed on the first two factors

$$\boldsymbol{R}_{gg_{LS}}\boldsymbol{R}_{g_{LS}g_{LS}}^{-0.5}=\boldsymbol{Q}_1\boldsymbol{D}{\boldsymbol{Q}_2}^{\text{H}}. \tag{4.44}$$

The best rank-p estimator is then

$$\begin{aligned}\boldsymbol{g}_p &= \boldsymbol{Q}_1\begin{bmatrix}\boldsymbol{D}_p & \boldsymbol{0}\\ \boldsymbol{0} & \boldsymbol{0}\end{bmatrix}{\boldsymbol{Q}_2}^{\text{H}}\boldsymbol{R}_{g_{\text{LS}}g_{LS}}^{-0.5}\boldsymbol{g}_{\text{LS}}\\ &= \boldsymbol{Q}_1\boldsymbol{D}'{\boldsymbol{Q}_2}^{\text{H}}\boldsymbol{R}_{g_{\text{LS}}g_{LS}}^{-0.5}\boldsymbol{g}_{\text{LS}} &(4.45)\end{aligned}$$

where $\boldsymbol{D}_p$ is the upper $p\times p$ left corner of $\boldsymbol{D}$, i.e. only the singular vectors associated to the p largest singular values are kept and the rest is set to zero. Hereby noise can be reduced by neglecting subspaces with low energy. The rank p is set as the estimated number of channel taps ($p=L$) [8]. It is also possible to further simplify (4.45) according to [18] in order to reduce the complexity. Equation (4.45) however is implemented in Matlab in order to compare this method with others.

4.6 Linear Interpolation

A simple way of performing interpolation is the to use linear interpolation. This is possible since the spacing between the reference symbols corresponds to the coherence bandwidth of the channel as described in Section 3.2.1.

4.7 Complexity of the Considered Estimators

The complexity of the frequency response estimation depends on the chosen method. The complexity is given in the form $O(N)$ in order to give an overview of the calculations. Table 4.7 lists the calculations and their complexity based on [10]. It should be noted that the listed complexity is for one OFDM symbol with N_{r} as the total number of estimates. From Table 4.7 it is clear that the reduced rank LMMSE estimator is the most complex because of the SVD calculation and matrix inversion. The LMMSE CIR requires one matrix inversion, while the calculation of downsampled CIR is only a matrix multiplication. The simplest method is the linear interpolation, which requires a constant number of floating point operations as a function of $(N_{\mathrm{r}} - 1)$. For a fixed signal to noise ratio however we can precompute most of the calculation and hereby reduce the calculation complexity. In this case the LMMSE CIR estimator requires step 3 and 4, while the reduced rank LMMSE estimator requires step 5. This yields a low-complexity approach from a calculation point of view to estimate the channel frequency response.

4.8 Summary

Estimation methods for calculation of the frequency response have been presented for the LTE downlink in the time-invariant channel. The performed estimation is based on transmitted reference symbols. The presented algorithms are LMMSE CIR estimator, downsampled CIR estimator, reduced rank LMMSE estimator and linear interpolation. The LMMSE CIR and downsampled CIR present a way to estimate the channel impulse response based on assumptions of the number of taps L. The downsampled CIR furthermore makes use of the fact that the LTE downlink only occupies $2/3$ of the transmitted bandwidth. The complexity of the algorithms have been reviewed and it is shown that the reduced rank LMMSE has the highest complexity, followed by LMMSE CIR and downsampled CIR. It is also shown that with a fixed SNR we can reduce the calculation complexity for the LMMSE CIR estimator and the reduced rank LMMSE estimator. The mobile channel is not time-invariant hence a method has to be found in order to also perform estimation in a time-varying channel. The next chapter introduces a method to cope with such channels.

Estimator	steps	Calculation	Complexity	Memory
LMMSE CIR	1	$\boldsymbol{R}_{y_\mathrm{r} y_\mathrm{r}}^{-1}$:	$O(N_\mathrm{r}^3)$	$\Gamma = \boldsymbol{X}_\mathrm{r}\boldsymbol{T}_\mathrm{r}\boldsymbol{R}_{h'h'}\boldsymbol{T}_\mathrm{r}^\mathrm{H}\boldsymbol{X}_\mathrm{r}^\mathrm{H} \in \mathbb{C}^{N_\mathrm{r}\times N_\mathrm{r}}$
	2	$\Phi = \boldsymbol{R}_{h' y_\mathrm{r}}\boldsymbol{R}_{y_\mathrm{r} y_\mathrm{r}}^{-1}$:	$O(N_\mathrm{BW}\cdot N_\mathrm{r}^2)$	$\boldsymbol{R}_{h' y_\mathrm{r}} \in \mathbb{C}^{L\times N_\mathrm{r}}$
	3	$\tilde{\boldsymbol{h}} = \Phi \boldsymbol{y}_\mathrm{r}$:	$O(LN_\mathrm{r})$	
	4	$\boldsymbol{g}_\mathrm{est} = \mathrm{fft}(\boldsymbol{h})$:	$O(N_\mathrm{IFFT}\log(N_\mathrm{IFFT}))$	
Reduced Rank LMMSE	1	$\boldsymbol{R}_{g_\mathrm{LS} g_\mathrm{LS}}^{-1} = \boldsymbol{R}_{g_\mathrm{LS} g_\mathrm{LS}}^{-0.5}\boldsymbol{R}_{g_\mathrm{LS} g_\mathrm{LS}}^{-0.5}$:	$O(N_\mathrm{r}^3)$	$\boldsymbol{T}_\mathrm{r}\boldsymbol{T}_\mathrm{r}^\mathrm{H} \in \mathbb{C}^{N_\mathrm{r}\times N_\mathrm{r}}$
	2	$\Psi = \boldsymbol{R}_{g g_{LS}}\boldsymbol{R}_{g_\mathrm{LS} g_\mathrm{LS}}^{-0.5}$:	$O(N_\mathrm{BW}\cdot N_\mathrm{r})$	$\boldsymbol{R}_{g g_{LS}} \in \mathbb{C}^{N_\mathrm{BW}\times N_\mathrm{r}}$
	3	svd(Ψ):	$O(N_\mathrm{BW}\cdot N_\mathrm{r}^2)$	
	4	$\Gamma = \boldsymbol{Q}_1\boldsymbol{D}'\boldsymbol{Q}_2{}^\mathrm{H}$:	$O(N_\mathrm{BW}\cdot L\cdot N_\mathrm{r})$	
	5	$\Phi = \Gamma\boldsymbol{R}_{g_\mathrm{LS} g_{LS}}^{-0.5}$:	$O(N_\mathrm{BW}N_\mathrm{r}^2)$	
	6	$\boldsymbol{g}_\mathrm{est} = \Phi\boldsymbol{g}_{LS}$:	$O(N_\mathrm{BW}N_\mathrm{r})$	
Downsampled CIR	1	$\boldsymbol{h}^\mathrm{DS} = \Gamma\cdot\boldsymbol{y}_\mathrm{r}$:	$O(L_\mathrm{DS}N_\mathrm{r})$	$\Gamma = \left(\boldsymbol{F}_r^{\mathrm{DS,H}}\boldsymbol{F}_r^\mathrm{DS}\right)^{-1}\boldsymbol{F}_r^{\mathrm{DS,H}}\boldsymbol{X}_\mathrm{r}{}^\mathrm{H} \in \mathbb{C}^{L\times N_\mathrm{r}}$
	2	$\boldsymbol{g}_\mathrm{est}$=$F_\mathrm{T}^\mathrm{DS}\boldsymbol{h}^\mathrm{DS}$:	$O(N_\mathrm{BW}L_\mathrm{DS})$	$\boldsymbol{F}_\mathrm{T}^\mathrm{DS} \in \mathbb{C}^{N_\mathrm{BW}\times L_\mathrm{DS}}$
Linear Interpolation		-	$O(N_\mathrm{r}-1)$	-

Table 4.1: *Complexity of frequency response calculation for the different methods described in this chapter. The required memory for complex elements is calculated as the product of the matrix dimensions. For the LMMSE CIR estimator and reduced rank LMMSE estimator we only have to perform the calculation after the horizontal line for a fixed signal to noise ratio, since all the other computations can be precomputed.*

Time-Varying Channel Estimation

5

The mobility of the UE and the surrounding objects leads to a time-varying channel which needs to be tracked. As described in Section 3.3.1 this results in a Doppler shift. In order to estimate the time-varying channel, the discrete prolate spheroidal (DPS) basis expansion is utilized. Firstly, the general idea behind time-varying channel estimation is introduced before describing the utilization of the DPS basis expansion in detail.

5.1 Initial Steps in the Time-Varying Channel Estimation

The goal of channel estimation is to estimate the time-varying channel frequency response for each OFDM symbol. In Section 3.3.2 it is concluded that the channel is constant within the duration of one OFDM symbol. In Chapter 4 it was investigated how to estimate the channel using scattered reference symbols in the frequency domain. Since the reference symbols are also scattered in the time-domain, it is necessary to estimate the channel in two dimensions, in the time-domain as well as in the frequency-domain. The principle of the estimation procedure is shown in Figure 5.1. The channel can also be represented by its impulse response instead of its frequency response and the time-varying behavior of the impulse response can be tracked. The methods to be used for these two different ways of tracking the channel are presented in the next sections.

5.1.1 Estimation of Subcarrier Coefficients

In order to track the channel frequency response, the subcarriers with reference symbols are used to find estimates of the channel for the subcarriers at OFDM symbols without reference symbols. This can be illustrated by Figure 5.1. Firstly, the channel is estimated in the time direction of all subcarriers with reference symbols using DPS sequences. This method allows a channel estimate to be found for each third subcarrier at each OFDM symbol. Secondly, the frequency response for each OFDM symbol is found by interpolating in the frequency-domain between the known estimates. Let us denote the number of reference symbols for subcarriers and OFDM symbols carrying them as N_{r} and M_{r} respectively. The notation M is used in order to emphasize that the reference symbols in time-domain are considered.

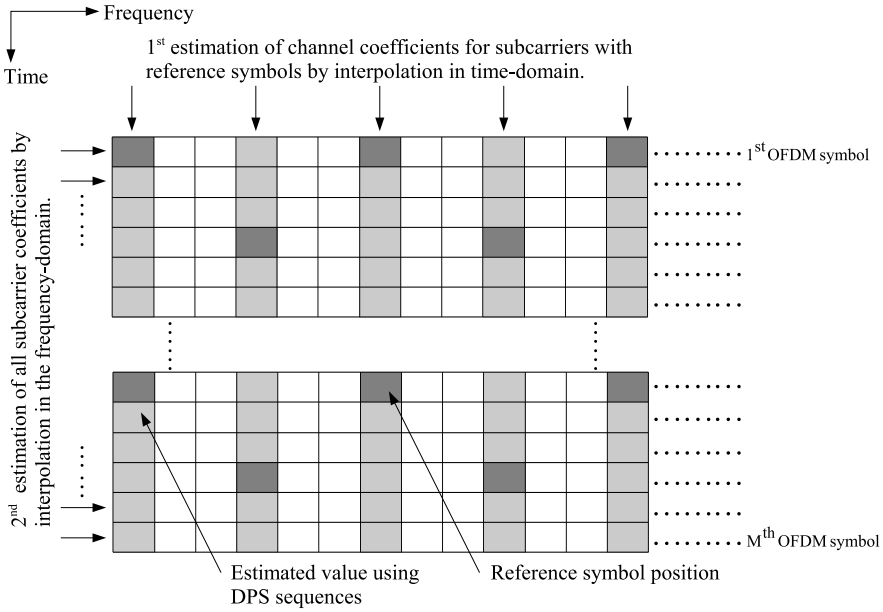

Figure 5.1: *Illustration of the estimation procedure. The horizontal axis is the channel frequency-response also referred to as frequency-domain, while the vertical axis corresponds to the time-varying behavior of the channel. The vertical dimension is referred to as time-dimension. The positions of reference symbols is according to Chapter 2 Section 2.4.2.*

Interpolation

Three interpolation methods are utilized.

- Linear interpolation between estimated subcarrier coefficients.
- Interpolation using the reduced rank LMMSE estimator.
- Interpolation using the DPS basis expansion.

The first two estimators are already known from Section 3.2.1 and 4.5 respectively. DPS sequences can be applied in the frequency dimension as well, which will be described in this chapter.

5.1.2 Estimation Using Channel Impulse Response

Instead of tracking the channel coefficients for subcarriers with reference symbols, the taps of the channel impulse response can be tracked, i.e we estimate the channel impulse response in the frequency-domain for OFDM symbols with reference symbols and then we track each tap in the time-domain.

Sections 4.3 and 4.4.2 presented two different approaches to estimate the channel impulse response. The task is now to firstly estimate a L-tap channel impulse response for each OFDM symbol carrying reference symbols. Hereafter each tap is tracked using DPS sequences instead of the subcarriers with channel estimates. In order to estimate the channel frequency response for each OFDM symbol, a FFT is performed on the estimated impulse response.

Common for all estimation methods is the use of DPS sequences, which will be explained in the following section.

5.2 Slepian Basis Expansion

In order to estimate the time-varying channel at the UE, an efficient representation of the channel is needed. The channel is estimated over a block of M OFDM symbols with a Doppler spectrum as defined in (3.22) with a maximum Doppler shift of ν_{Dmax}.
In order to model the time-varying channel, the effect of the Doppler shifts need to be modeled accurately. One way of modeling it is to make use of basis expansion models. In this thesis a basis expansion model based on DPS sequences will be utilized that is based on [28] and [26].
Slepian [22] investigated which sequences $u[m]$ are concentrated in a certain time interval of length M [28, p. 52 ff.],

$$\lambda(\nu_{\text{Dmax}}, M) = \frac{\sum_{m=0}^{M-1} |u[m]|^2}{\sum_{-\infty}^{\infty} |u[m]|^2}, \quad \text{with } 0 \leq \lambda \leq 1. \tag{5.1}$$

and simultaneously band-limited in frequency to the interval $\mathcal{W} = [-\nu_{\text{Dmax}}, \ldots, \nu_{\text{Dmax}}]$

$$u[m] = \int_{-\nu_{\text{Dmax}}}^{\nu_{\text{Dmax}}} U(\nu) e^{j2\pi m\nu} d\nu, \quad \text{where} \tag{5.2}$$

$$U(\nu) = \sum_{-\infty}^{\infty} u[m] e^{-j2\pi m\nu}. \tag{5.3}$$

The solutions for the optimization problems (5.1) (5.2) and (5.3) are the discrete prolate spheroidal sequences. The sequences $u_i[\ell, \nu_{\text{Dmax}}, M]$ are defined as the real solution of

$$\sum_{\ell=0}^{M-1} \frac{\sin(2\pi\nu_{\text{Dmax}}(\ell - m))}{\pi(\ell - m)} u_i[\ell, \mathcal{W}, M] = \lambda_i(\nu_{\text{Dmax}}, M) u_i[m, \mathcal{W}, M] \tag{5.4}$$

for $i \in \{0, \ldots, M-1\} = \mathcal{I}$ and $m \in \mathbb{Z}$. In the sequel a system with fixed parameters $(\mathcal{W}, M)$ is considered and the dependency on these parameters is dropped.
The DPS sequence $u_i[m]$ is a unique sequence which is exactly band-limited and having a high energy concentration within the time interval M. The sequences are doubly orthonormal on the infinite set $\{-\infty, \ldots, \infty\} = \mathbb{Z}$ as well as the finite set $\{0, \ldots, M-1\}$,

$$\sum_{m=0}^{M-1} u_i[m] u_j[m] = \lambda_i \sum_{-\infty}^{\infty} u_i[m] u_j[m] = \delta_{ij}, \tag{5.5}$$

where $i, j \in \{0, \ldots, M-1\}$. The eigenvalues λ_i of the sequences $u_i[m]$, expressed by (5.1) have the following property [28, p. 53]:

- The values of λ_i are clustered near 1 for $i \leq \lceil 2\nu_{\text{Dmax}} M \rceil + 1$

- For $i > \lceil 2\nu_{\text{Dmax}} M \rceil + 1$ they rapidly drop to zero.

Hence the dimension of the signal space [22] is approximately given by

$$D' = \lceil 2\nu_{\text{Dmax}} M \rceil + 1 \tag{5.6}$$

For the purpose of channel estimation, only the index set $m \in \{0, \ldots, M-1\}$ is of concern and these limited sequences are denoted as Slepian sequences. The vector $\boldsymbol{u}_i \in \mathbb{R}^M$ is now defined containing elements $u_i[m]$ for $m \in \{0, \ldots, M-1\}$ and equation (5.4) is written as:

$$\boldsymbol{C}\boldsymbol{u}_i = \lambda_i \boldsymbol{u}_i, \tag{5.7}$$

with matrix $\boldsymbol{C}$ defined as

$$[\boldsymbol{C}]_{i,\ell} = \frac{\sin(2\pi\nu_{\text{Dmax}}(i-\ell))}{\pi(i-\ell)}, \quad \text{for } i, \ell \in \{0, \ldots, M-1\}, \tag{5.8}$$

where $[\boldsymbol{C}]_{i,\ell}$ denotes the value of $\boldsymbol{C}$ at row i column ℓ.
The theory of time-concentrated and band-limited sequences developed by Slepian leads to a new approach for the time-varying channel estimation. The Slepian sequences span an orthonormal basis allowing a representation of time-limited snapshot of a band-limited signal using a minimum number of basis functions. The Slepian sequences expand the sequence $g[m]$ as follows:

$$g[m] \approx \tilde{g}[m] = \sum_{i=0}^{D-1} u_i[m]\gamma_i, \tag{5.9}$$

where γ_i is the weighting coefficients of the Slepian sequences and $m \in \{0, \ldots, M-1\}$. The dimension D has the constraints,

$$D' \leq D \leq M. \tag{5.10}$$

The choice of D affects the mean square error (MSE) defined as,

$$\text{MSE}_M = \frac{1}{M} \sum_{m=0}^{M-1} \mathbb{E}\left\{ |g[m] - \tilde{g}[m]|^2 \right\}. \tag{5.11}$$

5.2.1 Estimation of Channel Parameters

In order to utilize a basis expansion for channel estimation, the received OFDM signal is investigated. The received signal $y[m, q]$ for OFDM symbol at time index m for subcarrier q. For a fixed subcarrier, the index q is dropped resulting in

$$y[m] = g[m]d[m] + z[m], \tag{5.12}$$

where $g[m]$ is the channel attenuation, $d[m]$ the transmitted symbol and $z[m]$ is white Gaussian noise. Using a basis expansion (5.12) can be written as,

$$y[m] \approx \left(\sum_{i=0}^{D-1} u_i[m]\gamma_i \right) d[m] + z[m]. \tag{5.13}$$

If $d[m]$ has unit norm and is known for all m, an estimate of the channel coefficient $\hat{g}[m]$ is found as

$$\hat{g}[m] = y[m]d^*[m] = g[m] + z[m]d^*[m]. \tag{5.14}$$

The weighting coefficient $\hat{\gamma}_i$ for $i \in 0, \ldots, D-1$ is calculated as,

$$\hat{\gamma}_i = \sum_{m=0}^{M-1} \hat{g}[m]u_i^* = \sum_{m=0}^{M-1} y[m]d^*[m]u_i^*[m]. \tag{5.15}$$

The estimated sequence $\tilde{g}[m]$ is finally written as,

$$\tilde{g}[m] = \boldsymbol{f}^T[m]\boldsymbol{\gamma} = \left(\sum_{i=0}^{D-1} u_i[m]\hat{\gamma}_i \right), \tag{5.16}$$

where

$$\boldsymbol{f}[m] = \begin{bmatrix} u_i[m] \\ \vdots \\ u_{D-1}[m] \end{bmatrix} \in \mathbb{R}^D \tag{5.17}$$

and

$$\hat{\boldsymbol{\gamma}} = \begin{bmatrix} \hat{\gamma}_i \\ \vdots \\ \hat{\gamma}_{D-1} \end{bmatrix} \in \mathbb{C}^D. \tag{5.18}$$

It can be shown that the Slepian basis expansion is a reduced-rank channel estimation. The following section describes reduced-rank estimation in general.

5.2.2 Reduced-Rank Channel Estimation

Reduced-rank channel estimation is expressed in equation (5.9), which also can be written as [27],

$$g[m] \approx \tilde{g}[m] = \sum_{i=0}^{D-1} u_i[m]\hat{\gamma}_i = \boldsymbol{U}\hat{\gamma}, \quad \text{where} \tag{5.19}$$

$$\boldsymbol{U} = [\boldsymbol{u}_0, \ldots, \boldsymbol{u}_{D-1}], \quad \text{with} \tag{5.20}$$

$$\boldsymbol{u}_i = [u_i[0], u_i[1], \ldots, u_i[M-1]]^T, \quad i \in \{0, \ldots, D-1\}. \tag{5.21}$$

An estimate of the basis expansion coefficients $\hat{\gamma}$ is found the same way as in (5.15), but here expressed in a matrix-vector notation, simplified as [27],

$$\hat{\boldsymbol{\gamma}} = \boldsymbol{U}^{\mathrm{H}}\boldsymbol{g} \tag{5.22}$$

because of the orthonormality of the basis vectors. The reconstruction error per data block is defined as [27],

$$z = \frac{1}{M} ||\boldsymbol{g} - \hat{g}||^2 = \frac{1}{M} \left\|\boldsymbol{U}^{\mathrm{H}}\boldsymbol{n}\right\|^2 + \frac{1}{M} \left|\boldsymbol{V}^{\mathrm{H}}\boldsymbol{g}\right|^2, \tag{5.23}$$

where $\boldsymbol{V} = [\boldsymbol{u}_D, \ldots, \boldsymbol{u}_M]$ is the neglected subspace, orthogonal to the signal subspace spanned by the columns of $\boldsymbol{U}$ and $\boldsymbol{n} = [n[0], \ldots, n[M-1]]^T$ is the noise vector [27].
The mean square reconstruction error per data block is given by [27],

$$\begin{aligned} \text{MSE}_M &= \mathbb{E}\{z\} \\ &= \frac{D}{M}\sigma_n^2 + \frac{1}{M}\mathbb{E}\left\{\left|\boldsymbol{V}^{\text{H}}\boldsymbol{h}\right|^2\right\}. \end{aligned} \tag{5.24}$$

When using Slepian sequences, the subspace dimension D must be chosen such that reconstruction error is minimized.

5.2.3 Scattered Reference Symbols

In the LTE downlink the reference symbols are only located at some OFDM symbols $m \in \mathbb{P}_q$, where $\mathbb{P}_q$ is the set of positions of reference symbols of subcarrier q as depicted in Figure 5.1. Let us consider a fixed subcarrier q and neglect the notation q. Equation (5.15) is defined for a signal known for all $m \in \mathcal{I}$. The orthogonality of the Slepian sequences is lost by only taking some values of m. In order to correct the loss of orthogonality the instantaneous values the correlation matrix $\boldsymbol{G}$ is calculated [26].

$$\boldsymbol{G} = \sum_{m\in\mathbb{P}} \boldsymbol{f}[m]\boldsymbol{f}^{\text{H}}[m]\,|p[m]|^2 = \sum_{m\in\mathbb{P}} \boldsymbol{f}[m]\boldsymbol{f}^{\text{H}}[m], \tag{5.25}$$

where $p[m]$ is the value of the transmitted reference symbol at time m. According to Section 2.4.2 the norm of the reference symbols are always one, $|p[m]| = 1$.
Equation (5.15) is now calculated for all dimensions D as follows,

$$\tilde{\boldsymbol{\gamma}} = \boldsymbol{G}^{-1}\sum_{m\in\mathbb{P}} y[m]p^*[m]\boldsymbol{f}^*[m], \quad \text{where} \tag{5.26}$$

$$\tilde{\boldsymbol{\gamma}} = [\hat{\gamma}_0, \ldots, \hat{\gamma}_{D-1}]^T. \tag{5.27}$$

Let us define $\boldsymbol{U}_{\text{r}}$ as the truncated version of $\boldsymbol{U}$ with only rows corresponding to positions of reference symbols. Using the notation from Section 5.2.2, (5.25) is rewritten as follows,

$$\boldsymbol{G} = \boldsymbol{U}_{\text{r}}^{\text{H}}\boldsymbol{U}_{\text{r}}, \tag{5.28}$$

and (5.26) as,

$$\hat{\boldsymbol{\gamma}} = \boldsymbol{G}^{-1}\boldsymbol{U}_{\text{r}}^{\text{H}}\hat{\boldsymbol{g}}_{\text{mr}}, \tag{5.29}$$

where $\hat{\boldsymbol{g}}_{\text{mr}} \in \mathbb{C}^{M_{\text{r}}}$ is the vector containing the scattered estimates of the channel only.
The mean square error can be described by a square bias and a variance term [26],

$$MSE_M = \text{bias}_M^2 + \text{var}_M, \tag{5.30}$$

where bias_M^2 depends on the actual number of basis functions while var_M depends linearly on the noise term, the number of reference symbols J, and the number of basis functions D:

$$\text{var}_M \approx \sigma_z^2 \sum_{m=0}^{M-1} \boldsymbol{f}^{\text{H}}[m]\boldsymbol{G}^{-1}\boldsymbol{f}[m] \approx \sigma_z^2 \frac{D}{J}. \tag{5.31}$$

Equation (5.31) becomes exact for $\text{bias}_M^2 = 0$ [26].

5.3 Slepian Sequences Applied on the LTE Downlink

The theory behind Slepian sequences has now been reviewed and the following section will describe how to utilize Slepian sequences for channel estimation purposes in the LTE downlink.
As mentioned in Section 2.5 the user-plane latency should be below 5 ms. The time duration of one subframe which also corresponds to the TTI is 1 ms. Hence it is chosen to base the channel estimation using block length of 4 subframes, i.e. 8 slots with 4 ms duration. Taking a block of $N_{\text{sub}} = 4$ subframes into account results in a data block of 48 OFDM symbols.
According to the objectives of LTE [1], the performance should be optimized for speeds in range 0-15 km/h and high performance should be achieved for speeds up to 120 km/h. Based on these requirements it is chosen to design Slepian sequences for 120 km/h. In the following example parameters for the Slepian sequences are calculated.

The calculations are based on the listed parameters,

- Block length: $M = 48$.
- Maximum speed of UE: $v_{\text{max}} = 120$ km/h$= 33.3$ m/s.
- Carrier frequency: $f_C = 2$ GHz.

The normalized Doppler shift is calculated as follows,

$$\nu_{\text{Dmax}} = \frac{v_{\text{max}} f_C}{c_0} \cdot T_{\text{s}} = 0.0185. \tag{5.32}$$

The time-bandwidth product,

$$2\nu_{\text{Dmax}} M = 1.78. \tag{5.33}$$

The resulting minimum dimension of the signal space:

$$D' = \lceil 2\nu_{\text{Dmax}} M \rceil + 1 = 3. \tag{5.34}$$

The chosen dimension D must satisfy the condition [26]

$$D' \leq D \leq M_{\text{r}}. \tag{5.35}$$

There are two slots per subframe with each slot having 6 OFDM symbols (see Section 2.2). The total number of OFDM symbols (block length) is

$$M = 2N_{\text{sub}} \cdot 6 = 48. \tag{5.36}$$

There are two OFDM symbols with reference symbols within one slot, but the OFDM symbols do not have the reference symbols at same subcarrier positions. Hence only one reference OFDM symbol represents one reference subcarrier for each slot.

$$M_{\mathrm{r}} = 2N_{\mathrm{sub}} = 8. \tag{5.37}$$

The Slepian sequences are generated in Matlab with the command `dpss`. For this example the inputs are as follows `dpss(`M`,`$\nu_{\mathtt{Dmax}}M$`,D)`. With D set to 4 as an example, the generated Slepian sequences are depicted on Figure 5.2.

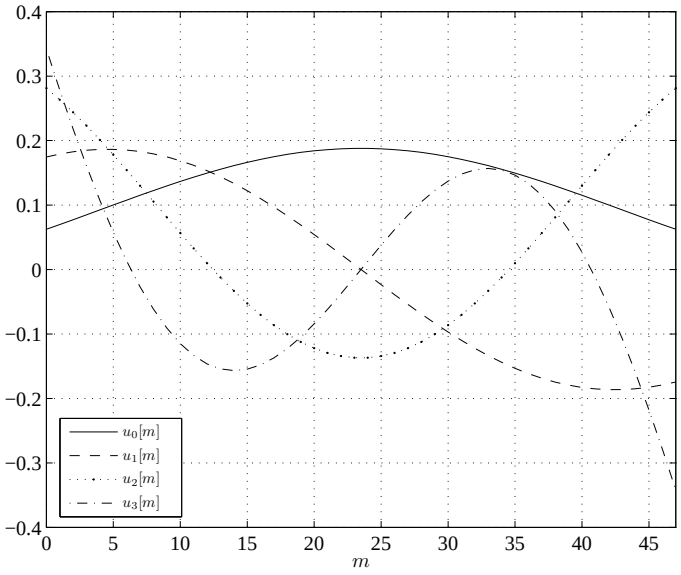

Figure 5.2: *Slepian sequences for $u_i[m]$ for $M = 48$ and $\nu_{Dmax} = 0.0185$.*

5.3.1 Slepian Sequences Applied in the Frequency Dimension

In Section 5.1.1 it was mentioned that Slepian Sequences could be applied in the frequency dimension as well. This is achieved as follows [25],

- For a fixed OFDM symbol m, the frequency response $\boldsymbol{g} \in \mathbb{C}^{N_{\mathrm{IFFT}}}$ spans a subspace that has dual properties to the Slepian subspace in the time-domain.
- The frequency index k is dual to the time index m,
- the block size of the sequence is N_{IFFT},
- and the normalized maximum delay $\theta_{\mathrm{max}} = \frac{L-1}{N_{\mathrm{IFFT}}}$ is dual to the maximum Doppler shift ν_{Dmax}.

The generated Slepian sequence here denoted as $\hat{u}_i \in \mathbb{C}^{N_{\mathrm{IFFT}}}$ for the frequency domain has the dimension $D_{\mathrm{f}} \leq \lceil \theta_{\mathrm{max}} N_{\mathrm{IFFT}} \rceil + 1 = L$. For the time-domain the Doppler spectrum is symmetric but the delays in interval $\theta \in [0, \theta_{\mathrm{max}}]$ are non-symmetric.

In order to take this into account, the Slepian sequence is shifted, i.e. $u_i[k] = \hat{u}_i[(k+\frac{N_{\text{IFFT}}}{2}) \bmod N_{\text{IFFT}}]$ [25]. With the shifted Slepian sequence the estimation of the channel parameters in frequency-dimension is achieved using the same steps as described in Section 5.2.1 and 5.2.3 but with the new parameters. It is worth noticing that only some positions of the frequency response are occupied (see Figure 2.2), hence we can reduce the size of basis vectors from $\boldsymbol{u}_i \in \mathbb{C}^{N_{\text{IFFT}}}$ to $\boldsymbol{u}_i \in \mathbb{C}^{N_{\text{BW}}}$. We denote the usage of Slepian sequences to estimate the frequency domain as 2x1D Slepian, since Slepian sequences are applied in the frequency-domain as well as in the time-domain.

5.4 Performance Comparison

The performance of the estimators are compared using the mean square error (MSE) between the estimated channel frequency response for used subcarriers and the true frequency response. The best estimator is the Wiener interpolation with known correlation functions of the channel frequency response and of the Doppler spectrum.

5.5 Wiener Interpolation

The optimal estimation is achieved using two-dimensional Wiener interpolation. Since 2D Wiener filters have a large computational complexity, cascading two 1 dimensional Wiener interpolators is a good trade-off between performance and complexity [13].
It can be shown that 2x1D interpolation and 2D interpolation in this case have same performance when the time and frequency dimensions are uncorrelated [13]. The cascaded 2x1D interpolater offers a joint estimation of channel coefficients using estimated values from the whole received data block. The interpolation is achieved as follows:

- The first interpolation is done in the frequency-dimension for all OFDM symbols carrying reference symbols.

- The second interpolation is done in the time-dimension for all subcarrriers.

5.5.1 Interpolation in Frequency-Dimension

The interpolation in frequency is similar to Section 4.3 where LMMSE estimation was used. Now the true autocorrelation of the channel is used, instead of assuming a uniform power delay profile. The interpolated frequency response, $\boldsymbol{g}_{\text{I}}$, is written as,

$$\boldsymbol{g}_{\text{I}} = \boldsymbol{R}_{g y_{\text{r}}} \boldsymbol{R}_{y_{\text{r}} y_{\text{r}}}^{-1} \boldsymbol{y}_{\text{r}} \tag{5.38}$$

$$= \boldsymbol{F} \boldsymbol{R}_{h'h'} \boldsymbol{T}_{\text{r}}^{\text{H}} \boldsymbol{X}_{\text{r}}^{\text{H}} \left(\boldsymbol{X}_{\text{r}} \boldsymbol{T}_{\text{r}} \boldsymbol{R}_{h'h'} \boldsymbol{T}_{\text{r}}^{\text{H}} \boldsymbol{X}_{\text{r}}^{\text{H}} + {\sigma_z}^2 \boldsymbol{I}_{N_{\text{r}}} \right)^{-1} \boldsymbol{y}_{\text{r}} \tag{5.39}$$

(5.39) is simply the Fourier transformation of (4.10).

5.5.2 Interpolation in Time-Dimension

The interpolation in the time direction requires information about the correlation, which depends on the Doppler shift. Let $y[m, q]$ denote a received value at time m for subcarrier q. For a fixed subcarrier, index q is dropped.
The signal $y[m]$ is only known at positions with reference symbols ($m \in \mathbb{P}$). $\boldsymbol{y}_{\text{mr}} \in \mathbb{C}^P$ denotes the vector containing only received reference symbols, while $\boldsymbol{y}_{\text{m}} \in \mathbb{C}^M$ contains the values of $y[m]$. Index m is added such that this vector is not confused with the notation $\boldsymbol{y}_{\text{r}}$ from Section 5.5.1. The channel frequency response is sought, hence it is estimated for all positions with reference symbols ($m \in \mathbb{P}$):

$$\hat{\boldsymbol{g}}_{\text{mr}} = \boldsymbol{X}_{\text{mr}} \boldsymbol{y}_{\text{mr}}, \tag{5.40}$$

where the matrix $\boldsymbol{X}_{\text{mr}} \in \mathbb{C}^{M_{\text{r}}}$ is the diagonal matrix containing the transmitted reference symbols on the time-dimension for a fixed subcarrier q and M_{r} is the number of reference symbols. The interpolated estimate in the time-dimension using Wiener interpolation is [14]:

$$\tilde{\boldsymbol{g}}_{\text{m}} = \boldsymbol{R}_{g_{\text{m}}\hat{g}_{\text{mr}}} \boldsymbol{R}^{-1}_{\hat{g}_{\text{mr}}\hat{g}_{\text{mr}}} \hat{g}_{\text{mr}}, \tag{5.41}$$

where $\tilde{g}_{\text{m}} \in \mathbb{C}^M$. The next task is to derive the values of the correlation matrices.
$\boldsymbol{R}_{g\hat{g}_{\text{mr}}} \in C^{M,P}$ is the cross-correlation between $\boldsymbol{g}$ and $\hat{\boldsymbol{g}}_{\text{mr}}$. The following example shows how the cross-correlation is found.

5.5.2.1 All Reference Symbols

For the scalar case $\tilde{g}[m]$ with reference symbols for all values of m, the interpolated value is found as,

$$\tilde{g}[m] = \boldsymbol{r}_{g_{\text{m}}\hat{g}_{\text{m}}}[m]^{\text{T}} \left(\boldsymbol{R}^{-1}_{\hat{g}_{\text{m}}\hat{g}_{\text{m}}} \right)^{-1} \hat{\boldsymbol{g}}_{\text{m}}. \tag{5.42}$$

The index r is dropped for indicating all reference symbols. The correlation vector $\boldsymbol{r}_{g_{\text{m}}\hat{g}_{\text{m}}}[m]$ can be written as,

$$\boldsymbol{r}_{g_{\text{m}}\hat{g}_{\text{m}}}[m] = \left[r_{g_{\text{m}}\hat{g}_{\text{m}}}[-m], r_{g_{\text{m}}\hat{g}_{\text{m}}}[-m+1], \ldots, r_{g_{\text{m}}\hat{g}_{\text{m}}}[m-M-1] \right]^T. \tag{5.43}$$

The corresponding matrix, $\boldsymbol{R}_{g_{\text{m}}\hat{g}_{\text{m}}}$, can be written as,

$$\boldsymbol{R}_{g_{\text{m}}\hat{g}_{\text{m}}} = \text{toeplitz}\left[r_{g_{\text{m}}\hat{g}_{\text{m}}}[0], r_{g_{\text{m}}\hat{g}_{\text{m}}}[1], \ldots, r_{g_{\text{m}}\hat{g}_{\text{m}}}[M-1] \right] \tag{5.44}$$

$$= \begin{bmatrix} r_{g_{\text{m}}\hat{g}_{\text{m}}}[0] & r_{g_{\text{m}}\hat{g}_{\text{m}}}[1] & \ldots & r_{g_{\text{m}}\hat{g}_{\text{m}}}[M-1] \\ r^*_{g_{\text{m}}\hat{g}_{\text{m}}}[-1] & r_{g_{\text{m}}\hat{g}_{\text{m}}}[0] & & r_{g_{\text{m}}\hat{g}_{\text{m}}}[M-2] \\ \vdots & \ldots & & \vdots \\ r^*_{g_{\text{m}}\hat{g}_{\text{m}}}[-M+1] & r^*_{g_{\text{m}}\hat{g}_{\text{m}}}[M] & \ldots & r_{g_{\text{m}}\hat{g}_{\text{m}}}[0] \end{bmatrix} \tag{5.45}$$

in order to find the vector $\tilde{\boldsymbol{g}}$, similar to (5.41).

5.5.2.2 Scattered Reference Symbols

The previous results (5.43) and (5.44) can be reused for the case with scattered reference symbols. For the scalar case $\tilde{g}[m]$ with reference symbols for $m \in \mathbb{P}$, the interpolated value is found as,

$$\tilde{g}[m] = \boldsymbol{r}_{g_{\mathrm{m}}\hat{g}_{\mathrm{mr}}}[m]\boldsymbol{R}^{-1}_{\hat{g}_{\mathrm{mr}}\hat{g}_{\mathrm{mr}}}\hat{\boldsymbol{g}}_{\mathrm{mr}}. \tag{5.46}$$

The estimated values for the channel is found on each third OFDM symbol since an interpolation in frequency direction was applied first, hence the crosscorrelation $\boldsymbol{r}_{g_{\mathrm{m}}\hat{g}_{\mathrm{mr}}}$ yields,

$$\boldsymbol{r}_{g_{\mathrm{m}}\hat{g}_{\mathrm{mr}}}[m] = [r_{g_{\mathrm{m}}\hat{g}_{\mathrm{m}}}[-m], r_{g_{\mathrm{m}}\hat{g}_{\mathrm{m}}}[-m+3], r_{g_{\mathrm{m}}\hat{g}_{\mathrm{m}}}[-m+6], \ldots, r_{g_{\mathrm{m}}\hat{g}_{\mathrm{m}}}[-m+46]]\,. \tag{5.47}$$

Using this knowledge, $\boldsymbol{R}_{g_{\mathrm{m}}\hat{g}_{\mathrm{mr}}}$ is found knowing $\boldsymbol{R}_{g_{\mathrm{m}}\hat{g}_{\mathrm{m}}}$. The rows of $\boldsymbol{R}_{g_{\mathrm{m}}\hat{g}_{\mathrm{mr}}}$ are the same as for $\boldsymbol{R}_{g_{\mathrm{m}}\hat{g}_{\mathrm{m}}}$, however, only the columns of $\boldsymbol{R}_{g_{\mathrm{m}}\hat{g}_{\mathrm{m}}}$ corresponding to the positions of the reference symbols taken into account.
The autocorrelation matrix is calculated next. It can be shown that

$$\boldsymbol{R}_{\hat{g}_{\mathrm{mr}}\hat{g}_{\mathrm{mr}}} = \boldsymbol{R}_{g_{\mathrm{mr}}g_{\mathrm{mr}}} + \boldsymbol{I}_{Mr}\sigma^2_{z'}, \tag{5.48}$$

where $\boldsymbol{R}_{g_{\mathrm{mr}}g_{\mathrm{mr}}}$ is found using the knowledge acquired from (5.44) and using it for the scattered case,

$$\boldsymbol{R}_{g_{\mathrm{mr}}g_{\mathrm{mr}}} = \text{toeplitz}\left\{[r_{g_{\mathrm{m}}g_{\mathrm{m}}}[0], r_{g_{\mathrm{m}}g_{\mathrm{m}}}[3], r_{g_{\mathrm{m}}g_{\mathrm{m}}}[6], \ldots, r_{g_{\mathrm{m}}g_{\mathrm{m}}}[3(M_{\mathrm{r}}-1)]]\right\} \tag{5.49}$$

The question is now how to estimate the correlation vector $\boldsymbol{r}_{g_{\mathrm{m}}\hat{g}_{\mathrm{mr}}}[m]$. An approximated analytical expression for the autocorrelation has been found in Section 3.4. However the autocorrelation for the SCME model is found through simulation, in order to obtain a better estimate.

5.6 Relation Between Slepian Sequences and Reduced Rank Wiener Interpolation

The theory of Slepian sequences has been introduced and the Wiener interpolation applied in order to compare the results. The utilization of Slepian sequences actually corresponds to a reduced rank Wiener interpolation and in this section the relationship will be shown. For the sake of simplicity the focus will be on a sequence $\hat{\boldsymbol{g}}$ with reference symbols only. This section follows the exact same reasoning as in [27], which investigates channel predicton, however in this case we focus on interpolation, i.e. channel estimation.

5.6.1 Reduced Rank Estimation

The Wiener interpolation for all reference symbols is expressed in (5.42). If covariance matrix $\boldsymbol{R}^{-1}_{\hat{g}_{\mathrm{m}}\hat{g}_{\mathrm{m}}} = \boldsymbol{R}^{-1}_{g_{\mathrm{m}}g_{\mathrm{m}}}$ that is if the noise is neglected and the optimum dimension is D, the estimated sequence for low-rank estimation can be written in general as [27],

$$\tilde{g}[m] = \underbrace{\boldsymbol{r}_g[m]^{\mathrm{H}}\boldsymbol{U}\boldsymbol{\Lambda}^{-1}}_{\boldsymbol{f}[m]}\underbrace{\boldsymbol{U}^{\mathrm{H}}\hat{\boldsymbol{g}}}_{\hat{\boldsymbol{\gamma}}} = \sum_{i=0}^{D-1} u_i\hat{\gamma}_i, \tag{5.50}$$

where $\mathbf{\Lambda} = \text{diag}\,(\lambda_0, \ldots, \lambda_{D-1})$ and $\boldsymbol{f}[m] = [u_0[m], \ldots, u_{D-1}[m]]^T$. The optimal dimension D is defined as [27]

$$D = \underbrace{\text{argmin}}_{D\in[1,\ldots,M]} \left(\frac{1}{M} \sum_{i=D}^{M-1} \lambda_i + \frac{D}{M}\sigma_z^2 \right). \tag{5.51}$$

The sequences $\boldsymbol{u}_i$ are defined as

$$\sum_{\ell=0}^{M-1} R_g[\ell - m]u_i[\ell] = \lambda_i u_i[m], \quad m \in \mathbb{Z}. \tag{5.52}$$

The sequences $\boldsymbol{u}_i$ for $m \in \mathcal{I}_M$ form orthogonal sets. Based on different assumptions on the covariace matrix $\boldsymbol{R}_{\hat{g}_\text{m}\hat{g}_\text{m}}$, different sets of $\boldsymbol{u}_i$ can be calculated.

5.6.2 Estimation Using Slepian Sequences

The utilization of Slepian sequences in based on the assumption of a flat Doppler spectrum $S(\nu, \mathcal{W})$. In order to relate it to a general reduced rank estimator, let us consider the sequence $\boldsymbol{u}_i(m, \mathcal{W})$. The index $\mathcal{W}$ is included to state that the Slepian sequences depends on the Doppler spectrum, which is band-limited in the region $\mathcal{W}$. In (5.7) and (5.8) it was shown how the Slepian sequences were found. Comparing this information to the covariance matrix of a given Doppler spectrum expressed in (3.23) in Section 3.4 yields,

$$C[k, \mathcal{W}] = |\mathcal{W}| R_\text{d}[k, \mathcal{W}] \tag{5.53}$$

We now express how the basis vectors of the Slepian sequences depend on R_d.

$$\begin{aligned} \boldsymbol{u}_i(\mathcal{W}) &= \frac{|\mathcal{W}|}{\lambda_i(\mathcal{W})} \sum_{\ell=0}^{M-1} R_\text{d}[\ell - m]^* u_i[\ell, \mathcal{W}] \\ &= \frac{|\mathcal{W}|}{\lambda_i(\mathcal{W})} \boldsymbol{r}_\text{d}[m, \mathcal{W}]^\text{H} \boldsymbol{u}_\mathcal{W}, \end{aligned} \tag{5.54}$$

where the knowledge of $C[k, \mathcal{W}] = |\mathcal{W}| R_\text{d}[k, \mathcal{W}]$ is first used and then $R_\text{d}[-k, \mathcal{W}] = R_\text{d}[k, \mathcal{W}]^*$ is applied [27]. Equation (5.50) and (5.17) associated with (5.54) yields

$$\boldsymbol{f}[m, \mathcal{W}]^T = \boldsymbol{r}_\text{d}[m, \mathcal{W}]^\text{H} \boldsymbol{U}(\mathcal{W}) \mathbf{\Lambda}^{-1}(\mathcal{W}), \tag{5.55}$$

with $\boldsymbol{r}_\text{d}[m, \mathcal{W}] = [R_\text{d}[m, \mathcal{W}], \ldots, R_\text{d}[m - (M-1), \mathcal{W}]]^T$, $\mathbf{\Lambda} = \frac{1}{|\mathcal{W}|}\text{diag}\,(\lambda_0, \ldots, \lambda_{D-1})$ and $\boldsymbol{U}(\mathcal{W}) = [\boldsymbol{u}_0(\mathcal{W}), \ldots, \boldsymbol{u}_{D-1}(\mathcal{W})]$. By inserting the information from equation (5.55) into the sequence estimation (5.16), equation (5.56) is obtained. It should be noticed that in (5.16) the index $\mathcal{W}$ is dropped, but it is used here.

$$\hat{g} = \boldsymbol{f}^T[m, \mathcal{W}]\boldsymbol{\gamma} \tag{5.56}$$

$$= \boldsymbol{r}_\text{d}[m, \mathcal{W}]^\text{H} \boldsymbol{U}(\mathcal{W}) \mathbf{\Lambda}^{-1}(\mathcal{W}) \boldsymbol{U}(\mathcal{W})^\text{H} \boldsymbol{y}, \tag{5.57}$$

which is exactly the same as (5.50) with reduced rank estimator for a constant Doppler spectrum, $R_g[k] = R_\text{d}[k]$, for $k \in \mathbb{Z}$. Hence both estimators are using the same subspace spanned by time-concentrated and band-limited sequences [27].

5.7 Complexity

The complexity of the time-varying channel estimation per data block of is divided into two parts, the first part is the estimation in the time-dimension and the second part is the frequency-dimension. This section considers the complexity in the time-dimension, since Section 4.7 already describes the complexity for estimation in the frequency-dimension. The complexity of Slepian sequences depends on whether the estimation is performed for the subcarriers with channel estimates or the impulse response. In general the complexity in the time-dimension for one subcarrier or tap can be expressed as in Table 5.1. The complexity of the projection depends on the number

Steps	Calculation	Complexity	Memory
1	$\hat{\gamma} = \boldsymbol{U}_{\mathrm{r}}^{\mathrm{H}} \hat{\boldsymbol{g}}_{\mathrm{mr}}$:	$D \cdot M_{\mathrm{r}}$	$\boldsymbol{U}^{\mathrm{H}} \in \mathbb{C}^{M \times D}$
2	$\tilde{\gamma} = \boldsymbol{G}\hat{\gamma}$:	D^2	$\boldsymbol{G} \in \mathbb{C}^{D \times D}$
3	$\tilde{g} = \boldsymbol{U}\tilde{\gamma}$	$D\dot{M}$	

Table 5.1: *Complexity of using Slepian sequences in time-domain.*

of channel estimates M_{r} and dimension D.

5.7.1 Estimation Using Subcarriers

The complexity of channel estimation by estimating the subcarriers firstly and then interpolating as described in Section 5.1.1 depends on which interpolation method is utilized and on the number of subcarriers to estimate.

The number of subcarriers with reference symbols is $N_{\mathrm{R}} = 2N_{\mathrm{r}}$, since scattered reference symbols are applied, see also Figure 5.1. The calculation described in Table 5.1 has to be performed $2N_{\mathrm{r}}$ times. After the first estimation in the time-domain there are $2N_{\mathrm{r}}$ estimates of the frequency response for each OFDM symbol. Hence N_{r} has to be replaced with N_{R} for reduced rank LMMSE estimator and linear interpolation in Table 4.7 and the stored matrices have to include the new positions of estimates as well in order to take them into account in the calculation.

5.7.1.1 Slepian Sequences in Frequency Dimension

The complexity of applying Slepian sequences in the frequency-dimension is not expressed in Table 4.7, hence it is calculated in Table 5.2.

5.7.2 Estimation Using the Impulse Response

Instead of estimating in the time-domain firstly, we estimate the channel impulse response in the frequency-domain for each OFDM symbol with reference symbols and then perform estimation in the time-domain. The number of OFDM symbols for which the taps are calculated is $M_{\mathrm{R}} = 2M_{\mathrm{r}} = 16$, see also Figure 5.1 and (5.37). The complexity of the calculation for each OFDM symbol is described in Table 4.7 for LMMSE CIR and downsampled CIR. Both impulse responses can be transformed into the frequency-domain and the channel estimates for each subcarrier can

Steps	Calculation	Complexity	Memory
1	$\hat{\gamma}_f = \boldsymbol{U}_{\mathrm{r}}^{\mathrm{H}} \hat{\boldsymbol{g}}_{\mathrm{r}}$:	$D_{\mathrm{f}} \cdot N_{\mathrm{R}}$	$\boldsymbol{U}_f^{\mathrm{H}} \in \mathbb{C}^{N_{\mathrm{BW}} \times D_{\mathrm{f}}}$
2	$\tilde{\gamma}_f = \boldsymbol{G}^{-1} \hat{\boldsymbol{\gamma}}$:	D_{f}^2	$\boldsymbol{G}^{-1} \in \mathbb{C}^{D_{\mathrm{f}} \times D_{\mathrm{f}}}$
3	$\tilde{g} = \boldsymbol{U}_f \tilde{\boldsymbol{\gamma}}_f$	$D_{\mathrm{f}} \cdot N_{\mathrm{BW}}$	

Table 5.2: *Complexity of frequency response estimation using the Slepian sequences.*

Steps	Calculation	Complexity	Memory
1	$\hat{\gamma} = \boldsymbol{U}_{\mathrm{r}}^{\mathrm{H}} \hat{\boldsymbol{g}}_{\mathrm{mr}}$:	$2DM_{\mathrm{r}}$	$\boldsymbol{U}^{\mathrm{H}} \in \mathbb{C}^{M \times D}$
2	$\tilde{\gamma} = \boldsymbol{G}^{-1} \hat{\boldsymbol{\gamma}}$:	D^2	$\boldsymbol{G}^{-1} \in \mathbb{C}^{D \times D}$
3	$\tilde{g} = \boldsymbol{U} \hat{\boldsymbol{\gamma}}$	$D \cdot M$	

Table 5.3: *Complexity of tracking the CIR using the Slepian sequences.*

be tracked. However it is chosen to track the taps of the impulse responses in the time-varying channel, because the number of taps is lower than the number of subcarriers. The complexity of applying the Slepian sequences is calculated using the same steps as in Table 5.1. Instead of considering one subcarrier we consider one tap. Table 5.3 lists the calculations for tracking one tap from the impulse response in the time-domain. Since we need to track all taps, the calculations in Table 5.3 need to be carried out L times and the found impulse response is transformed into the frequency domain M times.

5.7.3 2x1D Wiener Interpolation

Table 5.4 lists the calculation for the Wiener interpolation, which is the estimator that yields the lowest MSE, but has also the highest complexity, specially since it requires operation of an order of 3, i.e $O(M_{\mathrm{R}}^3)$ for step 1 . Hence the usage of Slepian sequences in the time-domain offers a low-complexity approach for estimation of the time-varying channel. By applying the Slepian sequences in time-domain for channel estimation and the different low-complexity estimators mentioned in Chapter 4 results in a low-complexity approach for the time-variant channel estimation.

Steps	Calculation	Complexity	Memory
1	$\boldsymbol{R}^{-1}_{\hat{g}_{\mathrm{mr}}\hat{g}_{\mathrm{mr}}}$:	$O(M_{\mathrm{R}}^3)$	$\Gamma = \boldsymbol{R}_{g_{\mathrm{mr}}\hat{g}_{\mathrm{mr}}} \in \mathbb{C}^{M_{\mathrm{R}} \times M_{\mathrm{R}}}$
2	$\Phi = \boldsymbol{R}^{-1}_{\hat{g}_{\mathrm{mr}}\hat{g}_{\mathrm{mr}}}\hat{g}_{\mathrm{mr}}$:	$O(M_{\mathrm{R}}^2)$	
3	$\boldsymbol{g}_{\mathrm{m}} = \boldsymbol{R}_{g_{\mathrm{m}}\hat{g}_{\mathrm{mr}}}\Phi$:	$M\dot{M}_{\mathrm{R}}^2$	$\boldsymbol{R}_{g_{\mathrm{m}}\hat{g}_{\mathrm{mr}}} \in \mathbb{C}^{L \times M_{\mathrm{R}}}$

Table 5.4: *Complexity of using Wiener interpolation in the time-domain.*

5.8 Summary

In this chapter methods to estimate the time-varying channel for the LTE downlink were presented. The channel is estimated using Slepian sequences in the time-dimension, while using LMMSE CIR, downsampled CIR, reduced rank LMMSE, linear interpolation and Slepian sequences as estimation methods in frequency-domain. Use of Slepian sequences in the time-domain corresponds to a reduced rank Wiener interpolation with a flat Doppler spectrum. Furthermore the Slepian sequences yields a low-complexity approach to estimate the time-varying channel in the time-domain. In order to evaluate the performance of the presented methods, they are compared to 2x1D Wiener interpolation with autocorrelation functions matching the channel. Combining the low-complexity channel estimation approach in the time-domain introduced by the Slepian sequences with the different estimators in the frequency-domain, we achieve a low-complexity alternative to the 2x1D Wiener interpolation. Beside the channel estimation it is also of importance to predict the mobile channel. The next chapter considers how this can be achieved by expanding the same methods utilized for channel estimation.

6 Channel Prediction

In Chapter 5 the channel estimation problem was considered, now channel prediction is investigated. The NodeB schedules resource blocks to the UEs for the each subframe. The scheduling is based on the state of the channel, reported by the UE in a frequency division duplex (FDD) system. However for mobile users at vehicular speed the channel state information gets outdated, hence the channel must be predicted for a proper scheduling [20]. This chapter introduces a method to predict the channel in UMTS LTE using Slepian sequences developed by [27].

6.1 Prediction using Slepian Sequences

As stated in Chapter 5 the utilization of Slepian sequences results in a time-concentrated and band-limited sequence. For prediction purposes channel estimates for $\ell > M-1$ are calculated. We denote the prediction as minimum-energy prediction since the Slepian sequences are concentrated in the interval $m \in \mathcal{I}_M$. The used Slepian sequences for channel estimation purpose were defined for $m \in \mathcal{I}_M$, hence the first task is to obtain Slepian sequences at times $\ell > M-1$.

6.1.1 Minimum Energy Band-Limited Sequences

By evaluating (5.4) in Section 5.2, basis vectors $\boldsymbol{u}_i$ were calculated for a block of finite length, i.e. $u_i[m]$ for $m \in \mathcal{I}_M$. The sequence $u_i[m]$ can be continued for m over $\mathbb{Z}$ in a minimum energy (ME) band-limited sense by evaluating (5.4) on the right hand side, as expressed in (6.1) [27].

$$u_i[\ell, \mathcal{W}, M] = \sum_{m=0}^{M-1} \frac{\sin(2\pi\nu_{\text{Dmax}}(m-\ell))}{\pi(m-\ell)} u_i[m, \mathcal{W}, M] \frac{1}{\lambda_i(\mathcal{W}, M)}. \tag{6.1}$$

The value for $u_i[\ell]$ at $\ell \notin \mathcal{I}$ can be calculated since the sequence $u_i[m]$ for $m \in \mathcal{I}$ and λ_i are already known.

6.1.2 Prediction

Using the minimum energy band-limited sequences and the same weighting $\hat{\boldsymbol{\gamma}}$ as for the channel estimation, the ME band-limited prediction of a time-variant channel for any $m \in \mathbb{Z}$ is finally

given as

$$\tilde{g}[\ell] = \sum_{i=0}^{D-1} u_i[l]\hat{\gamma}_i, \tag{6.2}$$

where $u_i[\ell]$ is the extended basis sequence at time indices $\ell \geq M$.Using the same methods as for channel estimation (Chapter 5), the channel can be predicted with the new knowledge from Section 6.1.1 and (6.2).

6.2 Wiener Predictor

Another solution for channel prediction is the Wiener predictor, which requires information about the second order statistics of the channel.
The structure of the Wiener predictor is based on Wiener interpolation as described in (6.3). For a sequence $\hat{g}_{\text{mr}}[m]$ with $m \in \mathcal{I}_M$ the predicted value at time index $\ell > M-1$ is as follows,

$$\tilde{g}[\ell] = \boldsymbol{r}_{g_{\text{m}}\hat{g}_{\text{mr}}}{}^{H}[\ell]\boldsymbol{R}^{-1}_{\hat{g}_{\text{mr}}\hat{g}_{\text{mr}}}\hat{g}_{\text{mr}}, \tag{6.3}$$

where $\boldsymbol{r}_{g_{\text{m}}\hat{g}_{\text{mr}}}[m]$ is found the same way as in (5.47). The Wiener predictor can be approximated by a reduced rank predictor where subspaces with small eigenvalues are truncated [27].

6.3 Relation Between Wiener Predictor and ME Predictor

In [27] it is shown that a reduced rank Wiener predictor approximates the Wiener predictor. Using the same procedure as in Section 5.6 but replacing time index m with an index ℓ greater than the block size ($\ell > M-1$), shows that ME band-limited prediction and reduced rank Wiener prediction assuming a constant Doppler spectrum spans the same subspace.

6.4 Summary

Using Slepian sequences it is possible to perform channel prediction such that the information about the channel is not outdated at NodeB. Furthermore the use of Slepian sequences for prediction is similar to the reduced rank Wiener prediction.

7 Simulation Results

The presented estimation and prediction methods are now simulated using Matlab. The written Matlab files can be found on the companion CD-ROM. The LTE downlink signal structure and SCME model offer several parameters to adjust. It was chosen to work with the downlink transmission bandwidths of 2.5 and 20 MHz, since the first use the same sampling frequency as the current UMTS 3G system while the latter is the maximum transmission bandwidth.

7.1 SCME Channel Model Configuration

The SCME channel model was used to generate channel realizations. In order to adjust it to the LTE downlink simulation, the model has to be configured appropriately.

7.1.1 Generation of Impulse Response

The SCME model takes several inputs which are described in [21]. A channel has to be generated for each OFDM symbol, which has a duration of T_s as described in Section 3.3.2. [21] does not give a detailed description of how to configure the model according the mentioned problem. Therefore the solution to this is given in this section.
In light of *line 531* in the Matlab file *'scm.m'* within the SCME package, the channel impulse response is generated for each OFDM symbol by configuring the parameter *scmpar.SampleDensity* as follows,

```
SlotDuration=0.5e-3; %0.5 ms
N.OFDM_symbol_pr_slot=6; % 6 symbols pr. slot
speed_of_light=2.99792458e8; %m/s
fcarrier=2e9; % 2GHz carrier frequency
wavelength=speed_of_light/fcarrier;
delta_t=SlotDuration/N.OFDM_symbol_pr_slot; %OFDM symbol duration
linkpar.MsVelocity=channel.vmax; % Velocity of UE is configured

%Configuring parameter to generate impulse response for each OFDM symbol.
scmpar.SampleDensity = wavelength / (linkpar.MsVelocity*2*delta_t);
```

The parameter *scmpar.SampleDensity* determines the delay between the generation of each channel impulse response.

7.2 Autocorrelation of Doppler Shift

Since some properties such as the power delay profile of the SCME model are unknown, they are determined by simulations. The SCME generates a number of impulse responses for each new channel generation.
For each channel generation the autocorrelation for each tap is found. The autocorrelation represents the correlation caused by the specific Doppler shifts of the generated channel. Let us denote the autocorrelation by vector $\tilde{\boldsymbol{r}}$, normalized such that $\tilde{r}[0] = 1$. The simulations are run over 4000 generated channels with each 100 impulse responses. Hereafter the correlation is averaged and the result is depicted on Figure 7.1. The autocorrelation vector is used as the a-priori Doppler

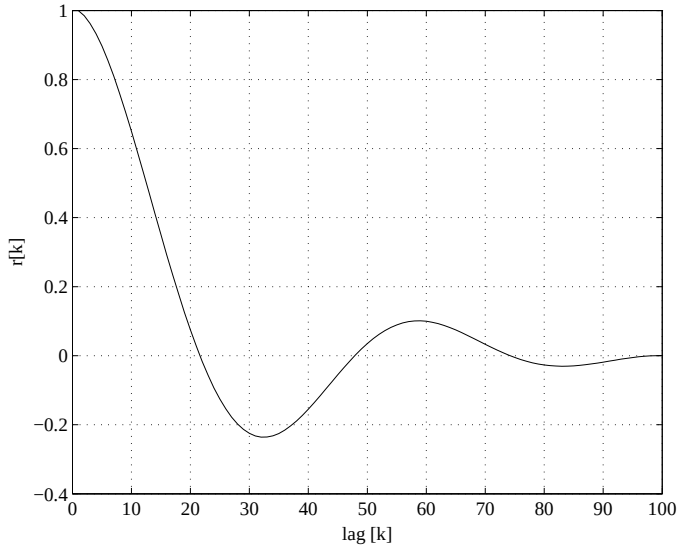

Figure 7.1: *Autocorrelation for the SCME channel model. The correlation is averaged over 4000 generated channels as well as over all taps.*

autocorrelation when the Wiener interpolator is used (see Section 5.5.2). The power delay profile is found as an average of power delay profiles from 2000 generated channels.

Figure 7.2 shows the power delay profile for 20 MHz transmission bandwidth. The chosen number of taps for this transmission bandwidth is 27.

7.3 Simulation Scenarios

In Chapter 5 different low-complexity estimation methods were presented for the time-varying channel. The utilized methods are as follows,

- LMMSE CIR estimator and downsampled CIR estimator:

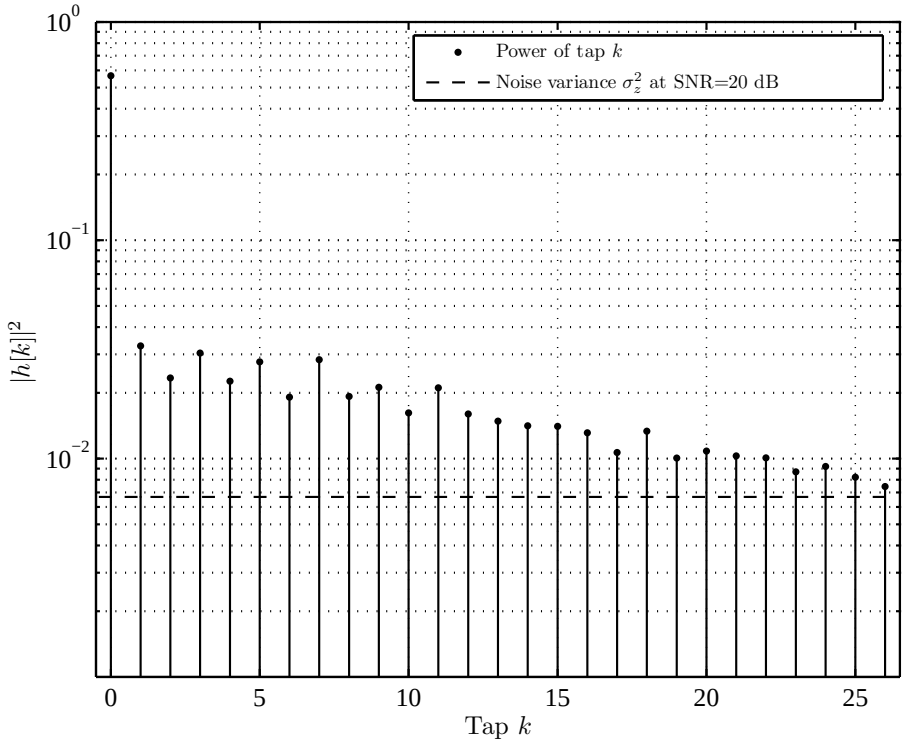

Figure 7.2: *Power delay profile for 20 MHz downlink transmission bandwidth using* $f_s = 30.72\ MHz$.

Channel is first estimated in the frequency domain

and then estimated in the time-domain using Slepian sequences

- Reduced rank LMMSE frequency response estimation, linear interpolation and 2x1D Slepian:

  The channel is first estimated in the time-domain using Slepian sequences

  and then in the frequency-domain.

- 2x1D Wiener Interpolation.

The last method is used as a reference since it has the best MSE performance.
Firstly the performance of the different estimators is evaluated at different signal-to-noise values at 120 km/h. All estimators use the Slepian sequences for estimation purpose in the time-domain.We adapt the Slepian sequences to 120 km/h and evaluate the performance for channel estimation as well as prediction at different speeds below 120 km/h. The evaluation scenarios can be listed as follows

- Channel estimation performance at SNR in the range $[0, \ldots, 20]$ dB with UE at 120 km/h.

- Channel estimation performance at 10 dB SNR with UE at speeds in the range $[0, \ldots, 120]$ km/h.

- Channel prediction performance at 10 dB SNR with UE at 120 km/h.

- Channel prediction performance at 10 dB SNR with UE at speeds in the range $[0, \ldots, 120]$ km/h.

In order to evaluate the performance we apply the 2.5 MHz and 20 MHz transmission bandwidths within the UMTS LTE. The SNR level at 10 dB is chosen since this is a typical value for wireless communications.

7.4 Evaluation

We apply the same procedure to investigate the 2.5 MHz bandwidth as for the 20 MHz bandwidth. The used parameters are listed in Table 7.1. The power delay profile for 2.5 MHz transmission bandwidth is depicted on Figure 3.3. For each OFDM symbol, the estimated frequency response

Parameters	Values
Channel model	Urban macro
Number of simulations	400
Taps	12 (27)
Cyclic Prefix	Long
Block size	48 OFDM symbols
Sampling frequency	3.84 MHz (30.72 MHz)
Dimension D for Slepian Sequences in time-domain	4 (5)
Speed of UE	120 km/h
Dimension D_f of Slepian sequences in frequency-domain	12 (27)

Table 7.1: *Parameters used in simulation for 2.5 MHz and 20 MHz downlink transmission bandwidth. For the latter case the changed parameters are specified in the round brackets.*

of the channel is compared to the true frequency response. The true frequency response is found as the Fourier transform of the channel impulse response. The performance of the estimators is measured in the MSE (mean square error) sense between the true channel and the estimated channel. The frequency response is compared in the range of the used subcarriers (see also Figure 2.2), since the estimates are used for these positions only.

7.4.1 Performance at Different SNR

The achieved mean square error for different SNR values are depicted on Figure 7.3 for 2.5 MHz transmission bandwidth and on Figure 7.4 for the 20 MHz bandwidth. The simulations are always conducted over 400 different channel iterations.

For the 2.5 MHz transmission bandwidth it is noticeable that the performance of LMMSE CIR estimator is close to the Wiener Interpolator. The downsampled CIR estimator again performs as well as LMMSE CIR for SNR up to 10 dB, hereafter the performance decreases. The reduced performance is caused by the aliasing due to the downsampling as described in Section 4.4.3. The

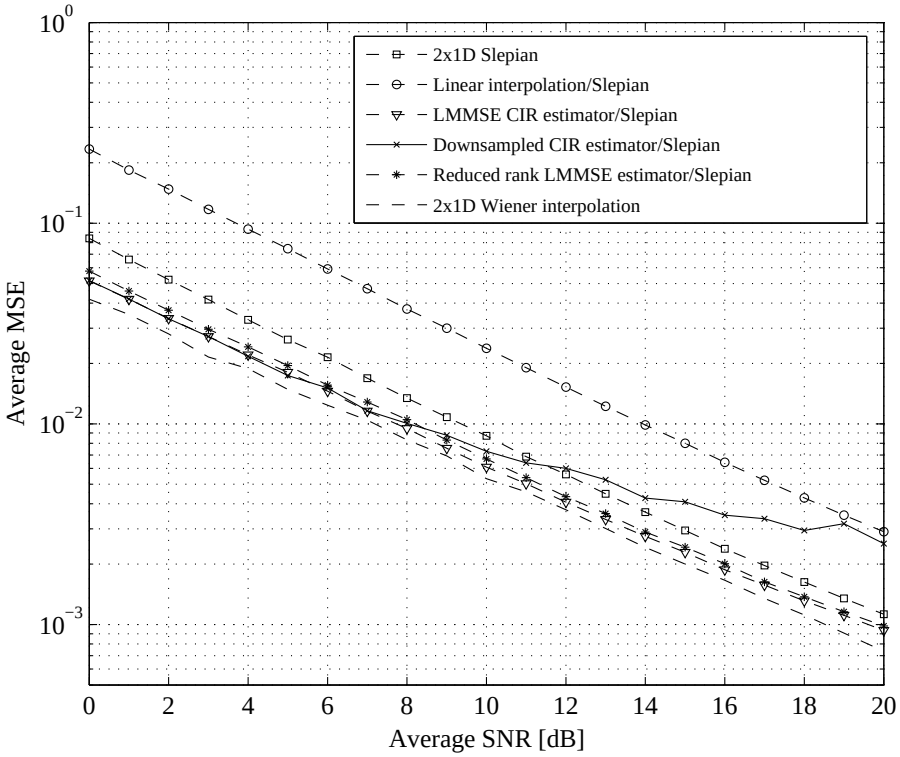

Figure 7.3: *MSE performance with 2.5 MHz transmission bandwidth at different SNR.*

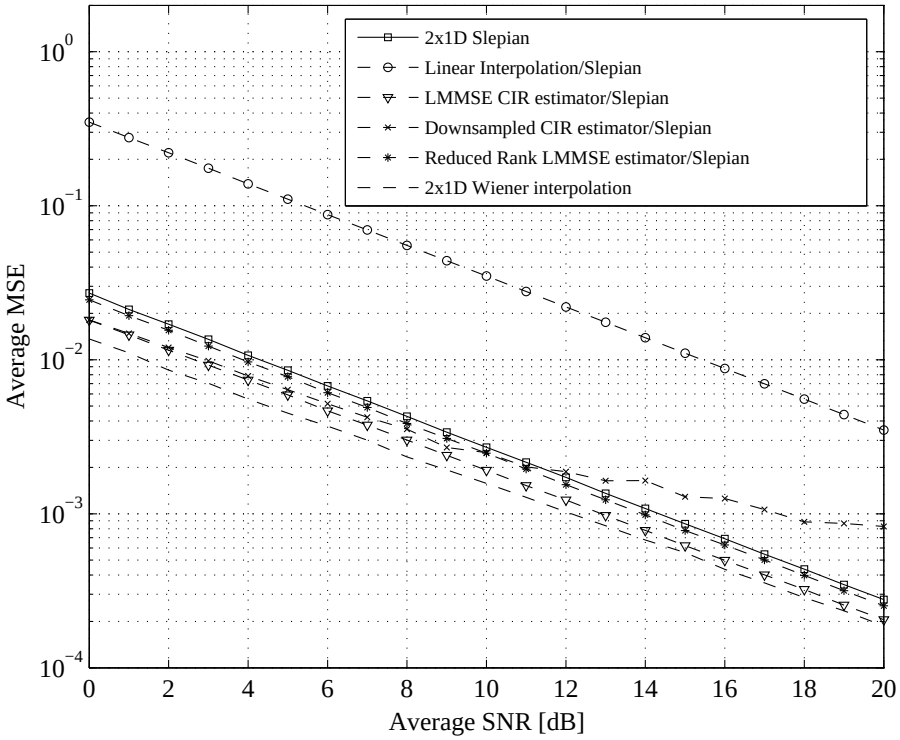

Figure 7.4: *MSE performance with 20 MHz transmission bandwidth at different SNR.*

reduced rank LMMSE estimator performs worse followed by 2x1D Slepian estimator. The linear interpolation has the worst performance of all estimators.

For the 20 MHz transmission bandwidth in general the mean square error is lower compared to 2.5 MHz transmission bandwidth. It is again noticeable that the performance of LMMSE CIR estimator is closest to the performance of the 2x1D Wiener interpolator. The downsampled CIR estimator performs as well as LMMSE CIR for SNR up to 10 dB. For higher SNR its performance decreases as for the 2.5 MHz case. Linear interpolation has the worst performance which differs by an order of one magnitude from the rest of the estimators.

7.4.2 Channel Estimation at Different Speeds

The estimators must also be able to perform at speeds below 120 km/h, hence the performance of channel estimation is investigated for the different estimators at speeds below 120 km/h but always with Slepian sequences adapted for 120 km/h. Figure 7.5 depicts the performance from 0 km/h to 120 km/h for the 2.5 MHz transmission bandwidth. Since the 2x1D Wiener interpolator is used as a reference its autocorrelation is adapted for the true speed. The Wiener interpolator

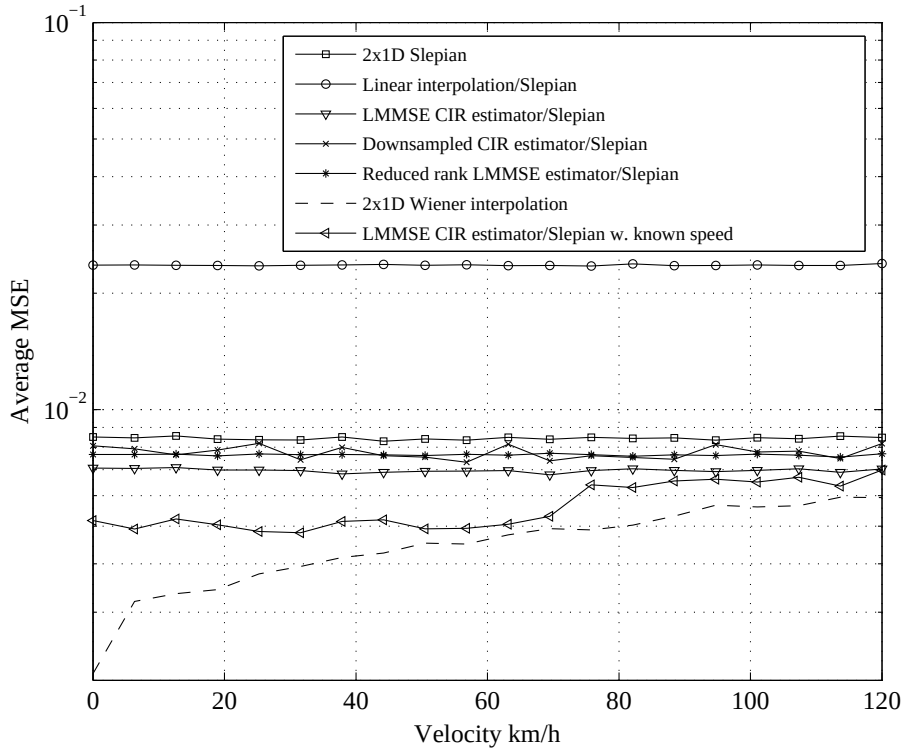

Figure 7.5: *MSE for channel estimation with 2.5 MHz transmission bandwidth at different speed.*

has the best performance, since the Doppler autocorrelation is adapted for each given speed. The estimation errors of all estimators using Slepian sequences adapted for 120 km/h have the same MSE for the different speeds. The LMMSE CIR estimator yields a better performance than the other low-complexity estimators, while the linear interpolator has the worst performance.
In order to see the performance when the Slepian sequences are designed for the specific speeds, the LMMSE CIR estimator is also applied with the mentioned sequences. The performance of this estimator is closest to the 2x1D Wiener interpolator. Figure 7.6 depicts the performance for

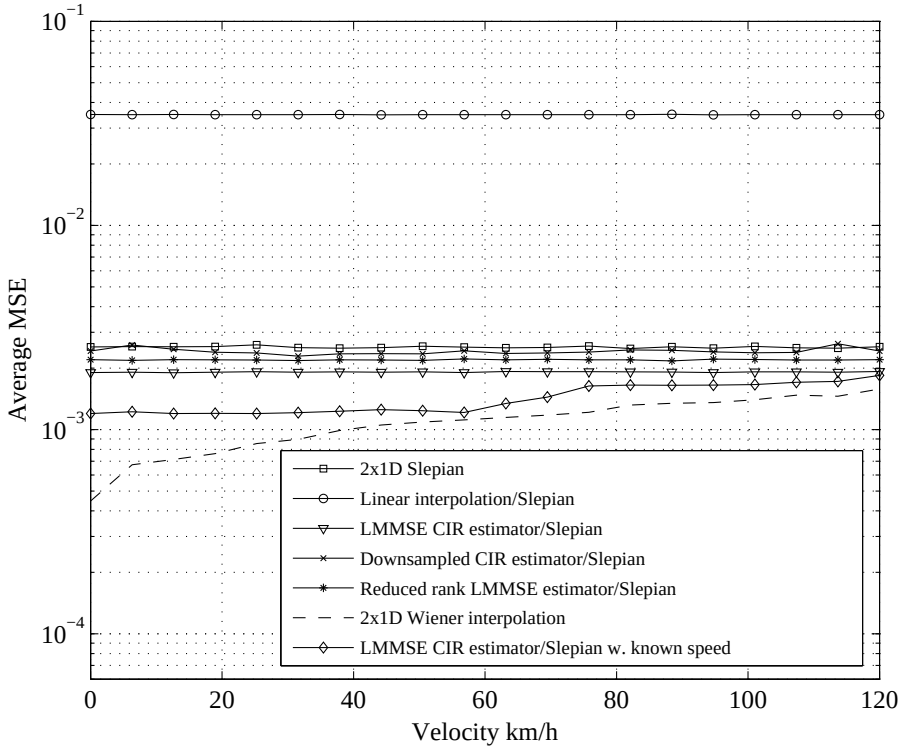

Figure 7.6: *MSE for channel estimation with 20 MHz transmission bandwidth at different speeds.*

the 20 MHz transmission bandwidth. In this case the MSE of all estimators are lower compared to 2.5 MHz transmission bandwidth. The Wiener interpolator has the lowest MSE, while the estimation errors of all estimators using Slepian sequences adapted for 120 km/h have the same MSE for the different speeds. We again apply the LMMSE CIR estimator with the adapted Slepian sequences for the different speeds. The performance of this estimator is closest to the 2x1D Wiener interpolator.

7.4.3 Channel Prediction

As mentioned in Chapter 6 channel prediction is also necessary. The prediction horizon is chosen as 2 subframes, i.e. 24 OFDM symbols and the number OFDM symbols over which the estimation is performed is still $M = 48$. Figure 7.7 depicts the measured MSE for 2.5 MHz transmission bandwidth. The channel is predicted for a UE with velocity 120 km/h. Since the channel is predicted after $m = 47$, the MSE is lower at $m < 48$ because the channel is estimated for this interval, while the MSE increases sharply after $m = 47$ because of the channel is now predicted. In general all estimators, except the linear interpolation, have the same MSE for channel prediction, however the downsampled CIR estimator has the performance closest to the Wiener predictor. The MSE performance for 20 MHz bandwidth is depicted on Figure 7.8. In this case the individual performance of the estimators are in general the same as for 2.5 MHz transmission bandwidth. The downsampled CIR estimator has the same performance for prediction as the other estimators. The resulting MSE increases sharply after $m = 47$. All predicted values have in general the same

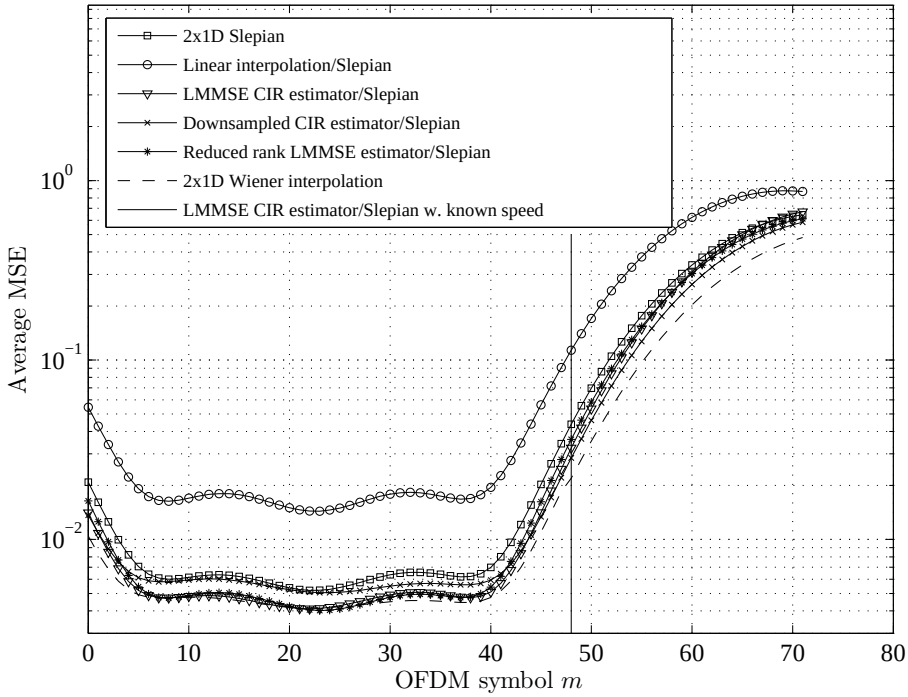

Figure 7.7: *MSE for channel prediction with 2.5 MHz transmission bandwidth at 120 km/h. The prediction starts after the thick vertical black line at $m = 47$. The 2x1D Wiener interpolator apply prediction for $m > 47$ and estimation otherwise.*

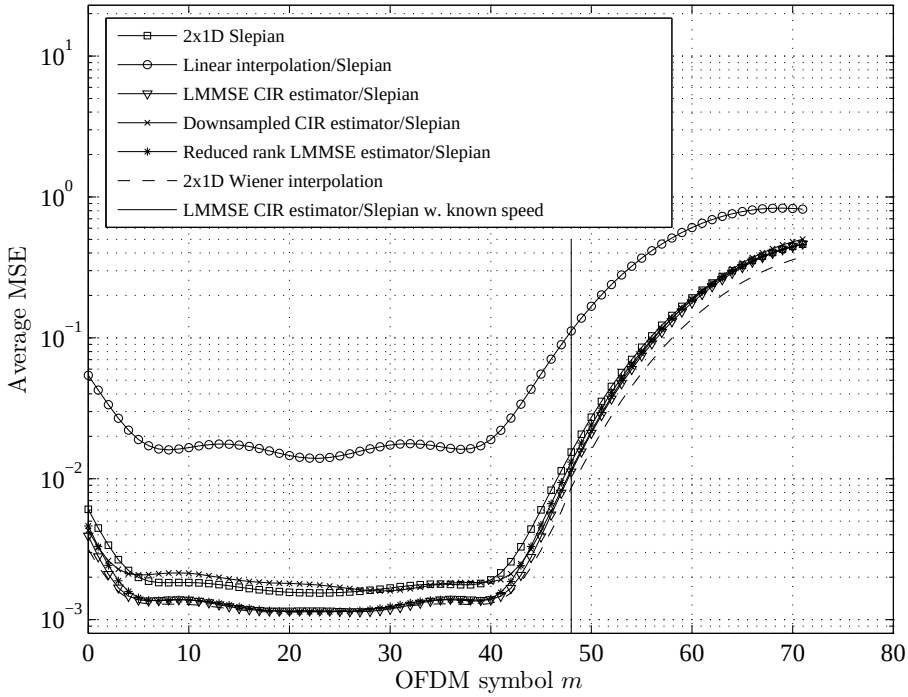

Figure 7.8: *MSE for channel prediction with 20 MHz transmission bandwidth at 120 km/h. The channel is predicted after $m = 47$.The 2x1D Wiener interpolator apply prediction for $m > 47$ and estimation otherwise.*

MSE. Excecpt for the linear interpolation the prediction error has its maximum at $m = 71$. This is the maximum horizon at which we can predict. This prediction horizon $\ell = 24$ corresponds to a covered distance in wavelength λ,

$$d = \frac{v_{\max} \ell T_s}{c_0 / f_c} = \frac{7}{16}\lambda, \tag{7.1}$$

by the UE. Hence we can predict the channel for a movement of maximum $\frac{7}{16}\lambda$ of the wavelength $\lambda = c_0/f_c$. It should be noted that we only calculate the distance at which we have the maximum prediction error. For practical usage the distance, i.e. the prediction horizon may be reduced.

7.4.3.1 Channel Prediction at Different Speeds

As for the channel estimation in Section 7.4.2 we investigate the performance of channel prediction at speeds below 120 km/h. The Slepian sequence used in time-domain is adapted for 120 km/h. The prediction is performed for OFDM symbol $m = 59$, i.e. the horizon is one subframe (12 OFDM symbols). Figure 7.9 depicts the MSE for the 2.5 MHz transmission bandwidth. As for

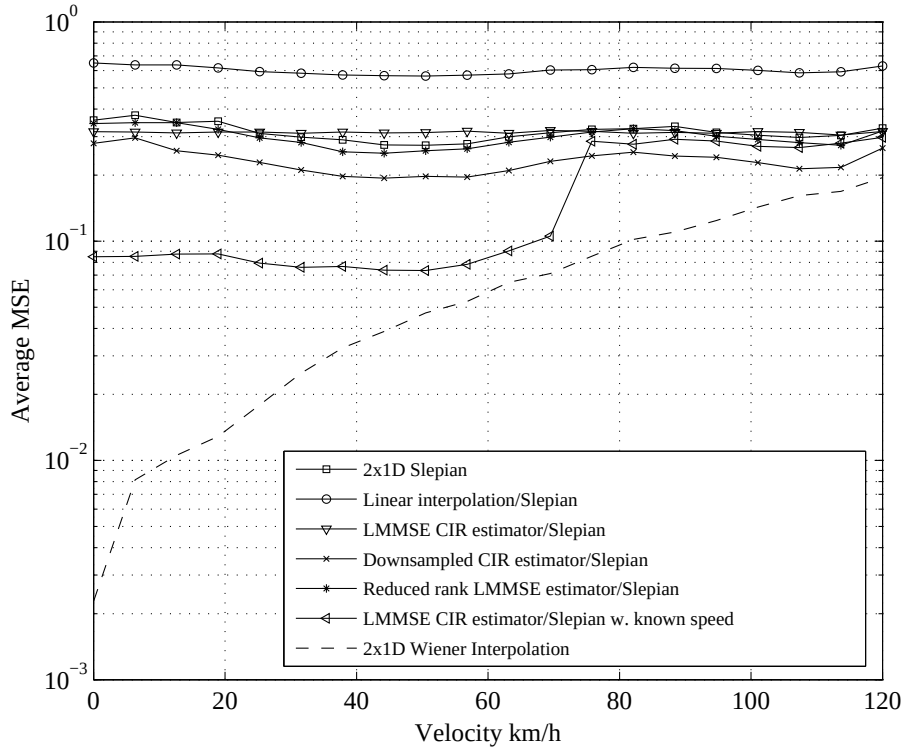

Figure 7.9: *MSE for channel prediction with 2.5 MHz at different speeds.*

the estimation case the prediction errors have the MSE for the estimators with Slepian sequences adapted for 120 km/h through out the range of chosen speeds. The downsampled CIR estimator has the lowest MSE compared to the other low-complexity estimators. Figure 7.10 depicts the same scenario for the 20 MHz transmission bandwidth. For this transmission bandwidth it is not possible to discriminate between the performance of the low-complexity estimators. Again the prediction errors have the MSE for the estimators with Slepian sequences adapted for 120 km/h.

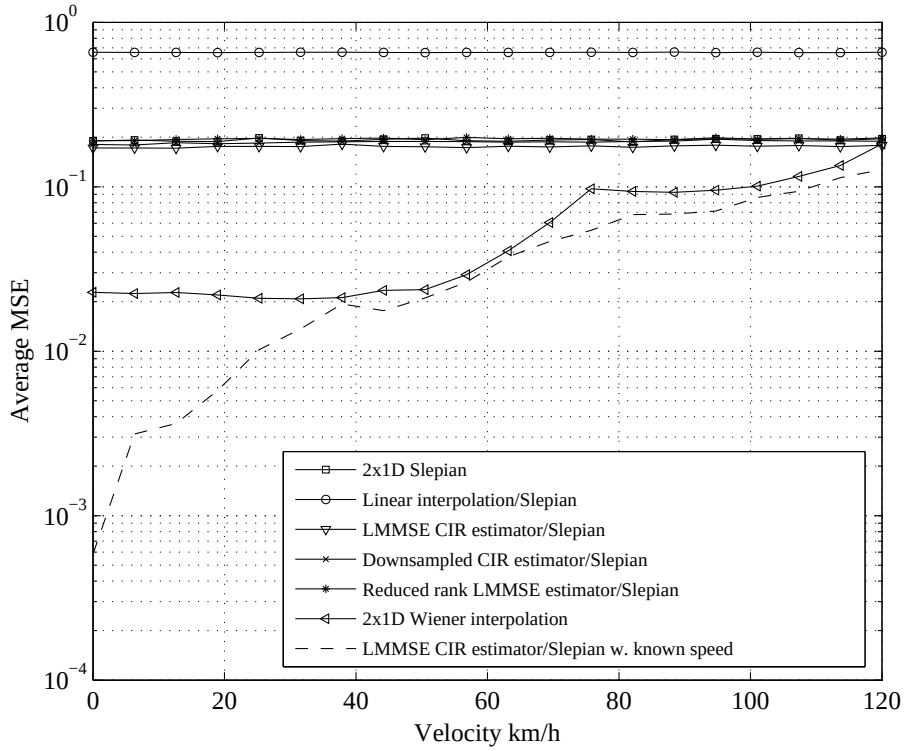

Figure 7.10: *MSE for prediction with 20 MHz transmission bandwidth at different speeds.*

However if the speed is known as for the LMMSE estimator using Slepian sequences adapted to the speed then the achieved MSE is lower and closest to the Wiener predictor.

7.5 Summary

The performance of the presented methods for time-variant channel estimation has been simulated with the SCME channel model. The autocorrelation of the Doppler spectrum from the SCME model is found numerically. The different estimators have been evaluated at 2.5 MHz and 20 MHz downlink transmission bandwidths. All estimators are compared to the 2x1D Wiener interpolation which is used as reference since it consistently yields the lowest MSE. In general the LMMSE CIR estimator using Slepian sequences shows the best MSE performance of all estimators, since it is closest to the 2x1D Wiener interpolator. Furthermore it is shown that the prediction horizon for 2.5 MHz as well as 20 MHz transmission bandwidths corresponds to a covered distance of approximately one half of the wavelength λ at 120 km/h.

8 Conclusion and Future Work

In order to ensure competitiveness for the next few years a long-term evolution of the 3GPP radio-access technology is currently developed. In this thesis important properties of the physical layer in UMTS-LTE downlink have been investigated based on specifications in Release 7 and on working assumptions in Release 8.

OFDMA is utilized as multiple access scheme in the downlink. One of the most important aspects in an OFDM system is a reliable and accurate channel estimation.

In order to perform realistic simulations, channel models with time-invariant and time-varying behavior have been investigated. The chosen channel model is the Spatial Channel Model Extended (SCME), which generates channel coefficients based on 3GPP channel model specifications. The channel model supports a typical urban area scenario as well as mobility of the UE. The SCME model is implemented with the LTE downlink structure in Matlab.

Different low-complexity estimation methods have been presented, all based on Slepian sequences. The channel is estimated using Slepian sequences in the time-dimension, while using LMMSE CIR estimator, downsampled CIR estimator, reduced rank LMMSE estimator, linear interpolation and also Slepian sequences as estimation method in the frequency-domain.

The LMMSE CIR and downsampled CIR present a way to estimate the channel impulse response based on assumptions of the number of taps L. The downsampled CIR furthermore makes use of the fact that the LTE downlink only occupies $2/3$ of the bandwidth.

The complexity of the algorithms have been reviewed and it is shown that the reduced rank LMMSE has the highest complexity, followed by LMMSE CIR estimator and downsampled CIR estimator respectively.

In order to investigate the performance of the presented methods, they are compared to 2x1D Wiener interpolation with perfectly known autocorrelation functions. Using Slepian sequences it is also possible to perform channel prediction in a minimum-energy (ME) band-limited sense such that the information about the channel does not get outdated at the NodeB. It is shown that the maximum prediction horizon at 120 km/h corresponds to a covered distance of one half of the wavelength. Using Slepian sequences for channel estimation as well as prediction in time-domain is similar to the reduced rank Wiener interpolation and prediction respectively with uniform Doppler spectrum assumption, since the subspaces spanned by both estimators are exactly

the same. The performance of the presented methods for time-varying channel estimation has been evaluated with the SCME channel model. The 2.5 MHz and 20 MHz downlink transmission bandwidths within the LTE have been investigated. It has been shown that the LMMSE CIR estimator with the Slepian sequence in general has the MSE performance, since it is closest to the Wiener interpolator. Hence the LMMSE CIR estimator is a good compromise between complexity and performance.

Future work

This thesis investigated channel estimators for the UMTS LTE downlink structure with transmission bandwidths 2.5 MHz and 20 MHz. For future research with other transmission bandwidths the implemented Matlab simulator can easily be reconfigured to evaluate the estimation performance. We have not considered coding in this thesis, hence this is left as future work. The different low-complexity estimators developed in this project can be used with the applied coding in order to find an appropriate estimator. Moreover the evaluation of the estimators shows that if the speed of the UE is below the speed at which the Slepian sequences are adapted, the performance decreases with respect to the Wiener interpolator. Hence possible future work is also to estimate the speed of the UE in order to improve the channel estimation as well as prediction. This work can be based on [27] which already presents an approach for this task.

Bibliography

[1] 3GPP. 3GPP TR 25.913 V7.3.0 Requirements for Evolved UTRA (E-UTRA) and Evolved UTRAN (E-UTRAN) . Technical report, 3GPP, September 2003.

[2] 3GPP. 3GPP TR 25.996 V6.1.0 Spatial Channel Model for Multiple Input Multiple Output (MIMO) simulations (Release 6). Technical report, 3GPP, September 2003.

[3] 3GPP. 3GPP TR 25.943 V6.0.0 Deployment Aspects (Release 6). Technical report, 3GPP, December 2004.

[4] 3GPP. 3GPP TR 25.814 V7.1.0 Physical Layer Aspects for Evolved Universal Terrestrial Radio Access (UTRA) (Release 7). Technical report, 3GPP, September 2006.

[5] 3GPP. 3GPP TS 36.211 V0.3.1 Physical Channels and Modulation (Release 8). Technical report, 3GPP, February 2007.

[6] Andrea Ancora, Calogero Bona, and Dirk T M Slock. Down-sampled Impulse Response Least-Squares Channel Estimation for LTE OFDMA. In *ICASSP 2007, 32nd IEEE International Conference on Acoustics, Speech, and Signal Processing, Honolulu, USA*, Apr 2007.

[7] P. Dent, G.E. Bottomley, and T. Croft. Jakes fading model revisited. In *Electronics Letters*, volume 29, pages 1162–1163, 24 June 1993.

[8] O. Edfors, M. Sandell, J. van de B., B. Wilson, and P. Börjesson. OFDM Channel Estimation by Singular Value Decomposition. In *IEEE Vehicular Technology Conference, Atlanta, USA, pp. 923-927,April 28-May 1.*, 1996.

[9] B.H. Fleury. An Uncertainty Relation for WSS Processes and Its Application to WSSUS Systems. *IEEE Transactions on Communications*, 44(12):1632–1634, Dec. 1996.

[10] G. H. Golub and C. F. Van Loan. *Matrix Computations*. Baltimore, MD, USA, second edition, 1989.

[11] S Haykin. *Adaptive Filter Theory*. Prentice-Hall, Inc., Upper Saddle River, NJ, USA, 1995.

[12] Harri Holma and Antti Toskala. *WCDMA for UMTS*. John Wiley & Sons, Inc., New York, NY, USA, 2002.

[13] Stefan Kaiser. *Multi-Carrier CDMA Mobile Radio Systems – Analysis and Optimization of Detection, Decoding, and Channel Estimation*. PhD thesis, University of Kaiserslautern, Germany, January 1998. VDI Verlag Düsseldorf, Series 10, No. 531, ISBN 3-18-353110-0.

[14] Steven M. Kay. *Fundamentals of Statistical Signal Processing: Estimation Theory*. Prentice-Hall, Inc., Upper Saddle River, NJ, USA, 1993.

[15] Louis Litwin and Michael Pugel. The principles of OFDM, January 2001.

[16] Andrew M. Odlyzko. Internet traffic growth: Sources and implications, 2003.

[17] Alan V. Oppenheim and Ronald W. Schafer. *Digital Signal Processing*. Prentice–Hall, 1989.

[18] M.K. Ozdemir, H. Arslan, and E. Arvas. Adaptive Low-Rank MIMO-OFDM Channel Estimation. In *Wireless and Microwave Technology, 2005. WAMICON 2005. The 2005 IEEE Annual Conference*, page 5pp., 2005.

[19] S. Parkvall, E. Englund, M. Lundevall, and J. Torsner. Evolving 3G Mobile Systems: Broadband and Broadcast Services in WCDMA. *IEEE Communications Magazine*, 44(2):30–36, Feb. 2006.

[20] A. Pokhariyal, G. Monghal, K. I. Pedersen, P. E. Mogensen, I. Z. Kovacs, C. Rosa, and T. E. Kolding. Frequency Domain Packet Scheduling Under Fractional Load for the UTRAN LTE Downlink. In *Vehicular Technology Conference, 2007. VTC2007-Spring. IEEE 65th*, pages 699–703, April 2007.

[21] Jari Salo, Giovanni Del Galdo, Jussi Salmi, Pekka Kyösti, Marko Milojevic, Daniela Laselva, and Christian Schneider. MATLAB implementation of the 3GPP Spatial Channel Model (3GPP TR 25.996). On-line, January 2005. http://www.tkk.fi/Units/Radio/scm/.

[22] D. Slepian. Prolate spheroidal wave functions, Fourier analysis, and uncertainty. V - The discrete case. *AT&T Technical Journal*, 57:1371–1430, June 1978.

[23] Antti Toskala, Harri Holma, Kari Pajukoski, and Esa Tiirola. Utran Long Term Evolution in 3GPP. In *IEEE 17th International Symposium on Personal, Indoor and Mobile Radio Communications*, pages 1–5, Sept. 2006.

[24] J.-J. van de Beek, O. Edfors, M. Sandell, S.K. Wilson, and P.O. Borjesson. On Channel Estimation in OFDM Systems. In *IEEE 45th Vehicular Technology Conference*, volume 2, pages 815–819vol.2, 25-28 July 1995.

[25] T. Zemen, H. Hofstetter, and G. Steinbock. Successive Slepian Subspace Projection in Time and Frequency for Time-Variant Channel Estimation, 2005.

[26] T. Zemen and C.F. Mecklenbrauker. Time-Variant Channel Estimation Using Discrete Prolate Spheroidal Sequences. *IEEE Transactions on Signal Processing,*, 53(9):3597–3607, Sept. 2005.

[27] T. Zemen and Fleury B. H. Mecklenbrauker, Kaltenberger F. Minimum-Energy Band-Limited Predictor with Dynamic Subspace Selection for Time-Variant Flat-Fading Channels. *IEEE Transactions on Signal Processing*, 2007. Accepted (2006-12-06), to be published.

[28] Thomas Zemen. *OFDM Multi-User Communication Over Time-Variant Channels*. PhD thesis, 2004. ISBN 3-902477-04-0.

Orthogonal Frequency Division Multiplexing systems

A

In high data rate, wideband communication through multipath fading channel, the received signals are affected by inter-symbol interference (ISI) due to the fact that the time spread of the channel is relatively large compared to the symbol duration. Reducing ISI is an important issue for enhancing the quality of wideband communications.
Normally ISI is removed by channel equalization, which is implemented either in the time or frequency domain, with symbol-by-symbol or sequence estimation algorithms.
If the symbol rate is reduced, while the information rate is remained, the impact of ISI becomes negligible and equalization becomes unnecessary. One method is to increase the constellation size in an Q-ary pulse modulation scheme. However, there is a limit on how large Q can be before modulation and demodulation becomes too complex.
Multicarrier modulation offers another approach. A serial high rate data stream is distributed into many parallel low rate data streams, transmitted through many orthogonal narrowband subcarriers, thus the symbol duration in each channel is large enough that the ISI can be negligible.
In this Appendix, the principle of multicarrier modulation is reviewed, followed by a review of OFDM, which is based on [15].

A.1 Multicarrier Modulation System

The concept of multicarrier modulation is illustrated in Figure A.1. The idea is to divide the transmitted bitstream into many different substreams and send them over many different subcarriers.
The data rate on each of the subcarriers is less than the total data rate, and the corresponding subcarrier bandwidth is less than the total system bandwidth. Multicarrier modulation can be seen as a parallel transmission scheme developed to eliminate ISI by extending the symbol interval. However, parallel transmission requires separate modulation and demodulation for each subcarrier. High data rate transmission requires a large number of subcarriers, which makes the implementation of multicarrier transmitter and receiver complex. A more feasible way to implement multicarrier modulation leads to the concept of OFDM.

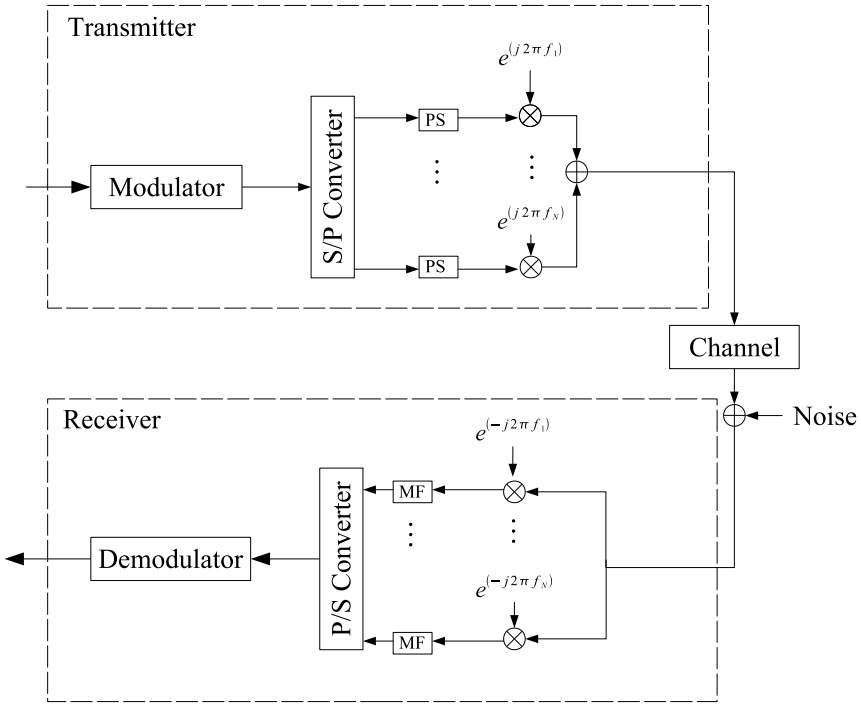

Figure A.1: *Basic structure of multicarrier modulation system. 'PS' is the pulse shaping filter at the transmitter side, while 'MF' is the matched filter at receiver side.*

A.2 Concept of OFDM System

OFDM is a feasible method to implement multicarrier modulation scheme which combats the ISI in multipath fading channel with spectral efficiency.

As mentioned above, the requirement for separate modulator and demodulator on each subcarrier is complex to be implemented. OFDM makes the modulation in parallel transmission be easily implemented. In OFDM, spectrum efficiency is increased by the fact that the spectrums of the subcarriers overlap, as shown in Figure A.3. The information transmitted over the carriers can still be separated because they are orthogonal. The orthogonal carriers can be created using inverse fast Fourier transformation ((IFFT)). The frequency spacing between the subcarriers is determined by the sampling frequency f_{s} and the number of points, N_{IFFT}, in the IFFT.

$$f_{\mathrm{space}} = \frac{f_{\mathrm{s}}}{N_{\mathrm{IFFT}}} \tag{A.1}$$

A.3 Orthogonality

An OFDM system is shown in Figure A.2. The Fast Fourier Transform (FFT) algorithms are used to generate orthogonal subcarriers due to their computational efficiency [15]. The IFFT operation results in the composite OFDM symbol of duration T_{s}. The idea behind using IFFT to modulate

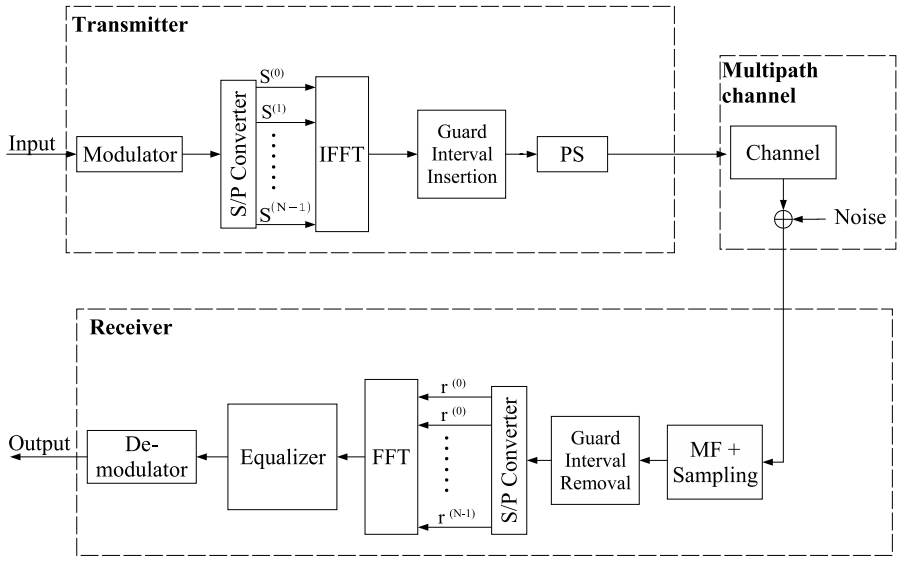

Figure A.2: *Basic structure of an OFDM system. 'PS' is the pulse shaping filter at the transmitter side while 'MF' is the matched filter at the receiver side.*

subcarriers starts by writing each modulated subcarrier as [15]

$$s_n(t) = A_n(t)e^{j(2\pi nft+\phi_n(t))} \tag{A.2}$$

where $s_n(t)$ is the n'th modulated subcarrier, $A_n(t)$ and $\phi_n(t)$ are the modulated amplitude and phase of the n'th subcarrier respectively, f is the frequency spacing between subcarriers, i.e. subcarriers are a group of harmonic sinusoids. The composite OFDM signal is then the summation of all N_{IFFT} subcarriers [15].

$$S(t) = \sum_{n=-\frac{N_{\text{IFFT}}}{2}}^{\frac{N_{\text{IFFT}}}{2}-1} s_{(t)} = \sum_{n=-\frac{N_{\text{IFFT}}}{2}}^{\frac{N_{\text{IFFT}}}{2}-1} A_n(t)e^{j(2\pi nft+\phi_n(t))} \tag{A.3}$$

where N is an even number of subcarriers and $S(t)$ is a baseband signal that is subsequently upconverted to the desired carrier frequency before transmission. Now sampling $S(t)$ over one OFDM symbol period T_{s}, with a sampling frequency of $f_s = \frac{1}{T_C}$, results in [15]

$$S(kT_{\text{C}}) = \sum_{n=-\frac{N_{\text{IFFT}}}{2}}^{\frac{N_{\text{IFFT}}}{2}-1} A_n e^{j(2\pi fknT_{\text{C}}+\phi)} \tag{A.4}$$

where $T_{\text{s}} = N \cdot T_{\text{C}}$ and the amplitude and phase of each subcarrier are constant in the duration of one OFDM symbol, i.e. $A_n(t) = A_n$ and $\phi_n(t) = \phi_n$. Therefore,

$$S(kT_{\text{C}}) = \sum_{n=-\frac{N_{\text{IFFT}}}{2}}^{\frac{N_{\text{IFFT}}}{2}-1} A_n e^{j\phi} e^{j\frac{2\pi}{N_{\text{IFFT}}}fknT_{\text{s}}} \tag{A.5}$$

Comparing with the IDFT equation [17],

$$S(kT_{\mathrm{C}}) = \sum_{n=-\frac{N_{\mathrm{IFFT}}}{2}}^{\frac{N_{\mathrm{IFFT}}}{2}-1} A_n e^{j\phi} e^{j\frac{2\pi}{N_{\mathrm{IFFT}}}kn} \tag{A.6}$$

shows that both equations are equal if $f = \frac{1}{T_{\mathrm{s}}}$. This condition ensures that all N subcarriers are orthogonal. Orthogonality is clear from examining the spectrum of the OFDM signal in Figure A.3. The IFFT block samples the spectrum at the peak of each sinc function to map A_n and ϕ_n to subcarriers. This results in no interference between subcarriers. The overlapping spectra is not of importance because the peak of each sinc functions coincides with zero crossings of all other sinc functions. In the time domain, orthogonality means that all subcarriers have an integer multiple of periods in each symbol period T_{s} as shown in Figure A.4.

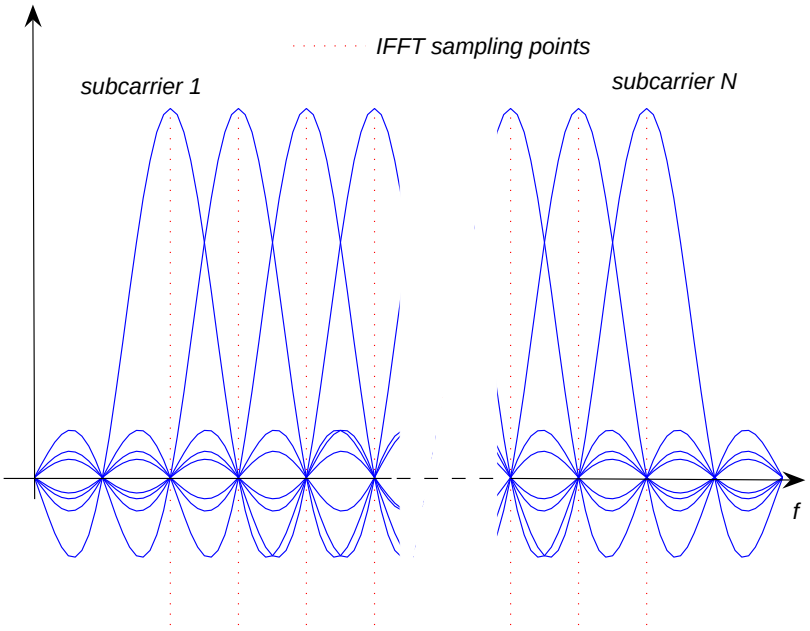

Figure A.3: *The spectrum of an OFDM signal consists of overlapping sinc functions. Each sinc function is sampled at its peak, which coincides with zero crossings of all other functions [15].*

A.4 Advantages of OFDM

A.4.1 Immunity to Frequency Selective Fading

Because of the nature of a mobile environment, multiple delays of the transmitted signal reach a mobile receiver. Delay spread results in a frequency selective fading channel response. Hence, some signal frequencies are enhanced while others suffer from deep fades. This affects both the amplitude and phase modulation of the carrier and consequently results in information loss. In order to combat frequency selective fading, OFDM uses a signal bandwidth that is much smaller than the coherence bandwidth associated with the estimated delay spread of the channel. This

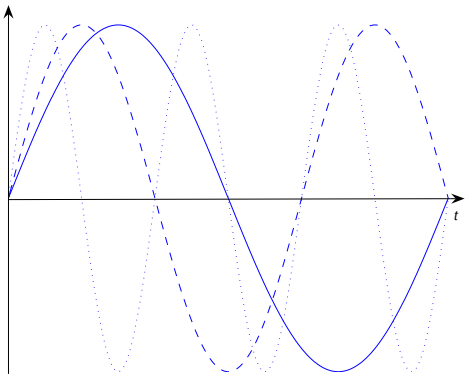

Figure A.4: *Orthogonality in the time domain means that all subcarriers in an OFDM signal have an integer number of periods during the period of one OFDM symbol [15].*

way, each subcarrier experiences fading and only some bits are lost if some of the subcarriers experience deep fades [15].

A.5 Immunity to Inter-Symbol Interference

In OFDM, dividing the incoming bit stream over N subcarriers increases the symbol duration by a factor of N. The symbol period is made greater than the delay spread of the channel. This way the effect of ISI is restricted to one symbol duration only, and only the first few samples of each period are distorted. Furthermore, to avoid such distortion, OFDM can use a cyclic prefix CP (or guard interval) before each OFDM symbol. Thus, all distortion due to ISI occurs in this CP, which would then be discarded at the receiver. The length of CP must be carefully chosen, as a very short CP does not totally remove ISI distortion while a very long CP decreases the throughput of the system. In CP-OFDM the last L_{CP} samples in each OFDM symbol are copied and added to the beginning of symbol as shown in Figure A.5. Adding a cyclic prefix CP also achieves continuous transmission required for transmitter/ receiver synchronization (as opposed to a zero-padding) [15]. In addition, such a cyclic prefix makes the signal appear periodic and that makes it possible to use frequency domain equalization.

A.6 Disadvantages of OFDM

A.6.1 High Peak-to-Average Power Ratio

Because an OFDM signal is composed of multiple subcarriers that are independently modulated, the amplitude of the signal's envelope can reach high peaks if all subcarriers add coherently. When compared to the envelope's average amplitude level, such peaks result in a high Peak-to-Average Power Ratio (PAPR) [15]. An OFDM signal composed of N_{IFFT} subcarriers can have a PAPR equal to 10 log N [15].

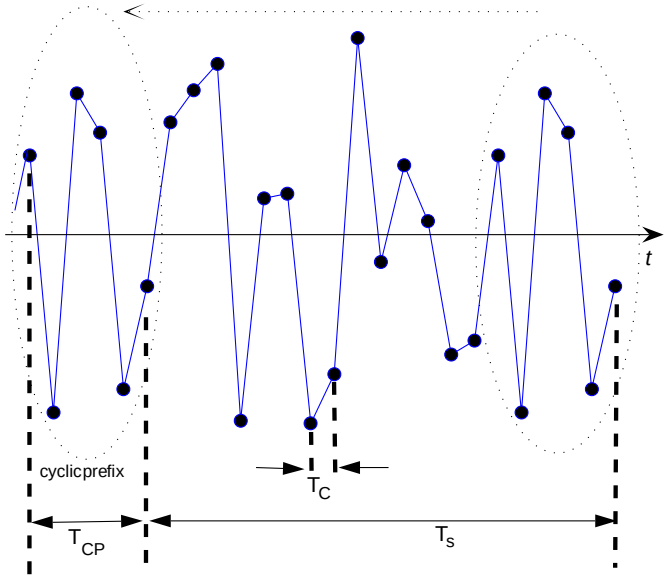

Figure A.5: *A cyclic prefix CP is added before each OFDM symbol [15]. This achieves continuous transmission of all subcarriers required for transmitter/receiver synchronization and makes it possible to use simple frequency domain equalization.*

A.6.2 Sensitivity to Frequency and Time Synchronization

An OFDM receiver's ability to separate the overlapping subcarriers of an OFDM signal relies on orthogonality of these subcarriers. In an OFDM system, frequency and time synchronization between the transmitter and the receiver are crucial to maintain orthogonality of the subcarriers. Loss of orthogonality results in inter carrier interference (ICI) and ISI [15]. The effect of imperfect frequency synchronization between the transmitter and receiver in an OFDM system can be shown by examining (A.5) once again [15],

$$S(kT_C) = \sum_{n=-\frac{N_{\text{IFFT}}}{2}}^{\frac{N_{\text{IFFT}}}{2}-1} A_n e^{j\phi} e^{j\frac{2\pi}{N_{\text{IFFT}}}kn}. \tag{A.7}$$

As mentioned in Section A.3, $S(kT_{\text{C}})$ is the baseband discrete-time OFDM signal. The upconverted transmitted signal, $S_{\text{UC}}(t)$, is then the analog version of $S(kT_{\text{C}})$. The analog version is a result of a convolution between pulse shaping filter and the discrete signal, which is also depicted on Figure A.2.

$S(t)$ is upconverted to the desired carrier frequency f_c [15],

$$S_{\text{UC}}(t) = S(t)e^{j2\pi f_c t} \tag{A.8}$$

Now, at the receiver side, $S_{\text{UC}}(t)$ should be downconverted to baseband by multiplying the signal with the term $e^{-j2\pi f_c t}$ to obtain $S(t)$ once again. However, if the receiver's local oscillator

frequency is $f_c + f_{\text{off}}$ instead of being exactly f_c, the baseband signal received, $S_{\text{offset}}(t)$, is then

$$S_{\text{offset}}(t) = S_{\text{UC}}(t)e^{-j2\pi(f_c+f_{\text{off}})t} = S(t)e^{-j2f_{\text{off}}t} \tag{A.9}$$

where f_{off} is the receiver's frequency error due to a frequency shift. The term $e^{-j2f_{\text{off}}t}$ accounts for ICI occurring due to the receiver's frequency error. In other words, subcarriers no longer have integer number of periods during an OFDM symbol period. Now, assuming a perfect matched filtering and sampling frequency at the receiver, $S(t)$ results in a discrete time signal, $S(kT_C)$, in the form [15]

$$S_{\text{offset}}(kT_{\text{C}}) = S(kT_C)e^{-j2f_{\text{off}}kT_C} = \sum_{n=-\frac{N_{\text{IFFT}}}{2}}^{\frac{N_{\text{IFFT}}}{2}-1} A_n e^{j\phi_n} e^{-j2f_{\text{off}}kT_{\text{C}}} e^{j\frac{2\pi}{N_{\text{IFFT}}}kn} \tag{A.10}$$

The receiver's FFT block then performs digital demodulation of $S_{\text{offset}}(kT_{\text{C}})$ to restore the transmitted constellation points. In effect, this is equivalent to multiplying $S(kT_{\text{C}})$ with the term $e^{j\frac{2\pi}{N_{\text{IFFT}}}kn}$. Therefore, when the distorted signal $S_{\text{offset}}(kT_{\text{C}})$ is applied to the FFT block, the received constellation points are [15]

$$S_{\text{c}}(k) = \sum_{n=-\frac{N_{\text{IFFT}}}{2}}^{\frac{N_{\text{IFFT}}}{2}-1} A_n e^{j\phi_n} e^{-j2f_{\text{off}}kT_{\text{C}}}, \tag{A.11}$$

where $S_{\text{c}}(k)$ are the constellation points obtained at the output of the FFT block.
Hence, the effect of imperfect frequency synchronization is a phase rotation of constellation points by an angle $\phi_{error} = 2f_{\text{off}}kT_{\text{C}}$. It can be seen that ϕ_{err} increases with both the frequency error and time.
Loss of orthogonality can also result from loss of timing synchronization. At the receiver side, the boundaries of OFDM symbols have to be located in order to apply the FFT window at the right time.

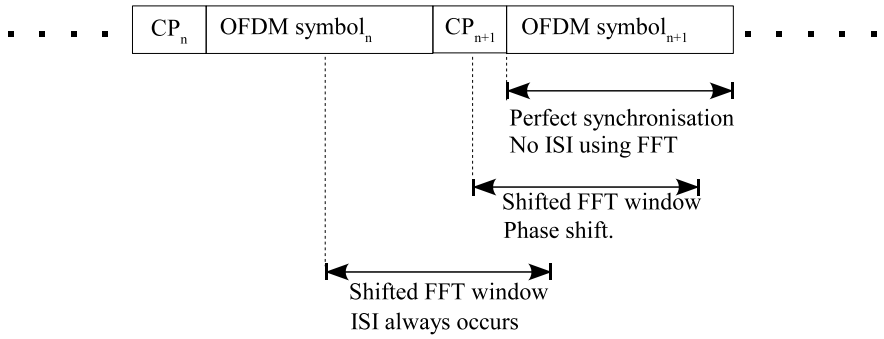

Figure A.6: *When there is a time shift, ISI occurs and hence received constellation points are distorted.*

A.7 OFDM Signal Model

The properties of OFDM transmission has now been described. This section intends to describe the OFDM transmission and the impact of the channel in mathematical terms following the same

structure as in [28, Sec. 2.3].

At the transmitter side, an OFDM symbol vector $\boldsymbol{d}[m] \in \mathbb{C}^{N_{\text{IFFT}}}$ is mapped into a chip vector $\boldsymbol{\mu}[m]$ at time index m,

$$\boldsymbol{\mu}[m] = \boldsymbol{T}_{\text{CP}} \frac{1}{\sqrt{N_{\text{IFFT}}}} \boldsymbol{F}_{N_{\text{IFFT}}}^{H} \boldsymbol{d}[m]. \tag{A.12}$$

The discrete time has the rate T_{s} and after parallel to serial conversion of $\boldsymbol{\mu}[m]$, the signal is transmitted over a multipath channel.

The N_{IFFT}-point DFT-matrix $\boldsymbol{F}_{N_{\text{IFFT}}} \in \mathbb{C}^{N_{\text{IFFT}} \times N_{\text{IFFT}}}$ with elements

$$[F_{N_{\text{IFFT}}}]_{i,l} = e^{\frac{-j2\pi il}{N_{\text{IFFT}}}}, \quad i, l \in \{0, 1, \ldots N_{\text{IFFT}} - 1\}. \tag{A.13}$$

The cyclic prefix is a result of matrix $\boldsymbol{T}_{\text{CP}}$,

$$\boldsymbol{T}_{\text{CP}} = \begin{bmatrix} \boldsymbol{0}_{N_{\text{IFFT}} - L_{CP}} & \boldsymbol{I}_{\text{CP}} \\ & \boldsymbol{I}_{N_{\text{IFFT}}} \end{bmatrix} \in \mathbb{R}^{P \times N_{\text{IFFT}}}. \tag{A.14}$$

Matrix T_{CP} copies the last L_{CP} chips of each OFDM symbol to the front.

If $\mu[n]$ denotes the chip sequence with rate $1/T_c$ to be transmitted, then

$$\boldsymbol{\mu}[m] = \begin{bmatrix} \mu[mP] \\ \vdots \\ \mu[mP + P - 1] \end{bmatrix} \in \mathbb{C}^{P} \tag{A.15}$$

is the chip sequence sequence of one OFDM symbol.

Let us assume that the multipath channel $h'[k]$ has an length L.

$$\boldsymbol{h}' = \begin{bmatrix} h'[0] \\ \vdots \\ h'[L-1] \end{bmatrix} \in \mathbb{C}^{L} \tag{A.16}$$

The received signal at the UE without noise is given by

$$x[n] = \sum_{k=0}^{L} h[k]\mu[n-k]. \tag{A.17}$$

The received signal $\boldsymbol{r}$ is also affected by white Gaussian noise $z[n]$ $(N)(0, \sigma_z^2)$,

$$r[n] = x[n] + z[n]. \tag{A.18}$$

The elements $x[n]$ and $z[n]$ has the following structure for each OFDM symbol,

$$\boldsymbol{x}[m] = \begin{bmatrix} x[mP] \\ \vdots \\ x[mP + P - 1] \end{bmatrix} \in \mathbb{C}^{P} \tag{A.19}$$

and

$$\boldsymbol{z}[m] = \begin{bmatrix} z[mP] \\ \vdots \\ z[mP+P-1] \end{bmatrix} \in \mathbb{C}^P. \tag{A.20}$$

The influence of the channel is included by taking the lower and upper triangular Toeplitz channel matrix into account.

$$\boldsymbol{H}^{(0)} = \begin{bmatrix} h'[0] & 0 & & & & 0 \\ \vdots & \ddots & & & & \vdots \\ h'[L-1] & & & & & \\ 0 & \ddots & & & & \\ \vdots & \ddots & & & & 0 \\ 0 & \dots & 0 & h'[L-1] & \dots & h'[0] \end{bmatrix} \in \mathbb{C}^{P\times P} \tag{A.21}$$

and

$$\boldsymbol{H}^{(1)} = \begin{bmatrix} 0 & \dots & 0 & h'[L-1] & \dots & h'[1] \\ & \ddots & & \ddots & \ddots & \vdots \\ & & & & & h'[L-1] \\ 0 & & & & & 0 \\ \vdots & & & & & \vdots \\ 0 & \dots & & & & 0 \end{bmatrix} \in \mathbb{C}^{P\times P} \tag{A.22}$$

are the upper and lower triangular Toeplitz channel matrix respectively.
Now the intersymbol interference is modeled as,

$$\boldsymbol{x}[m] = \boldsymbol{H}^{(0)}\boldsymbol{\mu}[m] + \boldsymbol{H}^{(1)}\boldsymbol{\mu}[m-1], \tag{A.23}$$

where the second term represents the inter-symbol interference between two consecutive OFDM symbols, which affect the first L samples of $\boldsymbol{x}[m]$.
At the receiver the cyclic prefix of length L_{CP} is removed by forming the product

$$\boldsymbol{R}_{\text{CP}}\boldsymbol{H}^{(1)} = \boldsymbol{0}_{N_{\text{IFFT}}\times P}, \quad \text{where} \tag{A.24}$$

$$\boldsymbol{R}_{\text{CP}} = [\boldsymbol{0}_{N_{\text{IFFT}}\times L_{CP}}\boldsymbol{I}_{N_{\text{IFFT}}}] \in \mathbb{R}^{N_{\text{IFFT}}\times P}, \tag{A.25}$$

with $\boldsymbol{0}_{N_{\text{IFFT}}\times P}$ and $\boldsymbol{0}_{N_{\text{IFFT}}\times L_{CP}}$ as matrices containing zeros with the dimensions $N_{\text{IFFT}} \times P$ and $N_{\text{IFFT}} \times L_{CP}$ respectively. Equation (A.24) only holds if the maximum channel delay $L-1$ is less than or equal to the cyclic prefix L_{CP}. The received signal is now written as,

$$\begin{aligned} \boldsymbol{y}[m] &= \boldsymbol{F}\boldsymbol{R}_{\text{CP}}(\boldsymbol{x}[m] + \boldsymbol{z}[m]) = \boldsymbol{F}\boldsymbol{R}_{\text{CP}}\boldsymbol{H}^{(0)}\boldsymbol{\mu}[m] + \boldsymbol{F}\boldsymbol{R}_{\text{CP}}\boldsymbol{z}'[m] \\ &= \boldsymbol{F}\boldsymbol{R}_{\text{CP}}\boldsymbol{H}^{(0)}\boldsymbol{T}_{\text{CP}}\boldsymbol{F}^H_{N_{\text{IFFT}}}\boldsymbol{d}[m] + \boldsymbol{F}\boldsymbol{R}_{\text{CP}}\boldsymbol{z}[m] \\ &= \boldsymbol{F}\bar{H}\boldsymbol{F}^H_{N_{\text{IFFT}}}\boldsymbol{d}[m] + \boldsymbol{R}_{\text{CP}}\boldsymbol{z}[m], \end{aligned} \tag{A.26}$$

where $\in \mathbb{C}^{N_{\text{IFFT}} \times N_{\text{IFFT}}}$ is the overall circulant channel matrix and can be decomposed as,

$$\bar{H} = \boldsymbol{R}_{\text{CP}} \boldsymbol{H}^{(0)} \boldsymbol{T}_{\text{CP}} = \boldsymbol{F}_{N_{\text{IFFT}}}^{H} \text{diag}(\boldsymbol{g}) \boldsymbol{F}_{N_{\text{IFFT}}}, \tag{A.27}$$

where $\boldsymbol{g} \in \mathbb{C}^{N_{\text{IFFT}}}$ is defined as the DFT of the channel impulse response $\boldsymbol{h}'$,

$$\boldsymbol{g} = \boldsymbol{F}_L \boldsymbol{h}', \tag{A.28}$$

with $\boldsymbol{F}_{\text{L}}$ as the truncated version of $\boldsymbol{F}$ with the first L columns. $\boldsymbol{H}^{(0)}$ has a Toeplitz structure and by inserting the cyclic prefix it is circularized. Hence the DFT-matrix are the eigenvectors, while the channel matrix diag$(\boldsymbol{g})$ is diagonal. Using Equation (A.26) and (A.27), the received signal can be expressed as,

$$\boldsymbol{y}[m] = \text{diag}(\boldsymbol{g}) \boldsymbol{d}[m] + \boldsymbol{z}[m]. \tag{A.29}$$

The elements of the noise vector, $\boldsymbol{z}[m]$ are white Gaussian with variance σ_z^2 and the covariance matrix of $\boldsymbol{z}[m]$ is diagonal with identical values

$$\begin{aligned} \boldsymbol{R}_{\boldsymbol{z}[m]} &= \mathbb{E}\left[\boldsymbol{F} \boldsymbol{R}_{\text{CP}} \boldsymbol{z}[m] \boldsymbol{z}[m]^H \boldsymbol{R}_{\text{CP}}^H \boldsymbol{F}^H\right] && \text{(A.30)} \\ &= \sigma_z^2 \boldsymbol{F} \boldsymbol{R}_{\text{CP}} \boldsymbol{R}_{\text{CP}}^H \boldsymbol{F}^H && \text{(A.31)} \\ &= \sigma_z^2 \boldsymbol{I}_{N_{\text{IFFT}}}. && \text{(A.32)} \end{aligned}$$

From Equation (A.29), each symbol vector $\boldsymbol{d}[m]$ is transmitted over an individual frequency-flat subcarrier.

A.8 Summary

Advances in DSPs have generated a great interest in OFDM as a spectrally efficient MCM scheme, that is capable of delivering high data rates. The FFT is the basic algorithm in any OFDM system, because it allows for a computationally efficient implementation. OFDM has high immunity against frequency selective fading and ISI which makes it suitable for mobile communication. OFDM transmission is also very sensitive to frequency and timing errors between the transmitter and the receiver, which result in loss of orthogonality and therefore, ICI and ISI.

Generation of Reference Symbols

B

B.1 Reference Symbol Sequences

The generation of reference symbols is based on [5].
As described in Section 2.4.2 the reference signal sequence $\boldsymbol{R}_{\text{ref}}$ is generated as a symbol-by-symbol product of an orthogonal sequence $\boldsymbol{R}^{\text{OS}} \in \mathbb{C}^{340\times 2}$ and a pseudo-random sequence $\boldsymbol{R}^{\text{PRS}} \in \mathbb{R}^{340\times 2}$. If $r_{m,n}$ is the entry at m'th row and n'th column of $\boldsymbol{R}_{\text{ref}}$, where $m = 0..339$ and $n = 0..1$, then

$$r_{m,n} = r^{\text{OS}}_{m,n} \cdot r^{\text{PRS}}_{m,n}, \tag{B.1}$$

There are $N_{\text{OS}} = 3$ different orthognal sequences and $N_{\text{PRS}} = 170$ different psudo-random sequences. The cells are divided into three identity groups at the physical layer level. There is a one-to-one mapping between the three identities and the three two-dimensional orthogonal sequences.

B.2 Orthogonal Symbol Sequences

The two-dimensional orthogonal sequence is generated as following:

$$r^{\text{OS}}_{m,n} = s_{m,n}, \tag{B.2}$$

where $s_{m,n}$ is the entry at the m'th row and the n'th column of the matrix S_i, defined as

$$S_i^{\text{T}} = \left[\underbrace{S_i^{\text{T}},\ S_i^{\text{T}},\ \ldots, S_i^{\text{T}}}_{114 \text{ repetitions}}\right],\ i = 0...2 \tag{B.3}$$

where

$$S_1^{\text{T}} = \begin{bmatrix} 1 & 1 \\ 1 & 1 \\ 1 & 1 \end{bmatrix} \quad S_1^{\text{T}} = \begin{bmatrix} 1 & e^{j4\pi/3} \\ e^{j2\pi/3} & 1 \\ e^{j4\pi/3} & e^{j2\pi/3} \end{bmatrix} \quad S_1^{\text{T}} = \begin{bmatrix} 1 & e^{j2\pi/3} \\ e^{j4\pi/3} & 1 \\ e^{j2\pi/3} & e^{j4\pi/3} \end{bmatrix} \tag{B.4}$$

B.3 Pseudo-Random Sequences

The definition of the pseudo-random sequences in LTE is still in progress and has not yet been determined. At present knowledge the pseudo-random sequences may vary from slot to slot and there exit 170 different sequences. In this project only one reference symbol is needed, hence it chosen to generate $\boldsymbol{R}^{\text{PRS}}$ as a random sequences of $+1$ and -1.

B.4 Mapping of Reference Symbols onto Resource Elements

The two-dimensional reference signal sequence $\boldsymbol{R}_{\text{ref}}$ is mapped to complex-valued modulation symbols $(a_{k,l}^{(p)}(i))$, where k is the OFDM symbol position in one slot and l is the position of the subcarrier, while p and i are the antenna port and slot number respectively:

$$a_{l,k}^{(p)}(i) = r_{m',n}, \tag{B.5}$$

where entry (m', n) of the reference symbol sequence is found as follows

$$m = 0, 1, \ldots, \lfloor \frac{N_{\text{BW}}}{N_{\text{BW}}^{\text{RB}}/2} \rfloor - 1 \tag{B.6}$$

$$m' = m + 170 - \lfloor \frac{N_{\text{BW}}}{N_{\text{RB}}} \rfloor \tag{B.7}$$

$$n = \begin{cases} 0 \text{ and } 1 & \text{if } p = 0 \text{ or } p = 1 \\ 0 & \text{if } p = 2 \text{ or } p = 3 \end{cases} . \tag{B.8}$$

The entry (l, k) of the reference symbol sequence is then calculated as following,

$$k = 6m + (v + f_{hop}(\lfloor i/2 \rfloor)) \text{ mod } 6 \text{ where} \tag{B.9}$$

$$l = \begin{cases} 0 & \text{if } n = 0 \text{ and } p = 0 \text{ or } p = 1 \quad (1) \\ 1 & \text{if } n = 0 \text{ and } p = 2 \text{ or } p = 3 \quad (2) \\ N_{sym} - 3 & \text{if } n = 1 \quad (3) \end{cases} . \tag{B.10}$$

B.4.1 Reference Symbol Mapping Example

In this example the number of transmitter antennas is 1 ($p = 0$), in order to make it as simple as possible. Using transmission bandwidth of 2.5 MHz, $N_{\text{BW}} = 150$ according to Table 2.1 and $N_{\text{RB}} = 12$ as explained in section . The number of OFDM symbols in one slot $N_{\text{sym}} = 6$ and it is chosen not to use frequency hopping.
The reference symbol to be transmitted is found in the following procedure:

- The index (m', n) is calculated.

  Since $p = 1$, $n = 0$ and $n = 1$ (Equation (B.8)).

  $m = m = 0, 1, \ldots, \lfloor \frac{150}{6/2} \rfloor - 1 = 0, 1, \ldots, 24$ (Equation (B.6)).

  $m' = m + 170 - \lfloor \frac{N_{\text{BW}}}{N_{\text{RB}}} \rfloor = 158, 159, \ldots, 182$ (Equation (B.7)).

- The entry (l, k) of the mapping positions are now found. Equation (B.10),1 and (B.10),2 are true, since $n = 0, 1$ and $p = 0$. Firstly the values (k, l) for $n = 0$ is calculated.

  For n=0, $k = 6m + (v + f_{hop}(\lfloor i/2 \rfloor)) \bmod 6 = 6m + (v \bmod 6) = 0, 6, \ldots, 144$. For n=0, l=1.

  For n=1, $k = 6m + (v \bmod 6) = 6m + (3 \bmod) 6) = 3, 9, \ldots, 147$. For n=1, $l = 3$.

In this example there is a reference symbol on the first and fourth OFDM symbol in one slot. There is always a spacing between the reference symbols of 6 subcarriers. The reference symbols are placed with an offset of 4 subcarriers at the fourth OFDM symbol.
An illustration of the structure is depicted on Figure B.1.

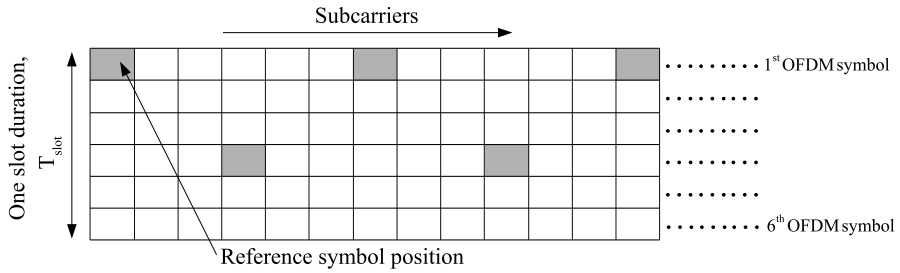

Figure B.1: *Example of the reference symbol structure for one slot with 6 OFDM symbols using one antenna. Note that only the used subcarriers are depicted.*